

State Space Models for Regional Epidemiological Indicators

Stefan Heyder

October 2023 – Draft v 0.1

Abstract

Short summary of the contents in English. . .

Zusammenfassung

Kurze Zusammenfassung des Inhaltes in deutscher Sprache. . .

Publications and Contributions

This thesis consists of mostly unpublished work. During my time as a PhD student I have, however, been fortunate to collaborate with many scientists on problems in mathematical epidemiology with a focus on COVID-19, which resulted in several publications. In this section I want to clarify what my contributions to these publications were and which contributions of the present thesis are new.

- [1] J. Bracher et al. “A Pre-Registered Short-Term Forecasting Study of COVID-19 in Germany and Poland during the Second Wave.” In: *Nature Communications* 12.1 (1 Aug. 27, 2021), p. 5173. ISSN: 2041-1723. DOI: [10.1038/s41467-021-25207-0](https://doi.org/10.1038/s41467-021-25207-0). URL: <https://www.nature.com/articles/s41467-021-25207-0> (visited on 09/30/2021).
- [2] Johannes Bracher et al. “National and Subnational Short-Term Forecasting of COVID-19 in Germany and Poland during Early 2021.” In: *Communications Medicine* 2.1 (1 Oct. 31, 2022), pp. 1–17. ISSN: 2730-664X. DOI: [10.1038/s43856-022-00191-8](https://doi.org/10.1038/s43856-022-00191-8). URL: <https://www.nature.com/articles/s43856-022-00191-8> (visited on 11/16/2022).
- [3] Jan Pablo Burgard et al. “Regional Estimates of Reproduction Numbers with Application to COVID-19.” Aug. 31, 2021. arXiv: [2108.13842 \[stat\]](https://arxiv.org/abs/2108.13842). URL: <http://arxiv.org/abs/2108.13842> (visited on 09/30/2021).
- [4] Sara Grundel et al. “How Much Testing and Social Distancing Is Required to Control COVID-19? Some Insight Based on an Age-Differentiated Compartmental Model.” In: *SIAM Journal on Control and Optimization* 60.2 (Apr. 2022), S145–S169. ISSN: 0363-0129, 1095-7138. DOI: [10.1137/20M1377783](https://doi.org/10.1137/20M1377783). URL: <https://epubs.siam.org/doi/10.1137/20M1377783> (visited on 11/16/2022).
- [5] Sara M. Grundel et al. “How to Coordinate Vaccination and Social Distancing to Mitigate SARS-CoV-2 Outbreaks.” In: *SIAM Journal on Applied Dynamical Systems* 20.2 (Jan. 1, 2021), pp. 1135–1157. DOI: [10.1137/20M1387687](https://doi.org/10.1137/20M1387687). URL: <https://epubs.siam.org/doi/abs/10.1137/20M1387687> (visited on 01/21/2022).
- [6] K. Sherratt et al. *Predictive Performance of Multi-Model Ensemble Forecasts of COVID-19 across European Nations*. June 16, 2022. DOI: [10.1101/2022.06.16.22276024](https://doi.org/10.1101/2022.06.16.22276024). URL: <http://medrxiv.org/lookup/doi/10.1101/2022.06.16.22276024> (visited on 11/28/2022). preprint.

Du musst bereit sein Dinge zu tun.

— A meme on the internet, 2022.

Acknowledgments

Put your acknowledgments here.

Contents

1	Introduction	1
2	Epidemiological considerations	3
2.1	Objectives of epidemiological modelling	4
2.2	Available data and its quality	6
2.3	Measures of epidemic spread	6
2.3.1	Growth Factor	6
2.3.2	Reproduction number	6
2.3.3	Other indicators	6
2.3.4	Usefulness of indicators	6
2.4	Dessiderata for epidemiological models	6
3	Importance Sampling in State Space Models	9
3.1	Modelling epidemiological dessiderata with state space models	12
3.2	Gaussian Linear State Space Models	12
3.3	Logconcave Gaussian state space models	14
3.4	Importance Sampling	16
3.4.1	Laplace approximation (LA)	19
3.4.2	The Cross-entropy method (CE-method)	19
3.4.3	Efficient importance sampling (EIS)	22
3.5	Gaussian importance sampling for state space models	25
3.5.1	The Gaussian linear state space model (GLSSM)-approach	26
3.5.2	The Markov-approach	29
3.6	Accounting for multimodality and heavy tails	36
3.7	Maximum likelihood estimation in state space models (SSMs)	36
3.8	Comparison of Importance Sampling method	36
3.8.1	Breakdown of methods	36
3.8.2	Computational complexity	38
3.8.3	Asymptotic variance	39
3.8.4	Numerical convergence	44
3.8.5	Performance of the optimal proposal	44
4	Analysis of selected models	49
4.1	Spatial reproduction number model	50
4.2	Regional growth factor model	50
4.3	Nowcasting hospitalizations	50
4.3.1	Context	50
4.3.2	Data	52
4.3.3	Model	53
4.3.4	Discussion	54
5	Discussion	59
A	Implementation in Python	61

B Proofs (?)**63**

Chapter 1

Introduction

The Coronavirus disease 2019 (COVID-19) pandemic put the scientific community to the test: how infectious, morbid and mortal was the disease? when and for how long did infected people become infectious? how effective are the countermeasures taken? how safe and effective are the vaccines that were developed at an unprecedented speed? Some of these questions, e.g. those about the epidemiology of COVID-19, are confined to well-established areas of research, while others, e.g. those about the efficacy of countermeasures, required collaboration across a wide range of disciplines: from infectious disease epidemiology, mathematical and statistical modeling, social and communication science to non-scientific actors such as legislators, journalists and politicians.

Although there is still a lot of scientific and societal follow-up work to be done, given the magnitude of this challenge, it is astonishing how well science and society as a whole have handled the pandemic. A key factor in this accomplishment is the large-scale availability of data surrounding the pandemic. In many countries, including Germany, data on reported cases, deaths, vaccinations and deaths were published daily by the respective national health authorities, i.e. the Robert Koch-Institut (RKI) [68, 69] in Germany. Additionally, mobility data from mobile communications providers allowed researchers to relate human movement to the spread of COVID-19 [54, 77]. As each day the news reported on the number of newly reported cases and deaths, numerous dashboards with analyses of COVID-19 data were made available and an abundant number of scientific works was created, effectively communicating with the public, whose cooperation with countermeasures was critical, became more and more important. To disseminate insights to the public, we need to understand and communicate to them the underlying dynamics of an epidemic.

An epidemic outbreak is inherently a random phenomenon [25]. Who becomes infected, for how long they stay infectious, whom they meet while they are infectious and whom they finally infect are all aspects that depend to a certain degree on chance. If one is interested in large-scale phenomena, e.g. effects of immunization in a large population, one may get away with a deterministic model [16], such as the classical S(E)IR model [49] or variants of it. However, as soon as one is interested in more detailed phenomena, as we are in this thesis, stochastic and statistical modeling becomes essential.

An epidemic outbreak is also inherently a local phenomenon, especially in the early phase of the epidemic. In the extreme case, there is only a single infectious person and, for the most part, their potential infectees will belong to the same spatial region as the infector. Therefore, we should incorporate this locality into our models. To fit such models to data, the data has to include spatial information. Luckily, the case and death data are available at the subnational level in most countries. In Germany, it is even available at the county (Landkreis, NUTS3) level [69].

As statisticians, having access to such a large amount of data is both a blessing and a curse. While more, and ideally better, data allows us to formulate and answer more relevant questions, the models we create to accommodate these data become more and more intricate. Intricate models require more care in modeling, fitting and interpretation, as more things can go wrong along the way. Thus we will tread carefully. As we incorporate more detailed effects into our models, fitting the models to

data becomes difficult to practically impossible using established techniques. While there are some remedies for this curse of dimensionality, e.g. exploiting as much available structure as possible, there is an ongoing need for new procedures enabling inference in these settings. Additionally, we need mathematical as well as practical insight into the performance of these procedures to make informed decisions in applied settings: which methods should we prefer under which circumstances?

These considerations set the stage for this thesis. Driven by the need for good statistical models that allow us to answer urgent questions in infectious disease epidemiology, with COVID-19 as a driving example, we will start with an analysis of what is required of these sought-after models. We will define and discuss the role of several epidemiological indicators, i.e. quantities that have an interpretation related to the epidemic. It turns out that we will usually be interested in quantifying the speed at which the epidemic proliferates, and we discuss several popular indicators that measure this speed. A useful statistical analysis should provide interpretable insight into the problem at hand, so we focus on how straightforward this interpretation is, giving recommendations on when to use which indicator. To estimate these indicators from data, we have to create statistical models that include them. Before we do so, we will create a list of desiderata from the context of COVID-19.

Once we have a clear view of the epidemiological problems at hand, we show that many of the desiderata can be covered by using SSMs, a flexible framework for modeling non-stationary time series. Unfortunately, we will require that these SSMs include integer-valued, non-Gaussian, observations, which makes fitting the models to data analytically impossible and numerically difficult, as one is essentially faced with a high-dimensional non-Gaussian Bayesian inference problem. Instead, inference will be based on simulation methods, most notably importance sampling. To apply these methods, the practitioner has some flexibility in the so-called proposal distribution, a tractable approximation to the Bayesian posterior. Different disciplines have developed simulation-based techniques that allow the user to choose optimal proposals, where optimality is based on different performance criteria for different methods. In this thesis, we focus on two methods: the cross-entropy method (CE-method) and efficient importance sampling (EIS). In the literature, a comparison between these two methods is missing: there are neither mathematical nor empirical results comparing the two. We fill this gap by first proving central limit theorems for both methods, allowing for a theoretical comparison. Additionally, we also provide simulation studies comparing the methods on instructive univariate and SSMs examples. To this end, we also develop a new algorithm that allows the CE-method to be applied to SSMs.

Finally, we demonstrate how to solve a selection of infectious disease epidemiology problems using the mathematical insights we gained. These examples focus on the COVID-19 epidemic in Germany and illustrate the modeling, computational and applied aspects of this thesis.

add some more refs?

Chapter 2

Epidemiological considerations

Contributions of this chapter

- ...

The spread of infectious diseases, such as COVID-19, is a complex phenomenon. For COVID-19 this complexity arises from the interplay of many factors. Studying these influences allows us to define the aims and challenges of epidemiological modeling in the context of this thesis. It also will guide us towards desirable and possible outcomes of our efforts from an applied perspective.

First of all, there is considerable heterogeneity in the way the disease progresses once an individual is infected [75]. Some infectees may show few to no symptoms but are still highly infectious [19], and disease progression is tightly linked to age and preexisting comorbidities [10]. Additionally, different variants of SARS-CoV-2 differ in key epidemiological characteristics such as the reproduction number [26] and mortality [44].

Second, the spread is highly dependent on the contact behavior in the population, as the infector has to be in close physical proximity to the infectee to infect them. These contact patterns are an essential component of any mathematical model for infectious diseases, as they define how the epidemic evolves. While there are some empirical studies [62, 85], capturing the contact behavior at certain points in time, in the context of an ongoing epidemic these patterns are subject to change, not only in intensity but also in shape [85]. As contact restrictions were put into place or lifted, mask-wearing was enforced and home office and schooling became commonplace, so did the number of contacts change and occur under different circumstances.

Finally, as the virus spread in the population and vaccinations became available, the population became partially immune against the disease, if not against infection

cite

. This immunity affects the spread as well: if an infector has contact with a partially immune individual, the probability of transmission is smaller. Additionally, partial immunity may lead infectors to develop fewer or no symptoms so they may not be aware of being infectious, foregoing quarantine.

As statisticians, we are faced with a difficult problem: Which of these factors should we include in our model and how? The answer certainly depends on the epidemiological question under consideration and the availability and quality of data.

2.1 Objectives of epidemiological modelling

Before considering the mathematical modeling of epidemics, let us make clear what the goals of our investigation are. In this thesis, we are interested in providing models that are informed by real-world data, allow us to learn about the past, current or future state of the epidemic and whose results are, ideally, easy to communicate to non-experts, e.g. political stakeholders. These time scales can be translated into the following three tasks for epidemiological modeling.

Retrospective Analysis Here we are interested in an ex-post analysis of a period of interest in the past. The goal here is either to infer intrinsic epidemiological quantities, such as the time-varying reproduction number R_t [1] or to evaluate the performance of non-pharmaceutical interventions (NPIs) taken [15, 34, 51]. The results of this analysis may inform future decisions on which countermeasures to implement, and as such we want a causal link between the NPIs prescribed and the reduction in reported cases. Naturally, this is a difficult objective to accomplish due to several aspects. The data at our disposal is observational and there are several quality issues, see Section 2.2. Additionally, the interplay between NPIs and change in the behavior of the population is intricate, where voluntary behavioral change may precede the enforced social distancing [38]. For some examples focusing on the efficacy of NPIs, we refer the reader to the excellent articles [15, 34, 51], especially the discussion and limitation sections therein. In these types of analyses, we can assume that all data related to that period is as complete as it will be. Methods used to perform these analyses range from estimating parameters for each day individually, e.g. using the EpiEstim [23] method [1], to constructing complex Bayesian mechanistic [34] and hierarchical models [15, 51].

Monitoring For monitoring, we are interested in real-time inference about the current state of the epidemic. This includes the recent past and near future and may include now- and forecasts of cases, hospitalizations or deaths. Here data is not yet final, and inference is complicated by slow reporting and data revisions, see Section 2.2. The results of monitoring can be used to inform current policy, i.e. whether current NPIs should be lifted or new ones enforced. Most online dashboards that emerged at the beginning of the pandemic fall into this category. The result of monitoring may either be an estimate of an epidemiological indicator, but may also consist of short-term forecasts. Examples of the former include the daily reproduction number estimates of the RKI [5], the Helmholtz Centre for Infection Research’s dashboard [50] or the dashboard of the authors team [43]. While some of these dashboards also provide forecasts of cases, a more concerted effort of forecasts is provided by the U.S. ForecastHub [65], its German/Polish [12, 13] and EU/EFTA [81] equivalents. These collaborative platforms gathered real-time forecasts of COVID-19 cases and deaths in the upcoming four weeks, based on an ensemble that aggregates predictions from several models provided by expert modelers. In a real-time setting, these forecasts can be evaluated which may inform practitioners as to which model to prefer. For forecasting, methods range from classical time series analysis methods [7] to compartmental models [50] and computationally intensive agent-based models [2].

Scenario Modeling Scenario modeling concerns itself with the impact that changes of current circumstances, e.g. variants, seasonality, policies, vaccination or NPIs, have on public health outcomes. Contrary to monitoring, the goal is to quantify the influence over longer periods with scenarios reaching multiple months into the future. The parameters of scenarios are assumed to be uncertain as well, making the task at hand challenging. These forecasts are difficult to evaluate, as the scenario specifications rely on assumptions that are hard to verify in practice. Nevertheless, these scenarios help policymakers make informed decisions [11].

In this thesis, we will forego scenario modelling

2.2 Available data and its quality

- surprising amount of data available, but quality questionable,
- in Germany have data on reported cases and deaths by gender, age group, county, with reporting date of case and for some cases even date of symptom onset
- reporting of cases is regulated by Infektionsschutzgesetz
- parallel dataset for reports of hospitalisations
- have description section from Nowcasting draft [here](#)
- descriptive statistics of German COVID-19 data set
- even larger datasets that compile this for europe + EFTA (?) by ECDC or by world (JHU)
- quality of reported case data is potentially too low
 - reporting delays
 - weekday effects
 - testing regime changing (2G/3G)
 - ...
- data on commuting

2.3 Measures of epidemic spread

This section consists of the ideas published in [39], but has been rewritten to fit better into this thesis.

- not only epidemic spread but also speed of proliferation is of interest, enables forecasts
- measuring speed difficult: data problems ... (look at AK book article)
-

2.3.1 Growth Factor

2.3.2 Reproduction number

2.3.3 Other indicators

2.3.4 Usefulness of indicators

2.4 Dconsiderata for epidemiological models

- we want models to be able to include as much data as possible, while still being numerically tractable

this paragraph to modelling chapter

The Poisson distribution arises from the law of small numbers: if there is a large population where every individual has, independently, a small probability of becoming infected in a small window of time then the total number of infections in that window of time is well approximated by the Poisson distribution. Indeed, the law of small numbers remains valid for small dependencies [6, 71]. However, incidences observed from the SARS-CoV-2 epidemic tend to follow a negative binomial distribution [20].

Regional dependencies and effects

- German case data are reported on Landkreis level, performing analysis of each individual is not sensible
- inhabitants travel between regions, and measures were taken on on regional level as well
- effects are not really spatial: euclidean distance is not so much of an issue but how closely connected regions are (give some examples)
- also want to account for other regional effects such as different socio-economic settings ...

Temporal correlation**Interpretability**

Chapter 3

Importance Sampling in State Space Models

Contributions

The main contribution of this chapter consists of a rigorous comparison of two important sampling frameworks: the Cross-entropy method (CE-method) and Efficient importance sampling (EIS). Both methods determine optimal importance sampling proposals, but have, until now, been studied in separate communities: the CE-method is popular in rare-event estimation and engineering disciplines, while EIS is popular in the financial time series community.

To facilitate this comparison, we prove central limit theorems for both methods (Sections 3.4.2 and 3.4.3), derive an efficient algorithm to apply the CE-method to state space models (Section 3.5.2), and extensively compare both methods on theoretical as well as practically relevant properties with instructive univariate and multivariate examples (Section 3.8).

We also proof Proposition 3.2

more explicit

Additionally, we show how one may use state space models to model the desiderata for epidemiological models identified in the last chapter (Section 3.1).

State space models (SSMs) form a versatile class of statistical models which allow to model non-stationary time series data and come along with straight-forward interpretation. The main idea of these models is to introduce unobserved **latent states** whose joint distribution is given by a Markov process and model the observed time series conditional on these states. By exploiting this structure, inference in SSMs becomes computationally efficient, i.e. the complexity of algorithms is linear in the number n of time points considered.

An additional advantage, that will become more explicit in Section 3.1, is that SSMs allow to interpret the modeled dynamics of latent states which makes

Definition 3.1 (State Space Model). A **SSM** is a discrete time stochastic process $(X_t, Y_t)_{t=0, \dots, n}$ taking values in the measurable space $(\mathcal{X} \times \mathcal{Y}, \mathcal{B}_{\mathcal{X}} \otimes \mathcal{B}_{\mathcal{Y}})$ such that

1. The marginal distribution of the **states** (X_0, \dots, X_n) is a discrete time Markov process, i.e. for $t = 1, \dots, n$

$$\mathbf{P}(X_t \in B | X_0, \dots, X_{t-1}) = \mathbf{P}(X_t \in B | X_{t-1}) \text{ a.s.} \quad (3.1)$$

for all measurable $B \in \mathcal{B}_{\mathcal{Y}}$.

2. Conditional on the state X_t and observation Y_{t-1} , Y_t is independent of X_s and Y_{s-1} , $s < t$, i.e.

$$\mathbf{P}(Y_t \in B | X_0, \dots, X_t, Y_0, \dots, Y_{t-1}) = \mathbf{P}(Y_t \in B | X_t, Y_{t-1})$$

for all measurable $B \in \mathcal{B}_{\mathcal{Y}}$.

For notational convenience we will write $X_{s:t} = (X_s, \dots, X_t)$ for the vector that contains all states from s to t , dropping the first index if we consider the whole set of observations up to time t , so $X_{:t} = X_{0:t}$. Similarly we set $Y_{s:t} = (Y_s, \dots, Y_t)$ and $Y_{:t} = Y_{0:t}$.

picture of dependency structure

Remark 3.1. Contrary to the standard definition of a SSM, our Definition 3.1 allows Y_t to depend on Y_{t-1} . This is not a limitation of the standard definition: given a SSM of the form in Definition 3.1 we can transform it to the standard form by choosing states $(X_t, Y_t) \in \mathcal{X} \times \mathcal{Y}$ and observations $Y_t \in \mathcal{Y}$ such that the SSM becomes a stochastic process on $(\mathcal{X} \times \mathcal{Y}) \times \mathcal{Y}$.

Additionally, most computations and inferences in this thesis will be conditioned on a single set of observations Y . We thus adopt a Bayesian perspective and as such Y may be treated as a fixed and Y_t only depends on X_t . We will not be interested in frequentist properties of the models concerning repeated sampling of Y .

As the models considered in Chapter 4 will make extensive use of SSMs with this dependency structure we opt to use this non-standard definition here.

In most models we consider in this thesis we use $\mathcal{X} = \mathbf{R}^m$, $\mathcal{Y} = \mathbf{R}^p$ or $\mathcal{Y} = \mathbf{Z}^p$ so that \mathcal{X} is m dimensional and \mathcal{Y} is p dimensional and equip these spaces with the usual σ -Algebras.

The models that we consider in this thesis will usually admit densities for the state transitions w.r.t. a common dominating measure $\mu_{\mathcal{X}}$ and similar for the observations w.r.t. a (potentially different) dominating measure $\mu_{\mathcal{Y}}$.

check whether models in Ch4 violate this

Notation 3.1 (Densities, conditional densities). I will use the standard abuse of notation for densities that makes the type of density „obvious“ from the arguments used. This means that $p(x)$ is the density for all states X , $p(x_t | x_{t-1})$ the conditional density of $X_t | X_{t-1}$ and similarly for observations: $p(y | x)$ is the density of all observations Y conditional on all states X .

Note that this notation also implicitly includes the time t and allows for changes in, e.g., the state transition over time.

When densities stem from a parametric model parametrized by $\theta \in \Theta \subseteq \mathbf{R}^k$ and the dependence of the model on θ is of interest, i.e. because we try to estimate θ , we indicate this by adding a subscript to the densities. If the dependence is not of interest, e.g. because θ is fixed, I will usually omit θ for better readability.

In this notation, the joint density of a parametric SSM factorizes as

$$\begin{aligned} p_\theta(x, y) &= p_\theta(x_0, \dots, x_{n-1}, y_0, \dots, y_{n-1}) \\ &= p_\theta(x_0) \prod_{t=1}^{n-1} p_\theta(x_t | x_{t-1}) \prod_{t=0}^{n-1} p_\theta(y_t | x_t, y_{t-1}), \end{aligned}$$

where $p_\theta(y_0 | x_0, y_{-1}) = p_\theta(y_0, x_0)$.

As inferences we make in this thesis depend on the SSM only through the likelihood we identify almost sure versions of (X, Y) with itself, i.e. all equations involving X or Y are understood almost surely.

Given data $(y_t)_{t=0, \dots, n-1}$ that may be modeled with a SSM the practitioner is confronted with several tasks, which provide the structure of this chapter:

1. Choosing a suitable, usually parametric, class of SSMs that include the effects of interest.
2. Fitting such a parametric model to the data at hand by either frequentist or Bayesian techniques.
3. Infer about the latent states X from the observations Y by determining, either analytically or through simulation, the smoothing distribution $X|Y$.

The first step, Item 1, requires that the practitioner specifies a joint probability distribution for the states and observations (Section 3.1). Due to the assumed dependency structure this boils down to specifying transition kernels for the states and observations. The setting Definition 3.1 is too abstract to perform inference in, so further assumptions on the types of distributions for the latent states and observations are needed. In this chapter we will discuss Gaussian linear state space model (GLSSM) (Section 3.2), where both the posterior distribution and the likelihood are analytically available. For the epidemiological application we have in mind these are however insufficient due to the non-linear behaviour of incidences and the low count per region (Section 2.4). Such observations are better modeled with distributions on the natural numbers, i.e. with a Poisson or negative binomial distribution, leading to the class of logconcave Gaussian state space models (Section 3.3).

Regarding the second step, Item 2, a frequentist practitioner will want to perform maximum likelihood inference on θ . While asymptotic confidence intervals for θ can be derived both theoretically and practically [27, Chapter 7], they are, in the context of this thesis, usually of little interest. We choose to view this fitting as an Empirical Bayes procedure and our main practical interest lies in analyzing the posterior distribution $X|Y$.

To obtain the maximum likelihood estimates $\hat{\theta}$ one needs access to the likelihood

$$p(y) = \int_{\mathcal{X}^n} p(x, y) dx, \quad (3.2)$$

which is usually not analytically available. Direct numerical evaluation of Equation (3.2) is hopeless due to the high dimensionality of the state space \mathcal{X}^n . Instead we will resort to simulation based inference by importance sampling (see Section 3.4), an alternative would be particle filters [22].

The performance of these simulations depends crucially on constructing distributions that are close to the posterior $p(x|y)$ but are easy to sample from. To this end, we construct suitable Gaussian state space models (Section 3.5) in which sampling from the posterior is analytically possible. This will be a good strategy if the target posterior $p(x|y)$ can be well approximated by a Gaussian distribution — otherwise, we may want to account for multiple modes by considering mixtures of Gaussian state space models or account for heavy tails with t-distributed errors (??).

3.1 Modelling epidemiological considerations with state space models

3.2 Gaussian Linear State Space Models

Gaussian linear state space models (GLSSMs) are the working horses of most methods used in this thesis because they are analytically tractable and computationally efficient. Indeed for fixed dimension of states m and observations p the runtime of algorithms that we consider in this thesis is $\mathcal{O}(n)$.

Definition 3.2 (GLSSM). A GLSSM is a state space model where states obey the transition equation

$$X_{t+1} = A_t X_t + u_t + \varepsilon_{t+1} \quad t = 0, \dots, n-1, \quad (3.3)$$

and observations obey the observation equation

$$Y_t = B_t X_t + v_t + \eta_t \quad t = 0, \dots, n. \quad (3.4)$$

Here $A_t \in \mathbf{R}^{m \times m}$ and $B_t \in \mathbf{R}^{p \times m}$ are matrices that specify the systems dynamics. The **innovations** ε_{t+1} and **measurement noise** η_t are independent from one another and from the starting value $X_0 \sim \mathcal{N}(\mathbf{E}X_0, \Sigma_0)$. Furthermore, $\varepsilon_{t+1} \sim \mathcal{N}(0, \Sigma_t)$ and $\eta_t \sim \mathcal{N}(0, \Omega_t)$ are centered Gaussian random variables and $u_t \in \mathbf{R}^m, t = 0, \dots, n-1, v_t \in \mathbf{R}^p, t = 0, \dots, n$ are deterministic biases.

The defining feature of a GLSSM is that the joint distribution of (X, Y) is Gaussian, as (X, Y) may be written as an affine combination of the jointly Gaussian $(X_0, \varepsilon_1, \dots, \varepsilon_n, \eta_0, \dots, \eta_n)$ and it is often useful to perform inferences in terms of innovations and measurement noise instead of states, see e.g. [27, Section 4.5].

As the joint distribution of (X, Y) is Gaussian, so are conditional distributions of states given any set of observations.

Lemma 3.1 (Gaussian conditional distributions). *Let (X, Y) be jointly Gaussian with distribution $\mathcal{N}(\mu, \Sigma)$ where*

$$\mu = (\mu_X, \mu_Y)$$

and

$$\Sigma = \begin{pmatrix} \Sigma_{XX} & \Sigma_{XY} \\ \Sigma_{YX} & \Sigma_{YY} \end{pmatrix},$$

for non-singular Σ_{YY} .

Then $X|Y = y$ is also a Gaussian distribution with conditional expectation

$$\mu_{X|Y=y} = \mathbf{E}(X|Y = y) = \mu_X + \Sigma_{XY} \Sigma_{YY}^{-1} (y - \mu_Y)$$

and conditional covariance matrix

$$\Sigma_{X|Y=y} = \text{Cov}(X|Y = y) = \Sigma_{XX} - \Sigma_{XY} \Sigma_{YY}^{-1} \Sigma_{YX}.$$

In particular, if $Y = BX + \varepsilon$ for a matrix $B \in \mathbf{R}^{p \times m}$ and $\varepsilon \sim \mathcal{N}(0, \Omega)$ for $\Omega \in \mathbf{R}^{p \times p}$ independent of X , then, as $\mu_Y = B\mu_X$, $\Sigma_{XY} = \Sigma_{YX}^T = \Sigma_{XX} B^T$ and $\Sigma_{YY} = B\Sigma_{XX} B^T + \Omega$, we have

$$\mu_{X|Y=y} = \mu_X + K(y - B\mu_X)$$

and

$$\Sigma_{X|Y=y} = \Sigma_{XX} - K \Sigma_{YY} K^T = (I - KB) \Sigma_{XX}$$

with $K = \Sigma_{XX} B^T (B\Sigma_{XX} B^T + \Omega)^{-1}$.

Proof. For the first statement, we refer the reader to [27, Chapter 4, Lemma 1]. The second statement follows from substituting the value of K .

□

Let us denote by $\hat{X}_{t|s}$ the conditional expectation of X_t given a set of observations $Y_{:s}$ and by $\Xi_{t|s}$ the conditional covariance matrix of X_t given $Y_{:s}$. Then $X_t|Y_{:s} \sim \mathcal{N}(\hat{X}_{t|s}, \Xi_{t|s})$. For a given t , three values of s are of particular interest: If $s = t - 1$ determining this conditional distribution is called a **prediction problem**, if $s = t$ this is a **filtering problem** and if $s = n$ a **smoothing problem**, and we call the distributions we seek the **predictive**, **filtering** or **smoothing distribution** respectively. Similarly we define $\hat{Y}_{t|s} = \mathbf{E}(Y_t|Y_{:s})$ to be the conditional expectation of Y_t given $Y_{:s}$, note that $\hat{Y}_{t|s} = Y_t$ if $s \geq t$. Finally, let $\Psi_{t|s} = \text{Cov}(Y_t|Y_{:s})$ be the conditional covariance matrix of Y_t given $Y_{:s}$. Again $\Psi_{t|s} = 0$ if $s \geq t$.

These distributions may be obtained efficiently using the celebrated Kalman filter (Algorithm 1) and smoother (Algorithm 2) algorithms, which we state here for completeness.

KF + KS literature review, historical comment

Algorithm 1 Kalman filter, with runtime $\mathcal{O}(n(m^2 + p^3))$

Require: GLSSM (Definition 3.2), observations Y_0, \dots, Y_n .

```

 $A_{-1} \leftarrow I \in \mathbf{R}^{m \times m}$  ▷ Identity Matrix
 $u_{-1} \leftarrow \mathbf{0} \in \mathbf{R}^m$ 
 $\hat{X}_{-1|-1} \leftarrow \mathbf{E}X_0$ 
 $\Xi_{0|-1} \leftarrow \Sigma_0$ 
for  $t \leftarrow 0, \dots, n$  do
     $\hat{X}_{t|t-1} \leftarrow A_{t-1}\hat{X}_{t-1|t-1} + u_{t-1}$  ▷ prediction
     $\Xi_{t|t-1} \leftarrow A_{t-1}\Xi_{t-1|t-1}A_{t-1}^T + \Sigma_t$ 
     $\hat{Y}_{t|t-1} \leftarrow B_t\hat{X}_{t|t-1} + v_t$ 
     $\Psi_{t|t-1} \leftarrow B_t\Xi_{t|t-1}B_t^T + \Omega_t$ 
     $K_t \leftarrow \Xi_{t|t-1}B_t^T\Psi_{t|t-1}^{-1}$  ▷ filtering
     $\hat{X}_{t|t} \leftarrow \hat{X}_{t|t-1} + K_t(Y_t - \hat{Y}_{t|t-1})$ 
     $\Xi_{t|t} \leftarrow \Xi_{t|t-1} - K_t\Psi_{t|t-1}K_t^T$ 
end for
```

In Algorithm 1 every time point $t = 0, \dots, n$ is processed in the same way, with a two-step procedure: first we predict the new observation Y_t based on $Y_{:t-1}$. Using the linearity of the system as well as the assumed conditional independence, this is achieved by applying the system dynamics to the current conditional expectation and covariance matrices. After Y_t has been observed, we can update the conditional distribution of the states by appealing to Lemma 3.1. For a rigorous derivation of the Kalman filter, we refer the reader to [27, Chapter 4] or the excellent monograph of Schneider, [79].

The Kalman filter is very efficient: each loop iteration requires inversion of the $p \times p$ matrix $\Psi_{t|t-1}$. Assuming this operation dominates the time complexity, e.g. because $m \approx p$, the time complexity of the Kalman filter is $\mathcal{O}(nm^3)$, a drastic improvement over the naïve $\mathcal{O}(n^3m^3)$, obtained by applying Lemma 3.1 to the joint distribution of Y . Similarly, the space complexity of Algorithm 1 is $\mathcal{O}(n(m^2 + p^2))$, and grows only linearly in the number of time steps n .

Depending on the situation at hand, one of the many variants of the basic algorithm presented in Algorithm 1 may be used. If the inversion of $\Psi_{t|t-1}$ is numerically unstable, the filtered covariance matrices $\Xi_{t|t}$ may become numerically non-positive definite. In this case, the square root filter and smoother [61] may be used. It is based on Cholesky roots of the involved covariance matrices, ensuring them to be positive-semi definite.

comment on information filter?

Algorithm 2 Kalman smoother

Require: todo

Notice that the Kalman filter calculates the likelihood $p(y)$ while filtering — this is possible because of the dependency structure of the state space model — this makes inference via maximum likelihood possible in GLSSMs.

To ensure numerical stability in these algorithms, the square root filter and smoother [61] may be used, see also [79] for an accessible introduction to it and other variants.

The Kalman smoother computes the marginal distributions $X_t|Y$ for $t = 0, \dots, n-1$ and, owing to the Markov structure of the states, these are enough to specify the joint distribution $X|Y$, allowing to simulate from it.

Algorithm 3 Forwards filter, backwards smoother [35, Proposition 1]

Require: TODO

The modeling capacity of GLSSMs is, however, limited: most interesting phenomena follow neither linear dynamics nor are well modeled by a Gaussian distribution. Nevertheless, linearization of non-linear dynamics suggests that GLSSMs may have some use as approximations to these more complicated phenomena, provided they are sufficiently close to Gaussian models, e.g. unimodal and without heavy tails. We start to move away from linear Gaussian models by allowing observations that are non-Gaussian.

3.3 Logconcave Gaussian state space models

The distribution of observations is never Gaussian - all we may hope for is that the data-generating mechanism is close enough to a Gaussian distribution that inferences made in the Gaussian model carry over. For epidemiological models, Gaussian distributions may be appropriate if incidences are high, e.g. during large outbreaks in a whole country. When case numbers are small, the discrete nature of incidences is better captured by a distribution on \mathbf{N}_0 , and standard distributions used are the Poisson and negative binomial distributions, see e.g. [58]. Both the Poisson and negative binomial belong to the class of exponential family distributions. As such, their densities have a convenient structure, allowing only for a linear interaction between the natural parameter and the densities argument. We refer to [18] for a comprehensive treatment of exponential families and use their definitions throughout this section.

Definition 3.3 (exponential family). Let μ be a σ -finite measure on \mathbf{R}^p and denote by

$$\Theta = \left\{ \theta \in \mathbf{R}^p : \int \exp(\theta^T y) \, d\mu(y) < \infty \right\}$$

the set of parameters θ such that the moment-generating function of μ is finite. For every $\theta \in \Theta$

$$p_\theta(y) = Z(\theta)^{-1} \exp(\theta^T y)$$

defines a probability density with respect to the measure μ , where

$$Z(\theta) = \int \exp(\theta^T x) \, d\mu(y)$$

is the normalizing constant. We call both the densities p_θ and induced probability measures

$$\mathbf{P}_\theta(A) = \int_A p_\theta(y) \, d\mu(y),$$

for measurable $A \subset \mathbf{R}^p$, a **standard exponential family**.

Conversely, let $\mathbf{P}_\theta, \theta \in \Theta$ be a given parametric family of probability measures on some space \mathcal{Y} that is absolutely continuous with respect to a common dominating measure μ . Suppose there exist a reparametrization $\eta : \Theta \rightarrow \mathbf{R}^p$, a statistic $T : \mathcal{Y} \rightarrow \mathbf{R}^p$ and functions $Z : \Theta \rightarrow \mathbf{R}$, $h : \mathcal{Y} \rightarrow \mathbf{R}$, such that

$$p_\theta(y) = \frac{d\mathbf{P}_\theta}{d\mu} = Z(\theta)h(y) \exp(\eta(\theta)^T T(y)),$$

then we call $\mathbf{P}_\theta, \theta \in \Theta$ and $p_\theta, \theta \in \Theta$ a **p -dimensional exponential family**. If $\eta(\theta) = \theta$ we call θ the canonical parameter. If $T(y) = y$, we call y the canonical observation. By reparametrization (in θ) and sufficiency (in y) every p -dimensional exponential family can be written as an equivalent standard exponential family, see the elaborations in [18, Chapter 1].

Exponential families have the attractive property that they are log-concave in their parameters. As such the Fisher-information is always positive semidefinite, which will be crucial in defining surrogate Gaussian models in Section 3.5.

Lemma 3.2 (log-concavity of exponential family distributions). *Let $p_\theta, \theta \in \Theta$ be a natural p -dimensional exponential family and Θ open in \mathbf{R}^p . In this case $\theta \rightarrow \log p_\theta(y)$ is concave for every $y \in \mathbf{R}^p$.*

Proof. As $\log p_\theta(y) = -\log Z(\theta) + \theta^T y$ it suffices to show that $\log Z(\theta)$ is convex. However,

$$\theta \mapsto \log Z(\theta) = \log \int \exp(\theta^T y) d\mu(y)$$

is the cumulant generating function of the base measure μ , which is convex [9, p. 148]. \square

We now generalize Definition 3.2 to allow for non-Gaussian observations by replacing the observation equation Equation (3.4) by more general exponential families.

Definition 3.4 (Logconcave state space model (LCSSM)). A **Logconcave state space model (LCSSM)** is a SSM where states obey the transition equation

$$X_{t+1} = A_t X_t + u_t + \varepsilon_{t+1}$$

and the conditional distribution of Y_t given X_t comes from an exponential family with respect to a base measure μ_t , i.e.

$$p(y_t|x_t) = h_t(y_t)Z_t(x_t) \exp(\eta_t(x_t)^T T_t(y_t))$$

for suitable functions h_t, Z_t, η_t, T_t .

If, additionally, matrices $B_t \in \mathbf{R}^{p \times m}$ exist, such that for the signal $s_t = B_t x_t \in \mathbf{R}^p$ it holds

$$p(y_t|x_t) = \prod_{i=1}^p h_t^i(y_t^i) Z_t^i(s_t^i) \exp(\eta_t^i(s_t^i)^T T_t^i(y_t^i)),$$

for functions $h_t^i : \mathbf{R} \rightarrow \mathbf{R}, Z_t^i : \mathbf{R} \rightarrow \mathbf{R}, \eta_t^i : \mathbf{R} \rightarrow \mathbf{R}, T_t^i : \mathbf{R} \rightarrow \mathbf{R}, i = 1, \dots, p$, we say the Logconcave state space model (LCSSM) has a **linear signal**.

Remark 3.2. To simplify notation we will usually assume that the functions h, Z and T are the same for all t (and i , if the LCSSM has a linear signal) and drop in our notation the dependence of h, Z , and T on t (and i). Similarly we assume that the base measure μ_t is the same for all relevant t .

As in the previous chapter, after having observed Y , one is interested in the conditional distribution of states X , given Y . If the observations are not Gaussian, this is a difficult task as the distribution is not analytically tractable. Instead approximations, e.g. the Laplace approximation (LA) (??), or simulation-based inference, e.g. importance sampling (Sections 3.4 and 3.5), sequential Monte Carlo [22] or MCMC-methods [17] are used. Similarly, fitting hyperparameters θ by maximum likelihood inference becomes more difficult as evaluating $\ell(\theta) = p(y) = \int p(x, y) dx$ is not analytically available, thus requiring numerical or simulation methods for evaluation and gradient descent or EM-techniques for optimization, see Section 3.7.

In this thesis, we will focus on importance sampling methods, which are the focus of the next section.

3.4 Importance Sampling

Importance sampling is a simulation technique that allows us to approximate integrals w.r.t a measure of interest, the target, by sampling from a tractable approximation, the proposal, instead, thus performing Monte-Carlo integration. To account for the fact that we did not sample from the correct probability measure, we weight samples according to their importance. As the user has freedom in the choice of approximation (except for some technical conditions), importance sampling also acts as a variance reduction technique with better approximations resulting in smaller Monte-Carlo variance. Thus the role that importance sampling plays is twofold: first, it allows to perform Monte-Carlo integration even if sampling from the target is not possible, and second it allows to do so in an efficient way by choosing, to be defined precisely below, the approximation in an optimal way.

Alternative approaches to importance sampling for performing inference in SSMs include Markov chain Monte Carlo (MCMC) and sequential Monte Carlo (SMC). Recall from the introduction to this chapter that this inference concerns three objectives: maximum likelihood estimation, i.e. evaluation and optimization of the likelihood, access to the posterior distribution $X_{:n}|Y_{:n}$ and prediction of future states and observations. Let us give a concise comparison of these alternative approaches, weighing their advantages and disadvantages over importance sampling, in particular for the SSMs that this thesis deals with.

MCMC [17] is a simulation technique that allows to simulation of correlated samples from a target distribution by constructing a Markov chain that has as its invariant distribution the desired distribution. For Metropolis Hastings MCMC, one needs access to the density of the sought distribution up to a constant to simulate a step in the Markov chain. While this method is very general, it fails in high dimensions and current research in MCMC methods investigates this

quotes

curse of dimensionality

cite something

.

MCMC vs. IS

SMC [22] or particle filters, use sequential importance sampling to provide a particle approximation to the filtering distributions $X_t|Y_{:t}$, essentially decomposing the problem into a n importance sampling steps. To avoid particle collapse, SMC is usually equipped with a resampling step once the effective sample size of the current set of particles drops below a specified level. Once the final filtering distribution $X_n|Y_{:n}$ is approximated, the smoothing distribution may be obtained in several ways ...

look up Chopin

.

Conveniently, SMC allows us to approximate the likelihood $\ell(\theta)$ for a single parameter by a single pass of the particle filter. However, the discrete nature of resampling makes the approximated likelihood non-continuous, complicating maximum likelihood inference. [22, Chapter 14] discusses several strategies: the first amounts to importance sampling of the order as discussed in this thesis, where one fixes a reference parameter θ_0 to perform importance sampling with $p_{\theta_0}(x|y)$ against $p_{\theta}(x|y)$. The second strategy only works in the univariate case and consists of approximating the non-continuous inverse CDFs appearing in the resampling step by continuous ones. Finally, if the dependence on the hyperparameters θ allows for application of the EM-algorithm, it may be used to

perform the optimization. Contrary to SMC, the global importance sampling approach we discuss in Sections 3.5 and 3.7 allows us to perform

...

This chapter proceeds with a general treatment of importance sampling. Subsequently, we will focus our attention on methods to obtain good importance sampling proposals.

Suppose we have a function $h : \mathcal{X} \rightarrow \mathbf{R}$ whose integral w.r.t. to some measure μ ,

$$\zeta = \int_{\mathcal{X}} h(x) d\mu(x),$$

we want to compute. Furthermore, suppose that we can write

$$\int_{\mathcal{X}} h(x) d\mu(x) = \int_{\mathcal{X}} f(x) d\mathbf{P}(x) = \mathbf{P}(f)$$

for a probability measure \mathbf{P} and function $f : \mathcal{X} \rightarrow \mathbf{R}$, e.g. because $\mathbf{P} = p\mu$ and $h(x) = f(x)p(x)$ μ -a.s. . Let \mathbf{G} be another measure on \mathcal{X} such that $f\mathbf{P}$ is absolutely continuous with respect to \mathbf{G} , $f\mathbf{P} \ll \mathbf{G}$, and let $v = \frac{d\mathbf{P}}{d\mathbf{G}}$ be the corresponding Radon-Nikodym derivative. Then

$$\zeta = \int_{\mathcal{X}} h(x) dx = \int_{\mathcal{X}} f(x) d\mathbf{P}(x) = \int_{\mathcal{X}} v(x) d\mathbf{G}(x)$$

which suggests to estimate ζ by Monte-Carlo integration:

$$\hat{\zeta} = \frac{1}{N} \sum_{i=1}^N v(X^i)$$

for $X^i \stackrel{\text{i.i.d.}}{\sim} \mathbf{G}$, $i = 1, \dots, N$. Here we call $\hat{\zeta}$ the importance sampling estimate of ζ .

The Monte-Carlo variance of $\hat{\zeta}$ is $\frac{\text{Var}(v(X^i))}{N}$, and so naturally we want $\text{Var}(v(X^i))$ to be small to ensure fast convergence of $\hat{\zeta}$. As v depends on the proposal \mathbf{G} , and we have the flexibility to choose \mathbf{G} , importance sampling acts as a variance reduction technique. A classical result is that the minimum MSE proposal \mathbf{G}^* has a closed form, which can be shown by a simple application of Jensen's inequality.

Proposition 3.1 ([22, Proposition 8.2]). *[minimum MSE proposal] The proposal \mathbf{G}^* that minimizes the MSE of importance sampling is given by*

$$\mathbf{G}^* = \frac{|f|}{\mathbf{P}(|f|)} \mathbf{P}.$$

Unfortunately, this optimality result has no practical use, indeed if f is positive we would need to obtain $\mathbf{P}(f)$ first, the overall target of our endeavor. Additionally, sampling from \mathbf{G}^* is not guaranteed to be practically feasible.

If one is not interested in a particular function f , we may instead think of

$$\hat{\mathbf{P}}_N = \frac{1}{N} \sum_{i=1}^N v(X_i) \delta_{X_i} \quad (3.5)$$

as a particle approximation of \mathbf{P} , in the sense that for sufficiently well behaved test functions f , $\mathbf{P}(f) \approx \hat{\mathbf{P}}_N(f)$. In this setting [3] shows that the random measure $\hat{\mathbf{P}}_N$ converges to \mathbf{P} at usual rate $\mathcal{O}\left(\frac{1}{\sqrt{N}}\right)$ in an appropriate metric on the space of random probability measures.

To perform importance sampling one must be able to evaluate the weights v . In a Bayesian setting, this is usually infeasible: if \mathbf{P} is a posterior distribution then the integration constant of its density is intractable. In this case, one can usually evaluate the weights up to a constant, i.e. $w(x) \propto_x \frac{d\mathbf{P}}{d\mathbf{G}}(x)$ is

available. The missing constant is then $\int w(x) d\mathbf{G}$ which is itself amenable to importance sampling. This leads to the self-normalized importance sampling weights $W_i = \frac{w(X_i)}{\sum_{i=1}^N w(X_i)}$ and Monte Carlo estimates $\hat{\zeta} = \sum_{i=1}^N W_i f(X_i)$ and particle approximation $\hat{\mathbf{P}}_N = \sum_{i=1}^N W_i \delta_{X_i}$.

In both cases, one can show that once the second moment of w w.r.t. \mathbf{G}

$$\rho = \int w^2 d\mathbf{G} = \int w d\mathbf{P},$$

exists the Monte-Carlo estimates are consistent and asymptotically normal at the usual rates, see [22, Chapter 8]. However, the finite sample variance of $\hat{\zeta}$, and thus the practical performance of the procedure, depends on the variance of $w \cdot f$ under \mathbf{G} , and thus on the proposal \mathbf{G} . [3] show that the supremum over bounded test function of the expected bias and variance of $\hat{\mathbf{P}}_N$ may be bounded, up to a constant, by the second moments of w . Thus, for bounded functions, ρ provides an upper bound on the speed of convergence of importance sampling. In addition, they provide bounds that involve the KL-divergence

$$\mathcal{D}_{\text{KL}}(\mathbf{P}||\mathbf{G}) = \int \log \frac{d\mathbf{P}}{d\mathbf{G}} d\mathbf{P} \leq \log \rho$$

fostering the intuition that \mathbf{G} should be close to \mathbf{P} for the particle approximation $\hat{\mathbf{P}}_N$ to be close to \mathbf{P} .

[21] provides the following theorem (using our notation), that relates the performance of importance sampling to both the Kullback Leibler divergence (KL-divergence) and the tail behavior of the log weights.

Theorem 3.1 ([21, Theorem 1.1]). *If $N = \exp(\mathcal{D}_{\text{KL}}(\mathbf{P}||\mathbf{G}) + t)$ for $t \geq 0$, and $f \in L^2(\mathbf{P})$ then*

$$\mathbf{G} |\mathbf{P}_N f - \mathbf{P} f| \leq \|f\|_2 + 2 \sqrt{\mathbf{P} \left(\log w > \mathcal{D}_{\text{KL}}(\mathbf{P}||\mathbf{G}) + \frac{t}{2} \right)}.$$

really \mathbf{P} in the log weights?

[21, Theorem 1.2] provides a similar result for autonormalised importance sampling.

To judge whether importance sampling has converged, several criteria are discussed in the literature. The classic effective sample size (ESS)[52]

$$\text{ESS} = \frac{1}{\sum_{i=1}^N W_i^2}$$

arises from an analysis of the asymptotic efficiency of importance sampling estimates and is easy to interpret. Assessing convergence through the variance of $\hat{\mathbf{P}}_N$ is, while natural, flawed [21] and should be avoided. As a remedy [21] suggest the heuristic $q_N = \mathbf{E}Q_N$ where

$$Q_N = \max_{1 \leq i \leq N} W_i.$$

This judges whether importance sampling has collapsed to just a few particles and is itself amenable to Monte-Carlo integration.

In the following sections, we will predominantly take the position that we are interested in finding a good particle approximation $\hat{\mathbf{P}}_N$ of the form Equation (3.5) over finding the optimal proposal \mathbf{G}^* Proposition 3.1 and assume that the importance sampling weights can only be evaluated up to a constant.

more clearly distinguish arguments for the two assumptions

This has several reasons: First of all, most problems considered in this thesis exist in a Bayesian context where \mathbf{P} is usually a posterior distribution, i.e. $\mathbf{P} = \mathbf{P}^{X|Y=y}$ for some random variables X

and Y . Should the appropriate densities exist, evaluating the weights amounts to calculating

$$\frac{d\mathbf{P}^{X|Y=y}}{d\mathbf{G}}(x) = \frac{p(x|y)}{g(x)} = \frac{p(y|x)p(x)}{g(x)p(y)} \propto \frac{p(y|x)p(x)}{g(x)}.$$

In these situations $p(y) = \int p(x, y) d\mu(x)$ is usually intractable. For \mathbf{G}^* we are in the same situation, where the evaluation of the integration constant $\mathbf{P}|f|$ is infeasible, but the density $f(x)p(x)$ is available. Second, focusing on the particle approximation allows us to consider multiple test functions f , e.g. focus on different marginals of \mathbf{P} . Finally, this allows us to simplify the notation used in this thesis. \mathbf{P} will always be the probability measure of interest and \mathbf{G} the proposal. In later parts of this thesis, we will predominantly perform Gaussian importance sampling, i.e. $\mathbf{G} = \mathcal{N}(\mu, \Sigma)$, hence a handy mnemonic is to think of \mathbf{G} as a **G**aussian proposal.

3.4.1 Laplace approximation (LA)

The Laplace approximation (LA) goes back to Laplace [55] who invented the technique to approximate moments of otherwise intractable distributions. Since [83, 84] rediscovered its use to approximate posterior means and variances, it has been a staple method for approximate inference. The method is based on a second-order Taylor series expansion of the log target density $\log p(x)$ around its mode \hat{x} , i.e. matching mode and curvature. Assuming the density is sufficiently smooth, we have

$$\log p(x) \approx \log p(\hat{x}) + \underbrace{\nabla_x \log p(\hat{x})}_{=0} (x - \hat{x}) + \frac{1}{2} (x - \hat{x})^T H (x - \hat{x}) \quad (3.6)$$

where H is the Hessian of $\log p$ evaluated at \hat{x} . As $\log p(\hat{x})$ does not depend on x , the right-hand side can be seen (up to additive constants) as the density of a Gaussian distribution with mean \hat{x} and covariance matrix $\Sigma = -H^{-1}$. Thus using $\mathbf{G} = \mathcal{N}(\hat{x}, -H^{-1})$ as a proposal in importance sampling seems promising. If \hat{x} is the unique global mode of p , H is negative definite and the LA yields an actual Gaussian distribution. To obtain the LA in practice, a Newton-Raphson scheme may be used, which conveniently tracks H as well.

The main advantage of the LA is that it is usually fast to obtain and, for sufficiently well-behaved distributions on a moderate dimensional space, provides reasonably high ESS. Additionally, the Newton-Raphson iterations to find the mode and Hessian are robust and require no simulation, unlike the other methods discussed further below. For the SSMs we consider in this thesis, the numerical methods can be implemented using the Kalman filter and smoother [28, 80], even in the degenerate case where H is indefinite [46], see also Section 3.5.1.

more theoretical background on LA?

However, as the LA is a local approximation, it may be an inappropriate description of the global behavior of the target, see Example 3.1 for a breakdown of LA and the simulation studies presented in Section 3.8. Additionally, even if LA works in principle, its ESS will usually degenerate quickly once the dimension increases whereas the cross-entropy method (CE-method) and efficient importance sampling (EIS) do so at a slower pace.

3.4.2 The Cross-entropy method (CE-method)

To provide a global approximation to the target, the CE-method [72, 73] selects from a family $(\mathbf{G}_\psi)_{\psi \in \Psi}$ of proposals the one that minimizes the KL-divergence to the target. Thus, the CE-method finds ψ_{CE} which solves the following optimization problem

$$\begin{aligned} \psi_{\text{CE}} &= \operatorname{argmin}_{\psi \in \Psi} \mathcal{D}_{\text{KL}}(\mathbf{P} || \mathbf{G}_\psi) \\ &= \operatorname{argmin}_{\psi \in \Psi} \int \log \frac{d\mathbf{P}}{d\mathbf{G}_\psi} d\mathbf{P}. \end{aligned}$$

If \mathbf{P} and \mathbf{G}_ψ possess densities p and g_ψ w.r.t. some common measure μ , the same for all ψ , we may reformulate the optimization problem to maximize the cross-entropy between p and g_ψ instead:

$$\begin{aligned}\psi_{\text{CE}} &= \operatorname{argmin}_{\psi \in \Psi} \int p(x) \log p(x) \, d\mu(x) - \int p(x) \log g_\psi \, d\mu(x) \\ &= \operatorname{argmax}_{\psi \in \Psi} \int p(x) \log g_\psi(x) \, d\mu(x),\end{aligned}\quad (3.7)$$

Note that the first integral does not depend on ψ . The assumption of such a dominating measure is not restrictive: otherwise the KL-divergence is infinite.

An attractive property of the CE-method is that if \mathbf{G}_ψ form an exponential family with natural parameter $\psi \in \mathbf{R}^p$, the optimal ψ_{CE} only depends on certain moments of \mathbf{P} . Indeed, for $\log g_\psi(x) = \log h(x) - \log Z(\psi) + \psi^T T(x)$ we have

$$\int p(x) \log g_\psi(x) \, d\mu(x) = \mathbf{P} \log h - \log Z(\psi) + \psi^T \mathbf{P} T.$$

As $\log Z(\psi)$ is the cumulant-generating function of \mathbf{G}_ψ it is smooth. Thus the optimal ψ_{CE} solves

$$\mathbf{P} T = \nabla_\psi \log Z(\psi_{\text{CE}}) = \mathbf{G}_{\psi_{\text{CE}}} T,$$

and the task at hand reduces to matching the moments of the sufficient statistic of the target and proposal. In many cases, this system of equations can be solved analytically or by gradient descent algorithms.

While $\mathbf{P} T$ is usually not available, it is itself amenable to importance sampling. Given a proposal \mathbf{G} we may estimate $\mathbf{P} T$ by $\hat{\mathbf{P}}_N T = \sum_{i=1}^N W^i T(X^i)$ for $X^1, \dots, X^N \stackrel{\text{i.i.d.}}{\sim} \mathbf{G}$ and auto-normalized importance sampling weights W^i and in turn estimate ψ_{CE} by $\hat{\psi}_{\text{CE}}$ solving

$$\hat{\mathbf{P}}_N T = \mathbf{G}_{\hat{\psi}_{\text{CE}}} T.$$

Thus $\hat{\psi}_{\text{CE}}$ is a Z-estimator, i.e. an estimator that arises from solving a random system of equations, and we can analyze its asymptotic behavior using standard results from the theory of Z-estimators. The following theorem of [87] will be useful in analyzing the asymptotic behavior of the estimators we consider in this thesis. We state it here, using our notation, for completeness.

Theorem 3.2 (asymptotic variance of Z-estimators, [87, Theorem 5.21]). *For every ψ in an open subset of \mathbf{R}^k , let $x \mapsto f_\psi(x)$ be a measurable vector-valued function such that, for every ψ_1 and ψ_2 in a neighborhood of ψ_0 and a measurable function \dot{f} with $\mathbf{G} \dot{f} < \infty$,*

$$\|f_{\psi_1}(x) - f_{\psi_2}(x)\| \leq \dot{f}(x) \|\psi_1 - \psi_2\|. \quad (\text{LL})$$

Assume that $\mathbf{G} \|f_{\psi_0}\| < \infty$ and that the map $\psi \mapsto \mathbf{G} f_\psi$ is differentiable at ψ_0 , with nonsingular derivative matrix B^{-1} . Let $X_1, \dots, X_N \stackrel{\text{i.i.d.}}{\sim} \mathbf{G}$ and $\hat{\mathbf{G}}_N = \sum_{i=1}^N \delta_{X_i}$. If $\hat{\psi}_N$ fulfills $\hat{\mathbf{G}}_N f_{\hat{\psi}_N} = o_P(N^{-\frac{1}{2}})$, and $\hat{\psi}_N \rightarrow \psi_0$ in probability, then

$$\sqrt{N} (\hat{\psi}_N - \psi_0) \xrightarrow{\mathcal{D}} \mathcal{N}(0, B M B^T), \quad (3.8)$$

where $M = \mathbf{G} f_{\psi_0} f_{\psi_0}^T$.

Notation 3.2 (central limit theorem for Z-estimators). The central limit theorems derived in this and the next section will make frequent use of Theorem 3.2. We will use the following consistent notation in the statement of theorems and their proofs:

- $f_\psi(x) : \mathbf{R}^k \rightarrow \mathbf{R}^k$ the estimating equation
- $B = (\mathbf{G} \partial_\psi f_\psi)^{-1}$ the bread matrix
- $M = \mathbf{G} f_\psi f_\psi^T$ the meat matrix

- $V = BMB$ the asymptotic covariance matrix
- $\log g_\psi(x) = \psi^T T(x) + \log h(x) - \log Z(\psi)$ the density of the natural exponential family considered
- $\dot{z}(\psi) = \nabla_\psi \log Z(\psi) = \mathbf{G}_\psi T$ the derivative of the log-normalizing constant $\psi \mapsto \log Z(\psi)$
- $\ddot{z}(\psi) = \partial_\psi \dot{z}(\psi) = \text{Cov}_{\mathbf{G}_\psi} T$ the Hessian of the log-normalizing constant $\psi \mapsto \log Z(\psi)$

The naming of B and M stems from the sandwich estimator [88], where the bread B is the Jacobian of the estimating equations $\mathbf{P}f_\psi = 0$ and the meat M is the covariance matrix of f_ψ under \mathbf{P} , thus making a „meat sandwich“.

Theorem 3.3 (consistency of $\hat{\psi}_{CE}$). from van der Vaart/Casella Berger

Theorem 3.4 (asymptotic normality of $\hat{\psi}_{CE}$). *Let \mathbf{G}_ψ form a natural exponential family with densities $g_\psi(x) = \frac{h(x)}{Z(\psi)} \exp(\psi^T T(x))$ w.r.t. μ . Let \mathbf{G}, \mathbf{P} be two other probability measures such that $\mathbf{G} \ll \mathbf{P}$ and let $W = \frac{d\mathbf{P}}{d\mathbf{G}}$ be the normalized importance sampling weights. Suppose further that*

- (A1) $\mathbf{G}_{\hat{\psi}_{CE}} T = \hat{\mathbf{P}}_N T$ μ -a.s. has a unique solution $\hat{\psi}_{CE}$,
- (A2) $\psi \mapsto \nabla_\psi \log Z(\psi)$ is locally Lipschitz around ψ_{CE} ,
- (A3) W, T and WT possess finite second moments w.r.t. \mathbf{G} ,
- (A4) the Fisher information $I(\psi_{CE})$ is positive definite and equal to $-\ddot{z}(\psi_{CE})$, additionally $\psi \mapsto I(\psi)$ is continuous, and
- (A5) the regularity conditions of Theorem 3.3 hold.

Then, as N goes to ∞ ,

$$\sqrt{N} \left(\hat{\psi}_{CE} - \psi_{CE} \right) \xrightarrow{\mathcal{D}} \mathcal{N}(0, V_{CE})$$

where

$$V_{CE} = B_{CE} M_{CE} B_{CE},$$

with

$$\begin{aligned} B_{CE} &= I(\psi_{CE})^{-1}, \\ M_{CE} &= \text{Cov}_{\mathbf{G}}(W(T - \mathbf{G}_{\psi_{CE}} T)). \end{aligned}$$

Moreover $\mathbf{G}(W(T - \mathbf{G}_{\psi_{CE}} T)) = 0$, so we may estimate V_{CE} consistently by plug-in:

$$\hat{V}_{CE} = I(\hat{\psi}_{CE})^{-1} \left(\sum_{i=1}^N W_i^2 \left(T(X^i) - \mathbf{G}_{\hat{\psi}_{CE}} T \right) \left(T(X^i) - \mathbf{G}_{\hat{\psi}_{CE}} T \right)^T \right) I(\hat{\psi}_{CE})^{-1}.$$

Proof. We check that the conditions of the central limit theorem for Z-estimators (Theorem 3.2) are fulfilled. This proof uses the notation established in Notation 3.2. Consider the estimating equations for ψ_{CE}

$$x \mapsto f_\psi(x) = \nabla_\psi (w(x) \log g_\psi(x)) = w(x)T(x) - w(x)\dot{z}(\psi),$$

where $w(x)$ are the unnormalized importance sampling weights. By (A1) $\hat{\mathbf{P}}_N f_{\hat{\psi}_{CE}} = 0$ μ -a.s., so it remains to show that $\hat{\psi}_{CE} \rightarrow \psi_{CE}$ in probability, which is implied by Theorem 3.3.

As

$$\|f_{\psi_1}(x) - f_{\psi_2}(x)\| = w(x) \|\dot{z}(\psi_1) - \dot{z}(\psi_2)\|$$

for all $\psi_1, \psi_2 \in \Psi$, $\mathbf{G}w < \infty$ and (A2) imply the local Lipschitz condition Equation (LL) in Theorem 3.2. Furthermore, by (A3) it holds

$$\mathbf{G} \|f_\psi\|^2 \leq \mathbf{G} w^2 \|\dot{z}(\psi)\|^2 + 2 \|\dot{z}(\psi)\| \mathbf{G} \|wT\| + \mathbf{G} \|wT\|^2 < \infty.$$

Additionally $\psi \mapsto \mathbf{G}f_\psi = (\mathbf{G}w)\dot{z}(\psi) + \mathbf{G}wT$ is differentiable everywhere, with Jacobian $(\mathbf{G}w)\dot{z}(\psi)$, where $\dot{z}(\psi) = \partial_\psi \dot{z}(\psi)$ is the Hessian of the cumulant generating function, which equals the negative Fisher information $-I(\psi_{\text{CE}})$ as $\mathbf{G}_\psi, \psi \in \Psi$ form a natural exponential family and the regularity conditions (A5) allow differentiation under the integral. Thus we see that

$$\mathbf{G}f_{\psi_{\text{CE}}} = \mathbf{P}(\dot{z}(\psi_{\text{CE}}) + T) = \dot{z}(\psi_{\text{CE}}) + \mathbf{P}T = 0,$$

by definition of ψ_{CE} , so

$$\text{Cov}_{\mathbf{G}}(w(T - \nabla_{\psi_{\text{CE}}} \log Z(\psi_{\text{CE}}))) = \text{Cov}_{\mathbf{G}}(f_{\psi_{\text{CE}}}) = \mathbf{G}f_{\psi_{\text{CE}}}f_{\psi_{\text{CE}}}^T.$$

As $W = \frac{w}{\mathbf{G}w}$ By Equation (3.8) the asymptotic covariance matrix is

$$V_{\text{CE}} = B_{\text{CE}}M_{\text{CE}}B_{\text{ce}}$$

which shows the asymptotic normality.

Estimating B_{CE} by $\hat{B}_{\text{CE}} = I(\hat{\psi}_{\text{CE}})$ and

$$M_{\text{CE}} = \mathbf{G}W^2(T - \mathbf{G}_{\psi_{\text{CE}}}T)(T - \mathbf{G}_{\psi_{\text{CE}}}T)^T = \mathbf{P}W(T - \mathbf{G}_{\psi_{\text{CE}}})(T - \mathbf{G}_{\psi_{\text{CE}}})^T$$

by

$$\hat{M}_{\text{CE}} = \hat{\mathbf{P}}_N W \left(T - \mathbf{G}_{\hat{\psi}_{\text{CE}}}T \right) \left(T - \mathbf{G}_{\hat{\psi}_{\text{CE}}}T \right)^T$$

yields the stated plug-in estimator. The promised consistency follows from (A3) and (A4). \square

The form of the asymptotic covariance matrix is that of the sandwich estimator [88], corrected for the importance sampling with \mathbf{G} . This is not surprising: the CE-method performs maximum likelihood estimation where the data come from the misspecified \mathbf{P} . Additionally, we have to correct the variance for performing importance sampling with \mathbf{G} , instead of sampling directly from \mathbf{P} .

If $\mathbf{G}_\psi, \psi \in \Psi$ do not form an exponential family, $\hat{\psi}_{\text{CE}}$ will still be consistent and asymptotically normal, provided the usual regularity conditions for M-estimators apply.

The CE-method is routinely used for estimating failure probabilities for rare events [41] and has been applied to Bayesian inference [30, 31] and optimal control problems [48, 90].

more lit. review CEM

3.4.3 Efficient importance sampling (EIS)

EIS[67] provides an alternative to the CE-method. Instead of minimizing the KL-divergence between the target \mathbf{P} and \mathbf{G}_ψ , EIS aims at minimizing the variance of the logarithm of importance sampling weights. The work by [21] [21], Theorem 3.1, suggests that this is worthwhile: the upper bound in their Theorems 1.1 and 1.2 involve tail probabilities of the distribution of log weights, which suggests minimizing their variance as well as the mean.

Thus, EIS finds ψ_{EIS} which solves

$$\begin{aligned} \psi_{\text{EIS}} &= \operatorname{argmin}_{\psi \in \Psi} \operatorname{Var}_{\mathbf{P}}(\log w_\psi) \\ &= \operatorname{argmin}_{\psi \in \Psi} \mathbf{P}(\log w_\psi - \mathbf{P} \log w_\psi)^2, \end{aligned}$$

where $\log w_\psi = \log p - \log g_\psi$. As $\mathbf{P} \log w_\psi$ is usually intractable as well, we include it in the optimization problem, utilizing the fact that the mean is the minimizer of the squared distance functional. Here unnormalized weights $w \propto \frac{d\mathbf{P}}{d\mathbf{G}}$ may be used, as the unknown integration constant gets absorbed by the unknown mean. In total, EIS solves

$$(\psi_{\text{EIS}}, \lambda_{\text{EIS}}) = \operatorname{argmin}_{\psi \in \Psi, \lambda \in \mathbf{R}} \mathbf{P}(\log p - \log g_\psi - \lambda)^2.$$

Under the usual regularity conditions allowing to differentiate under the integral, the estimating equations for ψ_{EIS} read

$$\begin{aligned}\mathbf{P}((\log p - \log g_\psi - \lambda) \nabla_\psi \log g_\psi) &= 0 \\ \mathbf{P}(\log p - \log g_\psi - \lambda) &= 0,\end{aligned}\tag{3.9}$$

which we will use to derive asymptotics for $\hat{\psi}_{\text{EIS}}$.

Similar to the CE-method we restrict our in-depth analysis to natural exponential family proposals where $\log g_\psi(x) = \psi^T T(x) - \log Z(\psi) + \log h(x)$. In this case Equation (3.9) simplifies to

$$\begin{aligned}\mathbf{P}((\log p - \psi^T T + \log Z(\psi) - \log h - \lambda)(T - \mathbf{G}_\psi T)) &= 0, \\ \lambda &= \mathbf{P}(\log p - \log g_\psi) = \mathcal{D}_{\text{KL}}(\mathbf{P} \parallel \mathbf{G}_\psi).\end{aligned}$$

As the first term is centered under \mathbf{P} , this is equivalent to $\log w_\psi$ and T being orthogonal in $L^2(\mathbf{P})$. Unfortunately, this formulation does not allow for an analytical solution of ψ_{EIS} , the problematic term being $\log Z(\psi)$, leading to an implicit equation for ψ . However, we can achieve an explicit equation by reparameterizing the nuisance parameter to $\lambda' = \lambda - \log Z(\psi)$, which results in a weighted linear least squares problem

$$\min_{\psi \in \Psi, \lambda' \in \mathbf{R}} \mathbf{P}(\log p - \log h - \psi^T T - \lambda')^2.$$

Thus the optimal $(\psi_{\text{EIS}}, \lambda'_{\text{EIS}})$ are given by the best linear prediction of $\log p - \log h$ by the sufficient statistic T under \mathbf{P} . Therefore, if $\text{Cov}_{\mathbf{P}} T$ is non-singular,

$$\begin{aligned}\lambda'_{\text{EIS}} &= \mathbf{P} \log p - \log h \\ \psi_{\text{EIS}} &= \text{Cov}_{\mathbf{P}}(T)^{-1} \text{Cov}_{\mathbf{P}}(T, \log p - \log h).\end{aligned}\tag{3.10}$$

Notice that ψ_{EIS} depends on second-order moments of the sufficient statistic T , as well as the shape of $\log p$, whereas the optimal parameter for the CE-method ψ_{CE} depends only on the first-order moments of T .

As the optimal ψ_{EIS} depends on several unknown quantities, EIS proceeds like the CE-method and employs importance sampling with a proposal \mathbf{G} , estimating ψ_{EIS} by

$$(\hat{\lambda}, \hat{\psi}_{\text{EIS}}) = \underset{\lambda, \psi}{\text{argmin}} \sum_{i=1}^N W^i (\log p(X^i) - \log g_\psi(X^i) - \lambda)^2,$$

where $X^1, \dots, X^N \stackrel{\text{i.i.d.}}{\sim} \mathbf{G}$. If $\mathbf{G}_\psi, \psi \in \Psi$ form an exponential family with natural parameter ψ , this optimization problem turns into a weighted least squares problem, so we can estimate ψ_{EIS} with the standard weighted least squares estimator

$$(\hat{\lambda}', \hat{\psi}_{\text{EIS}}) = (\mathbf{X}^T W \mathbf{X})^{-1} \mathbf{X}^T W y$$

where the random design matrix \mathbf{X} and diagonal weights matrix W are given by

$$\mathbf{X} = \begin{pmatrix} 1 & T(X^1)^T \\ \dots & \dots \\ 1 & T(X^N)^T \end{pmatrix}$$

and

$$W = \text{diag}(W_1, \dots, W_N),$$

and the observations are

$$y = (\log p(X^1) - \log h(X^1), \dots, \log p(X^N) - \log h(X^N))^T \in \mathbf{R}^N.$$

Alternatively, replacing \mathbf{P} by $\hat{\mathbf{P}}_N$ in Equation (3.10), we obtain the equivalent formulation

$$\hat{\psi}_{\text{EIS}} = \text{Cov}_{\hat{\mathbf{P}}_N}(T)^{-1} \text{Cov}_{\hat{\mathbf{P}}_N}(T, \log p - \log h), \quad (3.11)$$

as long as $\text{Cov}_{\hat{\mathbf{P}}_N} T$ is non-singular.

An attractive feature of EIS is that if the target \mathbf{P} is a member of the exponential family of proposals, i.e. there is a $\psi_{\mathbf{P}} \in \Psi$ such that $\mathbf{P} = \mathbf{G}_{\psi_{\mathbf{P}}}$, then EIS finds the optimal $\psi_{\text{EIS}} = \psi_{\mathbf{P}}$ a.s. for a finite number of samples.

Proposition 3.2 (Finite sample convergence of EIS). *Suppose $\mathbf{G}_{\psi}, \psi \in \Psi \subseteq \mathbf{R}^k$ for a natural exponential family w.r.t. Lebesgue measure, where both Ψ and the support of the sufficient statistic $\text{supp } T$ are open in \mathbf{R}^k . Furthermore let \mathbf{G} be a probability measure on \mathbf{R}^m that is equivalent to \mathbf{P} , i.e. $\mathbf{G} \ll \mathbf{P}$ and $\mathbf{P} \ll \mathbf{G}$.*

If there is a $\psi_{\mathbf{P}} \in \Psi$ such that $\mathbf{P} = \mathbf{G}_{\psi_{\mathbf{P}}}$, then $\hat{\psi}_{\text{EIS}} = \psi_{\mathbf{P}}$ a.s. for $N \geq k$.

Proof. As \mathbf{P} stems from the same exponential family as \mathbf{G}_{ψ} , the pseudo-observations are $\log p - \log h = \psi_{\mathbf{P}}^T T - \log Z(\psi_{\mathbf{P}})$. Thus $\text{Cov}_{\hat{\mathbf{P}}_N}(T, \log p - \log h) = \text{Cov}_{\hat{\mathbf{P}}_N}(T) \psi_{\mathbf{P}}$. If we can show that $\text{Cov}_{\hat{\mathbf{P}}_N} T$ is non-singular, Equation (3.11) implies that $\hat{\psi}_{\text{EIS}} = \psi_{\mathbf{P}}$ a.s..

If $\text{Cov}_{\hat{\mathbf{P}}_N} T$ were singular, there would exist a $\psi \in \Psi$ such that $\text{Cov}_{\hat{\mathbf{P}}_N}(\psi^T T) = 0$, as Ψ is open and contains 0. In this case the a.s. non-zero $W^i(X^i)T(X^i)$ would lie in the orthogonal complement ψ^\perp for all $i = 1, \dots, N$. As the weights are a.s. positive by the assumed equivalence of \mathbf{G} and \mathbf{P} , the same holds true for $T(X^i), i = 1, \dots, N$. If N is bigger than k , this is a contradiction to $\text{supp } T$ being open, so $\text{Cov}_{\hat{\mathbf{P}}_N} T$ is non-singular and the result is shown. \square

Theorem 3.5 (consistency of $\hat{\psi}_{\text{EIS}}$). *vdV, reg. conditions?*

Theorem 3.6 (asymptotic normality of $\hat{\psi}_{\text{EIS}}$). *Let \mathbf{G}_{ψ} form a natural exponential family with densities $g_{\psi}(x) = \frac{h(x)}{Z(\psi)} \exp(\psi^T T(x))$ w.r.t. μ . Let \mathbf{G}, \mathbf{P} be two other probability measures such that $\mathbf{G} \ll \mathbf{P}$ and let $W = \frac{d\mathbf{P}}{d\mathbf{G}}$ be the normalized importance sampling weights. Assume $\lambda(\psi) = \mathbf{P} \log w_{\psi}$ is known and the following conditions hold:*

(B1) $\mathcal{D}_{\text{KL}}(\mathbf{P} \parallel \mathbf{G}_{\psi}) < \infty$ for all ψ

prob. suffices locally

(B2) T and $\log w_{\psi_{\text{EIS}}}$ are square integrable w.r.t. \mathbf{P} ,

(B3) $\text{Cov}_{\mathbf{P}}(T)$ is positive definite and

(B4) the regularity conditions of Theorem 3.5 hold.

Without loss of generality, assume that $\mathbf{P}T = 0$. Then, as N goes to ∞ ,

$$\sqrt{N} \left(\begin{pmatrix} \hat{\lambda} \\ \hat{\psi}_{\text{EIS}} \end{pmatrix} - \begin{pmatrix} \lambda \\ \psi_{\text{EIS}} \end{pmatrix} \right) \xrightarrow{\mathcal{D}} \mathcal{N}(0, V_{\text{EIS}})$$

where

$$V_{\text{EIS}} = B_{\text{EIS}} M_{\text{EIS}} B_{\text{EIS}}$$

with

$$B_{\text{EIS}} = \begin{pmatrix} 1 & 0 \\ 0 & (\text{Cov}_{\mathbf{P}} T)^{-1} \end{pmatrix}$$

$$M_{\text{EIS}} = \mathbf{G} \left(W^2 \left(\log \frac{p}{h} - \psi_{\text{EIS}}^T T - \lambda_{\text{EIS}} \right)^2 \begin{pmatrix} 1 & T^T \\ T & TT^T \end{pmatrix} \right).$$

In particular, the asymptotic variance of $\hat{\psi}_{\text{EIS}}$ is

$$(\text{Cov}_{\mathbf{P}}T)^{-1} \mathbf{G} \left(W^2 \left(\log \frac{p}{h} - \psi_{\text{EIS}}^T T - \lambda_{\text{EIS}} \right)^2 T T^T \right) (\text{Cov}_{\mathbf{P}}T)^{-1}.$$

Proof. This proof follows the same strategy as that for Theorem 3.4 and uses the same notation (Notation 3.2). The estimating equations for λ and ψ_{EIS} are given by

$$x \mapsto f_{\lambda, \psi}(x) = \nabla_{\lambda} - \frac{1}{2} w(x) \left(\log \frac{p(x)}{h(x)} - \psi^T T(x) - \lambda \right)^2 = w(x) \left(\log \frac{p(x)}{h(x)} - \psi^T T(x) - \lambda \right) \begin{pmatrix} 1 \\ T(x) \end{pmatrix}.$$

For $\lambda_1, \lambda_2 \in \mathbf{R}$ and $\psi_1, \psi_2 \in \Psi$ the Lipschitz condition Equation (LL) are fulfilled, as

$$\begin{aligned} \|f_{\lambda_1, \psi_1} - f_{\lambda_2, \psi_2}\| &= |w(x)| |(\lambda_2 - \lambda_1 + T(x)(\psi_2 - \psi_1))| \left\| \begin{pmatrix} 1 \\ T(x) \end{pmatrix} \right\| \\ &\leq |w(x)| \underbrace{\left\| \begin{pmatrix} 1 & T^T(x) \\ T(x) & T(x)T^T(x) \end{pmatrix} \right\|}_{:=\dot{f}} \|(\lambda_2 - \lambda_1, \psi_2 - \psi_1)\|, \end{aligned}$$

and $\mathbf{G}\dot{f} < \infty$ by (B2).

At the optimal $\lambda_{\text{EIS}}, \psi_{\text{EIS}}$ it holds

$$\mathbf{G}f_{\lambda_{\text{EIS}}, \psi_{\text{EIS}}} = \mathbf{P} \left(\log \frac{p}{h} - \psi_{\text{EIS}}^T T - \lambda_{\text{EIS}} \right) \begin{pmatrix} 1 \\ T \end{pmatrix} < \infty,$$

as both T and $\log w(\psi_{\text{EIS}})$ are in $L^2(\mathbf{P})$ by (B2).

L2 definieren

By the assumed regularity conditions, $(\lambda, \psi) \mapsto \mathbf{G}f_{\lambda, \psi}$ is differentiable, with Jacobian

$$\begin{aligned} B_{\text{EIS}}^{-1} &= \partial_{\lambda, \psi} \mathbf{G}f_{\lambda, \psi} = \mathbf{P} \begin{pmatrix} 1 \\ T \end{pmatrix} \begin{pmatrix} 1 & T^T \end{pmatrix} \\ &= \mathbf{P} \left(\begin{pmatrix} 1 & T^T \\ T & T T^T \end{pmatrix} \right) = \begin{pmatrix} 1 & 0 \\ 0 & \text{Cov}_{\mathbf{P}}(T) \end{pmatrix}, \end{aligned}$$

as $\mathbf{P}T = 0$.

As $\hat{\psi}_{\text{EIS}}$ solves the estimating equations, we have $\hat{\mathbf{P}}_N f_{\hat{\psi}_{\text{EIS}}} = 0 = o_P(N^{-\frac{1}{2}})$. It remains to show that $\hat{\psi}_{\text{EIS}} \rightarrow \psi_{\text{EIS}}$ in probability, which follows by an application of Theorem 3.3. Finally, as $\mathbf{G}f_{\lambda_{\text{EIS}}, \psi_{\text{EIS}}} = 0$,

$$M_{\text{EIS}} = \mathbf{G} \left(f_{\lambda_{\text{EIS}}, \psi_{\text{EIS}}} f_{\lambda_{\text{EIS}}, \psi_{\text{EIS}}}^T = \mathbf{G} w^2 \left(\log \frac{p(x)}{h(x)} - \psi_{\text{EIS}}^T T - \lambda_{\text{EIS}} \right)^2 \begin{pmatrix} 1 & T^T \\ T & T T^T \end{pmatrix} \right)$$

□

discuss applicability of both CLTs

literature review EIS

3.5 Gaussian importance sampling for state space models

For the types of models considered in this thesis, importance sampling is used to infer the posterior distribution. Given a state space model of the form (3.1) and observations $Y = Y_{:n}$, let \mathbf{P} be the distribution of the states $X = X_{:n}$, conditional on Y and f be a function of interest. The task at hand is now to find a suitable proposal \mathbf{G} , using the methods presented in the last section. If n is

large, the posterior distribution lives in a high dimensional state of dimension $m \cdot n$, so to obtain \mathbf{G} efficiently, we should exploit the available structure. Additionally, we want \mathbf{G} to be tractable, so simulating from it is possible and evaluating the weights w up to a constant is possible.

The multivariate Gaussian distribution is a good candidate in this setting, as simulating from it is straightforward and its density can be evaluated analytically. However, naively performing the optimal importance sampling methods from the previous section for all multivariate Gaussians is computationally inefficient as the family of distributions has $\mathcal{O}((n \cdot m)^2)$ many parameters. We can, however, exploit the available structure of the SSM to find parameterizations with fewer parameters by either using smoothing distributions of GLSSMs (Section 3.5.1) or approximating with a Gaussian discrete-time Markov process (Section 3.5.2).

Using Gaussian proposals, while computationally efficient, also comes with some drawbacks. The whole procedure hinges on the assumption that there is a Gaussian that is, close to the target distribution. In the setting of SSMs this is not guaranteed, as the targets may contain multiple modes or heavy tails, features that may, in the worst case, lead to inconsistent importance sampling estimates. Additionally, even if there is a Gaussian distribution that facilitates consistent importance sampling, finding it in practice may be complicated, as the proposals generated by the LA, CE-method and EIS have deteriorating performance for fixed sample size N (in terms of ESS and convergence) with increasing dimension, see Section 3.8.5.

small lit. review

3.5.1 The GLSSM-approach

The first approach is motivated by the fact that the target posterior is again a Markov process, as are posteriors in GLSSMs. Additionally, the posterior distribution in GLSSMs is again Gaussian, and straightforward to simulate from by, e.g., the FFBS algorithm (Algorithm 3) or the simulation smoother [29]. Thus parameterizing the proposals \mathbf{G} by the posterior of a suitably chosen GLSSM may be a fruitful approach. For the models we consider in this thesis, the distribution of states is already Gaussian and the observations are conditionally independent given the states. Thus a natural GLSSM to use as a proposal consists of keeping the prior distribution of states and replacing the distribution of observations with conditionally independent Gaussian distributions and the actual observations by synthetic ones. By the assumed conditional independence, this model only needs $2p \cdot (n + 1)$ many parameters, $p \cdot (n + 1)$ for the synthetic observations and $p \cdot (n + 1)$ for their variances. We term this approach the **GLSSM-approach** to importance sampling.

In total, the GLSSM-approach considers parametric proposals \mathbf{G}_ψ of the form

$$\begin{aligned} \mathbf{G}_\psi &= \mathcal{L}(X|Z = z), \\ Z_t &= B_t X_t + \eta_t, \\ \eta_t &\sim \mathcal{N}(0, \Omega_t), \\ \Omega_t &= \text{diag}(\omega_t^2) = \text{diag}(\omega_{t,1}^2, \dots, \omega_{t,p}^2). \end{aligned} \tag{3.12}$$

where the distribution of X is given by (3.3), $\psi = (z, \omega^2)$ for $z = (z_0, \dots, z_n) \in \mathbf{R}^{n \times m}$ and $\omega^2 = (\omega_0^2, \dots, \omega_n^2) \in \mathbf{R}^{n \times m}$. Alternatively the natural parametrization $\psi = (z \oslash \omega^2, -1 \oslash (2\omega^2))$ may also be used, where \oslash is the Hadamard, i.e. entry-wise, division. Simulation from \mathbf{G}_ψ may be efficiently implemented by the FFBS algorithm, as \mathbf{G}_ψ is the smoothing distribution of a GLSSM.

In this setting, the importance sampling weights are given by

$$w(x) = \frac{p(x|y)}{g(x|z)} = \frac{p(y|x)p(x)g(z)}{g(z|x)p(x)p(y)} \propto \prod_{t=0}^n \frac{p(y_t|x_t)}{g(z_t|x_t)},$$

so they can be computed efficiently. Additionally, for a LCSSM with linear signals, $p(y_t|x_t)$ and $g(z_t|x_t)$ depend on x_t only through the signal $s_t = B_t x_t$, and we have

$$w(x) \propto \prod_{t=0}^n \frac{p(y_t|s_t)}{g(z_t|s_t)}, \tag{3.13}$$

which implies that auto-normalized weights may be calculated by using the signal smoother [46, Theorem 2]. As Durbin and Koopman [27, Section 4.5.3] argue, it is often computationally more efficient to treat only on the signals $(S_t)_{t=0,\dots,n}$ instead of the states $(X_t)_{t=0,\dots,n}$, the idea being that the dimension of S_t , p , is usually much smaller than that of X_t , m .

As the joint distribution of (X, S) is a Gaussian distribution, by Lemma 3.1 $X|S = s$ is again Gaussian, with known conditional mean and covariance matrix and density $p(x|s) = g(x|s)$. If $(\tilde{X}_t)_{t=0,\dots,n}$ is a draw from this conditional distribution a quick calculation reveals that a.s. $B_t \tilde{X}_t = S_t$, and so, as expected, the weights $w(\tilde{X}_t)$ are a.s. constant and given by (up to the integration constant) Equation (3.13). Producing a draw from this conditional distribution can be achieved by the FFBS algorithm (Algorithm 3), as (X, S) form a GLSSM with degenerate observation covariance matrices $\Omega_t = 0$.

By the assumed conditional independence of observations given signals, we have

$$p(x, s|y) \propto p(x|s)p(s|y),$$

and so if one is interested in the states, rather than the signals, importance sampling with the proposal Equation (3.12) can be achieved in a two-step procedure: first sample from $g(s|z)$, then run the FFBS algorithm to sample from $g(x|s) = p(x|s)$ using the same weights for MC-integration.

The GLSSM-approach is the standard approach for finding the LA in LCSSM [27, 28] and may even be applied when the observation densities are not log-concave[46]. The approach also leads to efficient implementation for EIS [53]. However, as will become apparent in the later part of this section, it is infeasible for the CE-method if n is large.

We now give a concise overview over how to perform the LA and EIS for LCSSM, but refer the reader for more details to the respective literature. The LA

elaborate on LA / EIS, Durbin Koopman book, EIS, MEIS, NEIS papers

Algorithm 4 The LA for LCSSM

Algorithm 5 EIS for LCSSM

For the CE-method, using the GLSSM-approach turns out to be difficult numerically. For a high-level argument of why this is true, let us ignore the Markov structure of the model for the moment. As the CE-method matches moments of the target and proposal, applying it to fit model (3.12) amounts to matching the moments of \mathbf{G}_ψ to those of the target posterior $\mathcal{L}(X|Y = y)$ in the SSM. Unfortunately, the covariance of \mathbf{G}_ψ is given by $(\Sigma^{-1} + B^T \Omega^{-1} B)^{-1}$, where Σ is the covariance of all states, $B = \text{block-diag}(B_0, \dots, B_n)$ and $\Omega = \text{block-diag}(\Omega_0, \dots, \Omega_n)$. Choosing the diagonal matrix Ω such that the covariance of \mathbf{G}_ψ matches this expression is numerically expensive: we either need to invert the large (dimension $(n+1)m \times (n+1)m$) covariance matrix, or solve numerically for the $(n+1)p$ parameters. The problem at hand is that we cannot decouple this into $(n+1)$ equations of dimension p as we did for EIS, because all entries of $(\Sigma^{-1} + B^T \Omega^{-1} B)^{-1}$ depend on all entries of Ω .

To make matters more concrete, the CE-method finds $\psi = (z, \omega^2)$ such that model (3.12) maximizes the cross entropy with the target $\mathbf{P}^{X|Y=y}$. For simplicity, let us assume that $m = p$, B is the identity and we only observe a single y . Using Lemma 3.1, we see that when $X \sim \mathcal{N}(\mu, \Sigma)$, the conditional distribution of X given $Z = z$, \mathbf{G}_ψ , is a Gaussian distribution with mean $\tilde{\mu} = \mu + \Sigma(\Sigma + \Omega)^{-1}(z - \mu)$ and covariance matrix $\tilde{\Sigma} = (\Sigma^{-1} + \Omega^{-1})^{-1}$ for $\Omega = \text{diag}(\omega^2)$, where $\omega^2 > 0$. Assuming that Σ is

non-singular, we can reparameterize the objective function of the CE-method by $\tilde{\mu}$,

$$\begin{aligned} \max_{z, \omega^2} \int p(x|y) \log g_\psi(x|z) dx &= \max_{\tilde{\mu}, \omega^2} \int p(x|y) \left(-\frac{1}{2} (x - \tilde{\mu})^T \tilde{\Sigma}^{-1} (x - \tilde{\mu}) - \frac{1}{2} \log \det \tilde{\Sigma} \right) dx \\ &= \max_{\tilde{\mu}, \omega^2} -\frac{1}{2} (\gamma - \tilde{\mu})^T \tilde{\Sigma}^{-1} (\gamma - \tilde{\mu}) - \frac{1}{2} \text{trace} \left(\tilde{\Sigma}^{-1} \Gamma \right) - \frac{1}{2} \log \det \tilde{\Sigma}, \end{aligned} \quad (3.14)$$

where $\gamma = \mathbf{E}(X|Y = y)$ and $\Gamma = \text{Cov}(X|Y = y)$. Thus the optimal $\tilde{\mu}$ is γ and to find the optimal ω^2 we have to minimize

$$\text{trace} \left((\Sigma^{-1} + \Omega^{-1}) \Gamma \right) - \log \det (\Sigma^{-1} + \Omega^{-1}).$$

Taking the derivative w.r.t. $\frac{1}{\omega^2}$, we see that

$$\Gamma_{i,i} = \left(\left(\Sigma^{-1} + \text{diag} \left(\frac{1}{\omega_1}, \dots, \frac{1}{\omega_p} \right) \right)^{-1} \right)_{i,i} = \left(\Sigma - \Sigma (\Sigma + \Omega)^{-1} \Sigma \right)_{i,i} \quad (3.15)$$

has to hold for all $i = 1, \dots, (p \times (n+1))$, i.e. we have to choose ω^2 such that the posterior marginal variances $\Gamma_{i,i}$ coincide with the marginal variances of \mathbf{G}_ψ .

Several problems arise: First of all, Equation (3.15) is not guaranteed to have a solution. For the i -th unit-vector $e_i \in \mathbf{R}^p$ we can reformulate Equation (3.15) to

$$\Sigma_{i,i} - \Gamma_{i,i} = e_i^T \Sigma^T (\Sigma + \Omega)^{-1} \Sigma e_i > 0$$

and so we require $\Gamma_{i,i} < \Sigma_{i,i}$. While the law of total covariance asserts that

$$\Sigma = \underbrace{\mathbf{E} \text{Cov}(X|Y)}_{=\Gamma} + \text{Cov}(\mathbf{E}(X|Y)),$$

it does not guarantee $\Gamma \prec \Sigma$, which would imply $\Gamma_{i,i} < \Sigma_{i,i}$.

Second, even if there is an analytical solution Ω to Equation (3.15), in the CE-method we replace $\Gamma_{i,i}$ by the observed marginal variances $\hat{\Gamma}_{i,i}$ obtained by importance sampling. The variation introduced by simulation can then lead to situations where $\hat{\Gamma}_{i,i} > \Sigma_{i,i}$. As an example take $X \sim \mathcal{N}(0, 1)$, and $Y = X + \eta$ for $\eta \sim \mathcal{N}(0, \omega^2)$. Then the conditional variance of X given $Y = y$ is $\Gamma = 1 - \frac{1}{1+\omega^2}$. Given N i.i.d. samples X^1, \dots, X^N from this distribution, their empirical variance $\hat{\Gamma} = \frac{1}{N} \sum_{i=1}^N (X^i - \bar{X})^2$ follows a scaled χ_{N-1}^2 distribution, i.e. $\frac{N\hat{\Gamma}}{\Gamma} \sim \chi_{N-1}^2$. Notice that we use the non-Bessel corrected version of the empirical variance here, as it is the maximum-likelihood estimate.

Then

$$\mathbf{P} \left(\hat{\Gamma} > 1 \right) = \mathbf{P} \left(\frac{N\hat{\Gamma}}{\Gamma} > \frac{N}{\Gamma} \right) = 1 - F_{\chi_{N-1}^2} \left(N \left(1 + \frac{1}{\omega^2} \right) \right)$$

is the probability that Equation (3.15) has no solution $\omega^2 \in \mathbf{R}_{\geq 0}$. Here $F_{\chi_{N-1}^2}$ is the cumulative distribution function of the χ_{N-1}^2 distribution. As ω^2 goes to ∞ , this probability approaches $1 - F_{\chi_{N-1}^2}(N)$ which, for large N , is approximately $1 - F_{\chi_{N-1}^2}(N-1) \approx \frac{1}{2}$, as $\chi_{N-1}^2 \approx \mathcal{N}(N-1, 2(N-1))$ [45, Section 18.5]. We illustrate this in Figure 3.1, displaying the probability of failure in this setting for various combinations of N and ω^2 . In this figure, we see that with growing N the threshold for ω^2 leading to non-negligible failure probability becomes larger, as expected. Thus, even in the very simple univariate Gaussian setting, for every N there is an ω^2 such that the CE-method fails for Equation (3.12) with practically relevant probability.

In higher-dimensional settings, e.g. when applying the CE-method to SSMs, we can expect this phenomenon to occur even more often. In the extreme case of independent marginals, i.e. when Σ is a diagonal matrix, Equation (3.15) reduces to $(n+1)p$ many decoupled equations, where $\hat{\Gamma}_{i,i}, i = 1, \dots, (n+1)p$ are independent. If all $q_i = \mathbf{P}(\Gamma_{i,i} > \Sigma_{i,i})$ are identical to $q \in (0, 1)$, e.g.

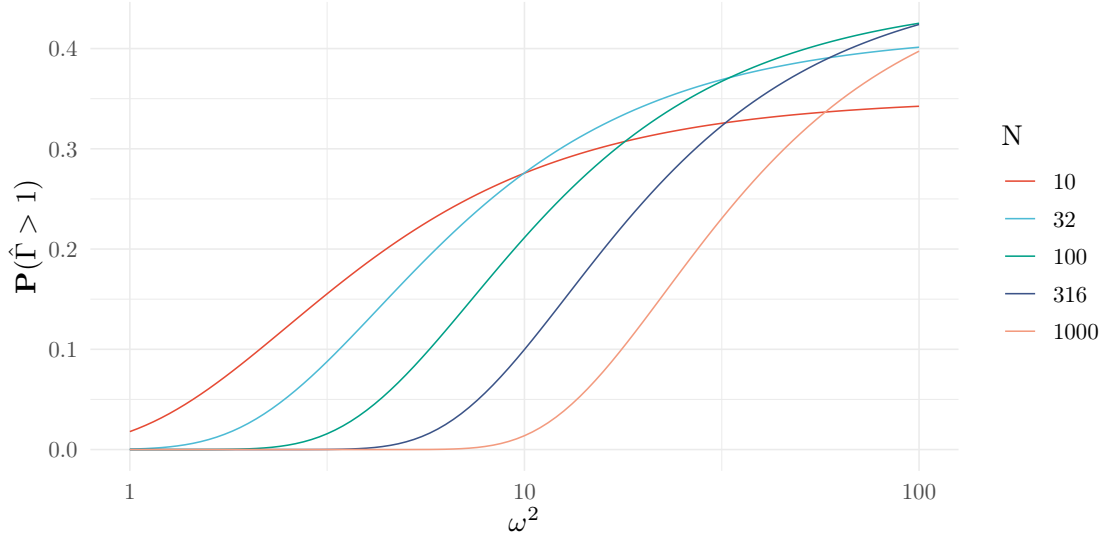


Figure 3.1: We show the probability that the estimated posterior variance $\hat{\Gamma}$ is bigger than the prior variance 1 when varying the noise variance ω^2 . **todo: ausführlicher beschreiben**

because Σ and Ω are multiples of the identity, the number of failures follows a Binom $((n+1)p, q)$ distribution, so that even small q may lead to a non-negligible number of failures if the number of observations is high.

Finally, in the multivariate setting, the system (3.15) has no analytical solution. Instead, we have to resort to numerical methods to find a solution Ω . Unfortunately, even evaluating the right-hand side of (3.15) requires $\mathcal{O}(m^3)$ operations, as we have to invert $\Sigma + \Omega$. Additionally, we cannot hope to reuse a singular-value, LR, or eigenvalue-decomposition for further evaluations, as Σ and Ω are not guaranteed to be jointly diagonalizable. In the SSM context we may use the Kalman-smoother to compute the marginal variances, but have to re-run the smoother for every evaluation.

If we admit noise variance ∞ in our optimization, then $\Gamma > 1$ implies that the CE-method chooses this as the estimate, i.e. $\mathbf{G}_{\hat{\psi}_{\text{CE}}}$ is $\mathcal{N}(0, 1)$, which is equal to the prior. We can interpret this as having a missing observation, which, going back to the SSM context, the Kalman-filter (Algorithm 1) can handle with only simple modifications, see e.g. [27, Section 4.10]. However, if there are a lot of failures, the optimally chosen $\mathbf{G}_{\hat{\psi}_{\text{CE}}}$ will still be close to the prior distribution of states X , and importance sampling is unlikely to be effective. Hence, we turn to another approach that allows us to apply the CE-method to SSMs.

3.5.2 The Markov-approach

An alternative family of Gaussian proposals is given by directly modeling a Gaussian Markov process on the states X_n . Again, this is sensible given the Markov structure of the target. This parametrization is more flexible than using the posterior of a GLSSM with fixed prior as the proposal. This flexibility, however, comes at the cost of requiring a larger number of parameters.

Here we propose with \mathbf{G}_ψ where

$$\begin{aligned} \mathbf{G}_\psi &= \mathcal{L}(U + v), \\ v &\in \mathbf{R}^{(n+1)m}, \\ U_0 &\sim \mathcal{N}(0, R_0 R_0^T), \\ U_t &= C_t U_{t-1} + R_t \nu_t, \\ C_t &\in \mathbf{R}^{m \times m}, \\ \nu_t &\sim \mathcal{N}(0, I), \\ R_t &\in \mathbf{R}^{m \times m} \text{ lower triangular with positive diagonal} \end{aligned} \tag{3.16}$$

for $t = 1, \dots, n$, with U_0 and ν_1, \dots, ν_n independent. The number of parameters in

$$\psi = (v, C_1, \dots, C_n, R_0, \dots, R_n)$$

is $(n+1) \cdot m$ for the mean v , $n \cdot m^2$ for the transition matrices C_t and $(n+1) \frac{m(m-1)}{2}$ for the Cholesky roots of innovation covariances, totaling $\mathcal{O}(n \cdot m^2)$ many parameters. While these are considerably more parameters than for the GLSSM-approach for large state dimension m , we will see in the later part of this section that finding the optimal parameters for the CE-method can be done analytically.

This approach, which we term the **Markov-approach**, was originally proposed by Richard and Zhang in [67] for general unnormalized transition kernels as EIS proposals. However, because of its lower number of parameters, one should favor the GLSSM-approach for EIS that operates on the signals, see [53].

To perform importance sampling with \mathbf{G}_ψ in model (3.16) we not only need to simulate from \mathbf{G}_ψ but also evaluate the unnormalized importance sampling weights $w(x) = \frac{p(x|y)}{g_\psi(x)}$. Simulation from \mathbf{G}_ψ is achieved by a simple recursion. For the weights note that

$$w(x) \propto \frac{p(y|x)p(x)}{g_\psi(x)} = \prod_{t=0}^n \frac{p(y_t|x_t)p(x_t|x_{t-1})}{g_\psi(x_t|x_{t-1})}, \tag{3.17}$$

where $p(x_0|x_{-1}) = p(x_0)$ and $g_\psi(x_0|x_{-1}) = g_\psi(x_0)$.

The Markov structure of model (3.16) implies that the precision matrix of \mathbf{G}_ψ is sparse, i.e. it has a block-tridiagonal form. This is a well-known property of the precision matrix of Gaussian random vectors, as the following two classical lemmas show. We show their proofs here for completeness. For a general treatment, we refer the reader to [56, Chapters 3 and 5].

Lemma 3.3. *Let (X, Y) be jointly Gaussian with distribution $\mathcal{N}(\mu, \Sigma)$ where*

$$\mu = (\mu_X, \mu_Y)$$

and

$$\Sigma = \begin{pmatrix} \Sigma_{XX} & \Sigma_{XY} \\ \Sigma_{YX} & \Sigma_{YY} \end{pmatrix},$$

are partitioned according to the dimensions of X and Y and Σ is non-singular. If

$$P = \Sigma^{-1} = \begin{pmatrix} \Sigma_{XX} & \Sigma_{XY} \\ \Sigma_{YX} & \Sigma_{YY} \end{pmatrix}^{-1} = \begin{pmatrix} P_{XX} & P_{XY} \\ P_{YX} & P_{YY} \end{pmatrix}$$

is the precision matrix of (X, Y) , partitioned as is Σ , then $\text{Cov}(X|Y) = P_{XX}^{-1}$.

Proof. Without loss of generality, assume that both X and Y are centered. The conditional density $p(x|y)$ is proportional (in x) to the joint density $p(x, y)$ with

$$\log p(x, y) = -\frac{1}{2} \begin{pmatrix} x & y \end{pmatrix} P \begin{pmatrix} x \\ y \end{pmatrix} + C = -\frac{1}{2} (x^T P_{XX} x + 2x^T P_{XY} y) + C',$$

for constants C, C' that do not depend on x . As the conditional distribution of X given $Y = y$ is Gaussian (by Lemma 3.1), its covariance matrix is P_{XX}^{-1} . \square

Lemma 3.4. *Let $(X, Y, Z) \sim \mathcal{N}(\mu, \Sigma)$ be jointly Gaussian with non-singular Σ . Then $X \perp Y|Z$ if, and only if, the sub-matrix of the precision matrix $P = \Sigma^{-1}$ whose rows correspond to the entries of X and columns correspond to the entries of Y is the 0 matrix.*

Proof. Partition the conditional covariance matrix into

$$\text{Cov}((X, Y)|Z) = \begin{pmatrix} \Sigma_{XX|Z} & \Sigma_{XY|Z} \\ \Sigma_{YX|Z} & \Sigma_{YY|Z} \end{pmatrix}.$$

Now as all distributions involved are Gaussian, $X \perp Y|Z$ is equivalent to $\text{Cov}((X, Y)|Z)$ being a block-diagonal matrix with blocks $\Sigma_{XX|Z}$ and $\Sigma_{YY|Z}$, which is equivalent to its inverse being a block-diagonal matrix with blocks $\Sigma_{XX|Z}^{-1}$ and $\Sigma_{YY|Z}^{-1}$. Its inverse is, by Lemma 3.3, the sub-matrix of P whose rows and columns correspond to X and Y . \square

Applying Lemma 3.4 to model (3.16), we see that its precision matrix P is sparse, i.e. it is a block-tri-diagonal matrix, as $U_t \perp U_s|U_{-t,-s}$ for $|t - s| > 1$ and $U_{-t,-s}$ being the vector of all U_0, \dots, U_n except for U_t, U_s . Thus, the only entries of P that are potentially non-zero are those whose row and column correspond to (U_t, U_t) for $t = 0, \dots, n$, (U_t, U_{t-1}) and (U_{t-1}, U_t) for $t = 1, \dots, n$.

The sparsity of P implies that $P = LL^T$ has a sparse Cholesky root L , which will make computations efficient. To see that L is sparse, we apply the following Theorem, slightly adapted to our notation, from the theory of Gaussian-Markov-Random-fields (GMRF), i.e. Gaussian models whose dependency structure is given by a graph, with edges between nodes indicating non-zero entries in the precision matrix.

Theorem 3.7 ([36, Theorem 12.14]). *Let $X = (X_0, \dots, X_n) \in \mathbf{R}^{(n+1)m}$ be a GMRF wrt to the labeled graph G , with mean μ and symmetric positive-definite precision matrix P . Let L be the Cholesky factor of P and define for $0 \leq t < s \leq n$ the future of t except s as*

$$F(t, s) = \{t + 1, \dots, s - 1, s + 1, n\}.$$

Then

$$X_t \perp X_s | X_{F(t,s)} \Leftrightarrow L_{t,s} = 0.$$

In the preceding theorem $X_{F(t,s)}$ is the vector of all X_u for $u \in F(t, s)$ and $L_{t,s} \in \mathbf{R}^{m \times m}$ is the sub-matrix of L whose rows correspond to X_t and columns to X_s . From Theorem 3.7 we immediately obtain the following:

Corollary 3.1 (sparsity of L in model (3.16)). *Let $U \sim \mathbf{G}_\psi$ as in Equation (3.16), $P \succ 0$ be the precision matrix of $\overleftarrow{U} = (U_n, \dots, U_0)$ and L be the Cholesky root of P . Then L is a lower-block-diagonal matrix, with at most $nm^2 + (n + 1)m^{\frac{m-1}{2}}$ non-zero entries:*

$$L = \begin{pmatrix} L_{n,n} & 0 & \cdots & \cdots & \cdots & 0 & 0 \\ L_{n-1,n} & L_{n-1,n-1} & 0 & \cdots & \cdots & 0 & 0 \\ 0 & L_{n-2,n-1} & L_{n-2,n-2} & 0 & \cdots & 0 & 0 \\ \vdots & \ddots & \ddots & \ddots & \ddots & 0 & 0 \\ 0 & 0 & 0 & \cdots & L_{1,2} & L_{1,1} & 0 \\ 0 & 0 & 0 & \cdots & 0 & L_{0,1} & L_{0,0} \end{pmatrix}, \quad (3.18)$$

where $L_{t,t} \in \mathbf{R}^{m \times m}$, $t = 0, \dots, n$ are lower triangular matrices with positive diagonal entries and $L_{t-1,t} \in \mathbf{R}^{m \times m}$, $t = 1, \dots, n$ are square matrices.

From L in Corollary 3.1 we obtain an iterative method of sampling from \mathbf{G}_ψ : If $v + U \sim \mathbf{G}_\psi$, then, as $\text{Cov}U = (LL^T)^{-1} = L^{-T}L^{-1}$, it holds that $L^T U \sim \mathcal{N}(0, I)$ follows a standard normal distribution. Thus to simulate from \mathbf{G}_ψ we may solve

$$L^T U = \overleftarrow{Z}$$

where $\overleftarrow{Z} = (Z_n, \dots, Z_0) \sim \mathcal{N}(0, I)$. Using the structure available in L , we see that this is equivalent to first solving

$$L_{0,0}^T U_0 = Z_0$$

and then recursively solving for $t = 1, \dots, n$

$$L_{t,t}^T U_t + L_{t-1,t}^T U_{t-1} = Z_{t-1}.$$

Rearranging terms, provided $L_{t,t}$ is non-singular, we end up with the Markov-process

$$U_t = L_{t,t}^{-T} L_{t-1,t}^T U_{t-1} + L_{t,t}^{-T} Z_t, \quad (3.19)$$

where Z_t is, by construction, independent of U_t . Thus for model (3.16), we obtain

$$\begin{aligned} R_t &= L_{t,t}^{-T} \text{ for } t = 0, \dots, n, \\ C_t &= L_{t,t}^{-T} L_{t-1,t}^T \text{ for } t = 1, \dots, n. \end{aligned} \quad (3.20)$$

Here we see why we chose to use \overleftarrow{U} in Corollary 3.1: had we applied Theorem 3.7 to U directly yields a Markov process in reverse time.

We now turn our attention to applying the CE-method to model (3.16). Following a similar argument as in the discussion surrounding Equation (3.14), we see that it suffices to choose P , the precision matrix of U , such that it minimizes

$$\frac{1}{2} \text{trace} \left(P \hat{\Gamma} \right) - \frac{1}{2} \log \det P \quad (3.21)$$

where $\hat{\Gamma}$ is the importance sampling estimate of the joint covariance matrix of all states X . This is equivalent to minimizing

$$\mathcal{D}_{\text{KL}} \left(\mathcal{N}(0, \hat{\Gamma}) \middle| \middle| \mathcal{N}(0, P^{-1}) \right).$$

Here P is restricted to precision matrices that may arise in model (3.16), i.e., by Corollary 3.1, $P = LL^T$ where L possess structure as in (3.18). At first glance, this problem seems more involved than solving Equation (3.15): after all, the optimal P depends on the whole covariance matrix $\hat{\Gamma}$. However, it turns out that the sparsity we enforce in L allows us to compute analytically the optimal \hat{L} that minimizes Equation (3.21). Additionally, due to the Markov-structure of our proposal, \hat{L} depends only on the block-tri-diagonal component of $\hat{\Gamma}$, i.e. only the covariances $\text{Cov}(X_t, X_{t-1})$ and $\text{Cov}(X_0)$ are required. This is sensible - all information about the Markov transitions is encoded in these covariances if we assume that X is a Gaussian Markov process.

To make this argument rigorous, let us apply the following result (stated in our notation).

Theorem 3.8 ([76, Theorem 2.1]). *Let Γ be a positive-definite matrix of size $n \times n$. Given a lower-triangular sparsity set $S \subset \{1, \dots, n\}^2$, i.e. $i \geq j$ for all $(i, j) \in S$, let*

$$\hat{L} = \underset{L \in \mathcal{S}}{\text{argmin}} \mathcal{D}_{\text{KL}} \left(\mathcal{N}(0, \Gamma) \middle| \middle| \mathcal{N}(0, (LL^T)^{-1}) \right)$$

be the Cholesky root of the closest Gaussian (wrt. the KL-divergence) with sparsity $\mathcal{S} = \{A \in \mathbf{R}^{n \times n} : A_{i,j} \neq 0 \Rightarrow (i, j) \in S\}$.

Then the following holds: The nonzero entries of the i -th column of \hat{L} are given by

$$L_{s_i, i} = \frac{\Gamma_{s_i, s_i}^{-1} e_1}{\sqrt{e_1^T \Gamma_{s_i, s_i}^{-1} e_1}}, \quad (3.22)$$

where $s_i = \{j : (i, j) \in S\}$, Γ_{s_i, s_i} is the restriction of Γ to the set of indices s_i and $e_1 \in \mathbf{R}^{|s_i|}$ is the first unit vector.

For the problem at hand, the sparsity pattern \mathcal{S} is given by the non-zero entries of L depicted in Equation (3.18) and the matrices Γ_{s_i, s_t} are sub-matrices of the covariances $\text{Cov}((X_{t-1}, X_t) | Y)$, for $t = 1, \dots, n$ and $\text{Cov}(X_0 | Y)$, i.e. we let $\Gamma = \text{Cov}(\bar{X} | Y)$ in Theorem 3.8.

Let $l_t^j \in \mathbf{R}^{2m \times m}$ be the j -th column of

$$\begin{pmatrix} L_{t,t} \\ L_{t-1,t} \end{pmatrix},$$

where $j \in \{1, \dots, m\}$. As $L_{t,t}$ is lower triangular, the first $j - 1$ entries of l_t^j are 0. We obtain the remaining nonzero entries by computing

$$\frac{\Gamma_{t,j}^{-1} e_j}{\sqrt{e_j^T \Gamma_{t,j}^{-1} e_j}},$$

for $\Gamma_{t,j} \in \mathbf{R}^{(2m-(j-1)) \times (2m-(j-1))}$ the joint covariance matrix of the last $m - (j - 1)$ components of X_t and all entries of X_{t-1} , conditional on $Y = y$, and $e_j \in \mathbf{R}^{2m-(j-1)}$ the first unit vector.

Putting everything together, we may apply the CE-method to estimate ψ in model (3.16) in the following way: Given importance samples U^1, \dots, U^N for $\mathcal{L}(X | Y = y)$ and associated unnormalized weights w^1, \dots, w^N , we estimate v by

$$\hat{v} = \frac{\sum_{i=1}^N w^i X^i}{\sum_{i=1}^N w^i} \quad (3.23)$$

and the empirical covariance matrices

$$\widehat{\text{Cov}}(X_t, X_{t-1}) = \frac{\sum_{i=1}^N w^i (X_{t:t-1}^i - \hat{v}_{t-1:t})(X_{t:t-1}^i - \hat{v}_{t-1:t})^T}{\sum_{i=1}^N w^i} \quad (3.24)$$

$$\widehat{\text{Cov}}(X_0) = \frac{\sum_{i=1}^N w^i (X_0^i - \hat{v}_0)(X_0^i - \hat{v}_0)^T}{\sum_{i=1}^N w^i}. \quad (3.25)$$

We then determine \hat{L} from these covariance matrices using Theorem 3.8. These steps are summarized in Algorithm 6.

improve: order to $\mathcal{O}(m^3)$

We can implement this more efficiently: Given sequential covariances $\text{Cov}(X_t, X_{t-1})$, there exists a Markov process with these covariances (Cholesky roots give L_t and R_t). As the optimal MP only depends on these covariances, we can also minimize KL-divergence to this MP. The KL divergence is thus minimized for this MP. Calculation of L_t and R_t then only take $\mathcal{O}((2m)^3) = \mathcal{O}(m^3)$ instead of the $\mathcal{O}(m^3)$ procedure presented until now.

To run Algorithm 6 we require an initial value for $\hat{\psi}^0$. If a suitable $\hat{\psi}^0$ is not available, we can obtain one from the LA by sampling X^1, \dots, X^N from the LA and performing steps 5 to 9 from the loop. Alternatively, we could also directly base our initial value on the smoothing distribution of the GLSSM that the LA is based on. The Kalman smoother (Algorithm 2) provides us with the analytically available covariances $\text{Cov}(X_t, X_{t-1} | Z = z)$ and the marginal covariance $\text{Cov}(X_0 | Z = z)$ can be computed as well.

The convergence criteria in Algorithm 6 is similar to that used for EIS: we stop until the absolute or entry-wise relative difference of $\hat{\psi}^l$ and $\hat{\psi}^{l+1}$ is smaller than a predetermined threshold, or a fixed number of iterations has passed. For the matrices involved, we use the Frobenius norm and the Euclidean distance for the mean v .

In Line 3 we use the standard praxis of common random numbers (CRNs) to ensure numerical convergence. This is similar to EIS and the maximum likelihood estimates from Section 3.7.

Algorithm 6 The CE-method for the Markov proposal (3.16)

Require: LCSSM (Definition 3.4), observations Y , initial estimate $\hat{\psi}^0 = (v^0, C^0, R^0)$, sample size N

- 1: set $l = 0$
- 2: **repeat**
- 3: sample $U^1 + v^l, \dots, U^N + v^l \stackrel{\text{i.i.d.}}{\sim} \mathbf{G}_{\hat{\psi}^l}$ with fixed seed ▷ Equation (3.16)
- 4: determine unnormalized weights w^1, \dots, w^N ▷ Equation (3.17)
- 5: estimate \hat{v}^{l+1} ▷ Equation (3.23)
- 6: estimate $\widehat{\text{Cov}}(U_t, U_{t-1}), t = 1, \dots, n, \widehat{\text{Cov}}(U_0)$ ▷ Equation (3.24)
- 7: determine \hat{L}^{l+1} ▷ Theorem 3.8
- 8: determine C^{l+1} and R^{l+1} from \hat{L}^{l+1} ▷ Equation (3.20)
- 9: set $\hat{\psi}^{l+1} = (\hat{v}^{l+1}, C^{l+1}, R^{l+1})$
- 10: set $l = l + 1$
- 11: **until** $\hat{\psi}^l$ converged
- 12: **return** $\hat{\psi}_{\text{CE}} = \hat{\psi}^l$

step	time complexity	space complexity
simulation (Line 3)	$\mathcal{O}(N n m^2)$	$\mathcal{O}(N n m)$
weights (Line 4)	$\mathcal{O}(N n m^2)$	$\mathcal{O}(N)$
estimating v (Line 5)	$\mathcal{O}(N n m)$	$\mathcal{O}(n m)$
estimating covariances (Line 6)	$\mathcal{O}(N n m^2)$	$\mathcal{O}(n m)$
determining L (Line 7)	$\mathcal{O}(n m^4)$	$\mathcal{O}(n m^2)$
determining C and R (Line 8)	$\mathcal{O}(n m^3)$	$\mathcal{O}(n m^2)$

Table 3.1: Time and space complexities of individual steps in Algorithm 6.

We give an overview of the time and space complexities of each line in Algorithm 6 in Table 3.1. The total time complexity of single iteration of Algorithm 6 is $\mathcal{O}(N n m^2 + n m^4)$ and its space complexity is $\mathcal{O}(N n m + n m^2)$. Let us elaborate on the complexities of each step:

- Line 3 Generate N i.i.d. samples from model (3.16), where each simulation requires $\mathcal{O}(n)$ matrix-vector multiplications of dimension m .
- Line 4 To evaluate the weights, Equation (3.17), we have to evaluate for every sample $\mathcal{O}(n)$ -times the density of a m -variate Gaussian distribution, while this usually has time-complexity $\mathcal{O}(m^3)$, we have access to the Cholesky root R_t , so this step has only time-complexity $\mathcal{O}(m^2)$. In Equation (3.17) we also need to compute $p(y_t|x_t)$ and $p(x_t|x_{t-1})$. Assuming conditional independence of observations, $p(y_t|x_t) = \prod_{i=1}^m p(y_t^i|(B_t x_t)^i)$, evaluating the first term requires only $\mathcal{O}(m^2)$ operations. For the second term, if we allow pre-computation of the Cholesky roots of innovations off-line (in $\mathcal{O}(m^3)$ time), this step reduces to $\mathcal{O}(m^2)$ as well.
- Line 5 Calculating the weighted mean $\hat{v} \in \mathbf{R}^{(n+1)m}$, Equation (3.23), requires $\mathcal{O}(N n m)$ operations.
- Line 6 Calculating the weighted covariance matrices, Equation (3.24), requires $(n+1)$ times multiplying N many $m \times 1$ with $1 \times m$ vectors.
- Line 7 To determine $L_{t,t}$ and $L_{t-1,t}$ we have to solve m times the linear systems of equations given in Equation (3.22), where the dimension of the system is $2m, \dots, m+1$. This requires $\mathcal{O}(m^4)$ many operations, and we have to perform it for every one of the $n+1$ time points. The result is L with sparsity structure given by Equation (3.18), which has $\mathcal{O}(n m^2)$ many non-zero entries.
- Line 8 For each of the $\mathcal{O}(n)$ many C_t and R_t we have to invert a triangular matrix of dimension m .

An efficient implementation of Algorithm 6 can improve on some of the other steps involved. There is no need to calculate the C_t and R_t matrices explicitly, instead we can calculate $C_t U_{t-1}$ efficiently

by solving the linear system $L_{t,t}^T (C_t U_{t-1}) = L_{t-1,t}^T U_{t-1} t$ by back-substitution, as $L_{t,t}^T$ is an upper triangular matrix. Similarly, to compute $R_t Z_t$ we solve $L_{t,t}^T (R_t Z_t) = Z_t$ by back-substitution. However, the main bottleneck for the time-complexity of Algorithm 6 is determining L with time complexity $\mathcal{O}(nm^4)$, which we have not been able to improve upon.

If the main bottleneck for space lies in the $\mathcal{O}(Nnm)$ simulation part, we may reduce this by simulating twice from model (3.16) using CRNs, and only storing the samples for a single time step (dimension $\mathcal{O}(Nm)$) in each simulation. In the first pass, we only calculate the weights, and in the second pass, we calculate \hat{v} and the required covariance matrices. For this, we only need the $2N$ samples of dimension m from time t and $t+1$, i.e. $\mathcal{O}(Nm)$ space. This reduces the total space complexity to $\mathcal{O}(Nm + nm^2)$.

We demonstrate these improvements in Algorithm 7. Additionally, we calculate the weights on the log scale for numerical stability.

Algorithm 7 Time and space improved version of Algorithm 6. Instructions involving the free index i are to be performed for all $i = 1, \dots, N$ samples.

Require: LCSSM (Definition 3.4), observations Y , initial estimate $\hat{\psi}^0 = (v^0, L^0)$, sample size N

set $l = 0$

repeat

simulate $Z_0^1, \dots, Z_0^N \stackrel{\text{i.i.d.}}{\sim} \mathcal{N}(0, I)$

set $U_0^i = (L_{0,0}^l)^{-T} Z_0^i$ ▷ backsubstitution

set $X_0^i = v_0^l + U_0^i$

set $\log w^i = \log p(y_0 | X_0^i) + \log p(X_0^i) + \frac{1}{2} \|Z_0^i\|^2$ ▷ $\log g(X_0^i) = -\frac{1}{2} \|Z_0^i\|_2^2 + C$

store current RNG state

for $t \leftarrow 1, \dots, n$ **do**

simulate $Z_t^1, \dots, Z_t^N \stackrel{\text{i.i.d.}}{\sim} \mathcal{N}(0, I)$

set $U_t^i = (L_{t,t}^l)^{-T} (L_{t-1,t}^l)^T U_{t-1}^i + (L_{t,t}^l)^{-T} Z_t^i$ ▷ backsubstitution

set $X_t^i = v_t^l + U_t^i$

set $\log w^i = \log w^i + \log p(y_t | X_t^i) + \log p(X_t^i | X_{t-1}^i) + \frac{1}{2} \|Z_t^i\|^2$

end for

set $\log w^i = \log w^i - \max_{i=1, \dots, N} \log w^i$ ▷ ensure $\log w^i \leq 0$

set $w^i = \exp(\log w^i)$

set $W^i = \frac{w^i}{\sum_{i=1}^N w^i}$ ▷ auto-normalized weights

set $v_0^{l+1} = \sum_{i=1}^N W^i X_0^i$

restore RNG state

for $t \leftarrow 1, \dots, n$ **do**

simulate $Z_t^1, \dots, Z_t^N \stackrel{\text{i.i.d.}}{\sim} \mathcal{N}(0, I)$

set $U_t^i = (L_{t,t}^l)^{-T} (L_{t-1,t}^l)^T U_{t-1}^i + (L_{t,t}^l)^{-T} Z_t^i$ ▷ backsubstitution

set $X_t^i = v_t^l + U_t^i$

set $v_t^{l+1} = \sum_{i=1}^N W^i X_t^i$

set $\widehat{\text{Cov}}(X_{t-1}, X_t) = \sum_{i=1}^N W^i (X_{t-1:t}^i - v_{t-1:t}^l) (X_{t-1:t}^i - v_{t-1:t}^l)^T$

end for

determine \hat{L}^{l+1} ▷ Theorem 3.8

set $\hat{\psi}^{l+1} = (\hat{v}^{l+1}, \hat{L}^{l+1})$

set $l = l + 1$

until $\hat{\psi}^l$ converged

return $\hat{\psi}_{\text{CE}} = \hat{\psi}^l$

The advantage of Algorithms 6 and 7 over applying the CE-method to the GLSSM model (3.12) are multiple: First of all, as long as the involved covariance matrices are positive definite, the two algorithms produce valid proposals, i.e. they do not have the degeneracy problem we observed in Section 3.5.1. Additionally, determining the optimal parameters (v, C, R) or (v, L) is numerically stable, involving only inversion of small matrices. Compare this with solving Equation (3.15), where

we need to employ a numerical scheme to solve for the diagonal entries of Ω .

After having determined $\hat{\psi}_{\text{CE}}$ for model (3.16), generating N samples requires only $\mathcal{O}(Nnm^2)$ operations, whereas sampling from model (3.12) requires $\mathcal{O}(nm^3 + Nnm^2)$ operations, as we need an initial run of the Kalman filter. Unless $N < m$, this difference is negligible, and the case where $N < m$ is not really of interest, as we would expect importance sampling to require at least as many samples as there are dimensions, i.e. $N \gg m$.

However, the two algorithms presented in this section also come with some drawbacks, especially if the dimension m of states is large. This affects the algorithms in multiple ways: when m is large, computation of L becomes more time-intensive. Additionally, the dimension of the parameter ψ increases quadratically in m , so we expect convergence to be slower, requiring a larger sample size N to find the optimal $\hat{\psi}_{\text{CE}}$. For an empirical study in this direction, see Section 3.8.

To improve the speed of computation of both algorithms, L has to be computed faster.

3.6 Accounting for multimodality and heavy tails

3.7 Maximum likelihood estimation in SSMs

3.8 Comparison of Importance Sampling method

We now have three tools to produce Gaussian importance sampling proposals: the LA, the CE-method and EIS. Naturally, we want to choose the optimal tool for the problem at hand. In this section, we investigate under which circumstances which method is to be preferred over the others. To judge the performance of each method, we will discuss the following quality criteria:

- breakdown of methods,
- time and space complexity of the method,
- speed of stochastic convergence, as indicated by the asymptotic variance, for the CE-method and EIS,
- speed of numerical convergence, as indicated by the number of iterations until Algorithms 5 and 7 reach numerical convergence for fixed sample size N and precision ϵ , and
- performance of the optimal proposal, as measured by the efficiency factor, especially as n or m comes larger.

Let us elaborate on these criteria. With a breakdown of the methods, we mean settings in which either the numerical scheme diverges, produces parameters that lead to invalid proposals, i.e. negative variances, or where the proposals fail to produce consistent importance sampling estimates. Time and space complexity allow us to compare the methods theoretically, i.e. be independent of implementation details. The speed of stochastic convergence is relevant as well: The smaller the asymptotic variance, the smaller we can choose the sample size N and thus decrease computation time. Similarly, numerical convergence directly affects computation time.

reformulate this paragraph nicer

Finally, if one method has vastly better performance at the optimum, we might be willing to spend more time initially to save time later when we use the proposal to perform inference. Of special interest is the performance for long (large n) or fat (large m) time series, as the models we fit in Chapter 4 usually fall into one of these categories.

3.8.1 Breakdown of methods

Let us start with a classical example in which the LA fails to produce consistent importance sampling estimates.

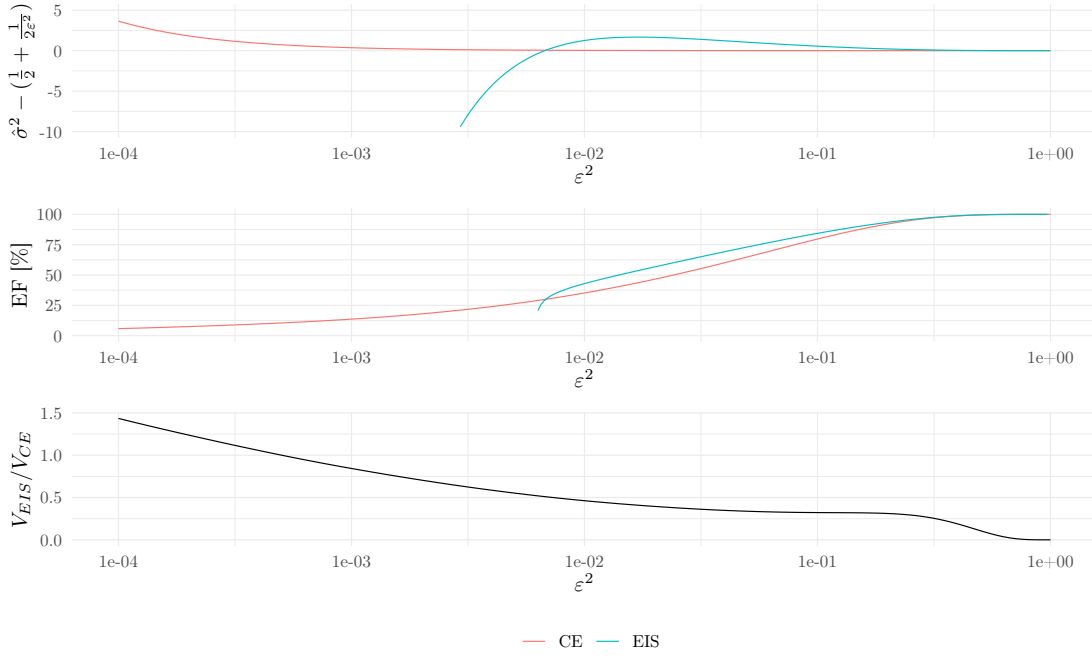


Figure 3.2: TODO

Example 3.1 (Failure of LA). Consider the Gaussian scale mixture $\mathbf{P} = \frac{1}{2} (\mathcal{N}(0, 1) + \mathcal{N}(0, \varepsilon^{-2}))$ with mode $x^* = 0$. The LA is $\mathbf{G}_{\text{LA}} = \mathcal{N}\left(0, \frac{1}{\varepsilon^2 - \varepsilon + 1}\right)$, whose variance goes to 1 as ε goes to 0, so the LA will miss close to $\frac{1}{2}$ of the total mass. For ε small enough, the variance of the LA will be smaller than $\frac{1}{2\varepsilon^2}$, whence the second moment of the weights is infinite and importance sampling with \mathbf{G}_{LA} is inconsistent.

The CE-method minimizes the KL-divergence between \mathbf{P} and \mathbf{G}_ψ , is given by $\mathbf{G}_{\text{CE}} = \mathcal{N}(0, \sigma^2)$, where $\sigma^2 = \frac{1}{2} (1 + \varepsilon^{-2})$ is the variance of \mathbf{P} . As $\sigma^2 > \frac{1}{2}\varepsilon^{-2}$, the weights have finite second moment, and importance sampling with \mathbf{G}_{CE} is consistent.

add proof for $\frac{1}{2}$ to appendix

As EIS does not yield analytically tractable proposals in this setting, we resort to a simulation study. Using the same setup as described in Example 3.2, we replicate $M = 100$ times $\hat{\psi}_{\text{CE}}$ and $\hat{\psi}_{\text{EIS}}$ for varying levels of ε^2 . The resulting excess variances, i.e. $\sigma^2 - \left(\frac{1}{2} + \frac{1}{2\varepsilon^2}\right)$, efficiency factors and asymptotic efficiencies are displayed in Figure 3.2. We see that for small ε^2 , EIS is inconsistent, while the CE-method stays consistent. However, as is to be expected, for small ε^2 , the efficiency factor becomes very small.

This is more of a technical counter-example, in practice the LA produces good importance sampling proposals, especially for LCSSMs.

In the LCSSM setting EIS may produce invalid proposals, as estimates of the variance component in the weighted least squares regression are not guaranteed to be negative. Thus EIS may produce negative variances. To deal with this, the original EIS paper [67, Section 3.2] recommends either inflating the prior or setting the parameters in question to arbitrary fixed values. Alternatively using a more expensive constrained linear least squares solver, such as a conjugate-gradient method [14] or the BVLS (bounded variable least squares) solver [82] may be appropriate, as is re-running the EIS procedure with a different random seed. Finally, in the LCSSM setting, we could also identify the corresponding observation as missing, similar to the argument presented in Section 3.5.1 for the CE-method.

method	single iteration (time)	single iteration (space)	simulation (time)
LA	$\mathcal{O}(np^3)$	$\mathcal{O}(np^2)$	$\mathcal{O}(n(p^3 + m^3 + N m^2))$
EIS	$\mathcal{O}(n(m^2 + p^3 + N p^2))$	$\mathcal{O}(N p + n(p^2 + m^2))$	$\mathcal{O}(n(p^3 + m^3 + N m^2))$
CE-method	$\mathcal{O}(n(N m^2 + m^4))$	$\mathcal{O}(N m + n m^2)$	$\mathcal{O}(N n m^2)$

Table 3.2: Computational complexities of importance sampling algorithms.

The CE-method presented in Section 3.5.2 (Algorithm 7) depends on the fact that the covariance matrix of the posterior $\text{Cov}(X|Y = y)$ is symmetric positive definite (SPD), i.e. non-singular. This might be violated if, e.g., the model contains seasonal components whose associated innovations have variance 0. In this case, the Cholesky roots involved will not be unique. Still Algorithm 7 will, as $N \rightarrow \infty$ converge a globally optimal solution, though it may not be unique.

3.8.2 Computational complexity

Throughout this section, we assume that the model in question is a LCSSM with linear signal (c.f. Definition 3.4) to simplify the treatment. This benefits the LA and EIS approaches, as they may then be implemented in terms of the simulation and signal smoother. If the observation dimension p is smaller than that of states m , this is more efficient and we'll assume this as well. An overview of computational complexities is given in Table 3.2. Note that most operations can be parallelized in one way or the other, e.g. sampling from the proposals, and so the time-complexities are not necessarily indicative of real-world-performance. Still they provide theoretical insight into the performance of the three methods considered.

Let us begin with a discussion of the computational complexity involved in finding the optimal parameters, ψ_{LA} , ψ_{EIS} and ψ_{CE} . Here we focus on a single iteration and treat the number of iterations empirically in Section 3.8.4.

As the LA is based on the Kalman-smoother, the time complexity of a single iteration is $\mathcal{O}(n(m^2 + p^3))$. The CE-method and EIS need to generate N samples from the current proposal. For the CE-method this amounts to $\mathcal{O}(N n m^2)$ operations (see Section 3.5.2). For EIS, using the simulation smoother [29] requires $\mathcal{O}(n(m^2 + p^3 + N p^2))$ operations: we need to run the Kalman filter once, while preparing the matrices required for the simulation smoother. Then, provided Cholesky roots of the innovation covariance matrices Σ_t are already available, only matrix-vector multiplications are necessary for the simulation smoother. Obtaining the EIS model parameters is efficient, requiring only $\mathcal{O}(n(N p^2 + p^3))$ operations for constructing the $n p \times p$ design matrices and estimating the optimal parameters.

Another concern is the time required to generate N samples from the fitted model. For both the LA and EIS this requires using either the simulation smoother or the FFBS algorithm. This necessitates inverting $p \times p$ matrices in the Kalman filter and $m \times m$ matrices when simulating the states. Fortunately, these steps can be performed offline, after which the simulation of a single sample requires only $\mathcal{O}(n)$ matrix-vector multiplications. The CE-method simulation is based on applying Equation (3.16), which only requires $\mathcal{O}(n m^2)$ time per sample.

Concerning space complexity, the LA has to run the Kalman filter with $\mathcal{O}(n(p^2 + m^2))$ space and store $\mathcal{O}(np)$ parameters. EIS has the same space requirement, but needs additional $\mathcal{O}(Np)$ storage for the simulated signals. As the weights w_t in EIS depend only on the current signals S_t^1, \dots, S_t^N , they may be discarded afterwards. See Section 3.5.2 for the derivation of the $\mathcal{O}(N m + n m^2)$ space requirement of the CE-method.

The LA has the fastest and most space-efficient iteration of the three methods, because it does not require simulation of N samples. This makes it an ideal candidate as an initial guess for the other two methods.

cem faster, only need m^3

For $p \ll m$, EIS is faster than CE-method as it is based on the signals S only, thus having access to

the efficient simulation and signal smoother algorithms. The same is true for the space complexity. If, however, $p \approx m$, there is no linear signal or the observations are not conditionally independent given the states or signals, the speed of EIS and CE-method should be comparable. While theoretically, the CE-method performs sampling faster than the other two methods, for large numbers of samples N the difference is negligible because the additional computations only have to be performed once.

3.8.3 Asymptotic variance

As we have seen in the previous section, the number of samples N used to estimate ψ_{CE} and ψ_{EIS} enter linearly into the computational complexities. Naturally, we want to know how big a sample size we should choose for our procedures and whether one of the two simulation-based procedures requires fewer samples than the other. To answer this question we turn to the two central limit theorems, Theorems 3.4 and 3.6. If N is large, the asymptotic variances (or rather: the asymptotic standard deviations) tell us how much stochastic variation we should expect around the optimal value, and can thus guide us in choosing N . We start with two examples in a univariate setting, where both the CE-method and EIS use Gaussian proposals with either fixed variance (Example 3.2) or mean (Example 3.3). This allows us to compare the methods for either the mean (variance) if the variance (mean) is fixed and potentially misspecified, i.e. not the global optimum. Additionally, the univariate setting allows us, in some cases, to derive analytical expressions of the efficiencies involved, allowing us to interpret them.

rewrite this more clearly

To compare both methods we will determine the asymptotic relative efficiencies, i.e. $\frac{\text{Var}(\hat{\psi}_{\text{EIS}})}{\text{Var}(\hat{\psi}_{\text{CE}})}$, with values smaller than 1 indicating that EIS requires (asymptotically) fewer samples for the same precision as the CE-method. Let us note that we are comparing the efficiencies of parameters ψ , not those of derived parameters such as the standard deviation or the ESS. However, should both methods have the same optimal value the relative efficiencies are the same for all parameters derived from ψ , by the delta method. By a continuity argument, the same is approximately true if the optimal values of the CE-method and EIS are close.

Example 3.2 (univariate Gaussian, σ^2 fixed). Consider the probability space $(\mathbf{R}, \mathcal{B}(\mathbf{R}), \mathbf{P})$ where $\mathbf{P} = p\lambda$ for the Lebesgue measure λ which is symmetric around 0, i.e. $p(-x) = p(x)$ for λ -a.e. $x \in \mathbf{R}$ and possesses up to third order moments. Let $\mathbf{G} = \mathbf{P}$, so $W \equiv 1$ and let $\mathbf{G}_\psi = \mathcal{N}(\sigma\psi, \sigma^2)$ be the single parameter natural exponential family of Gaussians with fixed variance $\sigma^2 > 0$. Then

$$\log g_\psi(x) = \psi T(x) - \frac{\psi^2}{2} + \log h(x),$$

where $T(x) = \frac{x}{\sigma}$ and $h(x)$ is the density of $\mathcal{N}(0, \sigma^2)$ w.r.t. Lebesgue measure. Note that T is centered under \mathbf{P} . To compare the asymptotic behavior of the CE-method and EIS we compute the asymptotic variances arising from their respective central limit theorems (Theorems 3.4 and 3.6).

By symmetry, both ψ_{CE} and ψ_{EIS} are equal to 0. Then $I(\psi) = 1$ for all ψ , so

$$V_{\text{CE}} = \text{Cov}_{\mathbf{P}}(T) = \frac{\tau^2}{\sigma^2}, \quad (3.26)$$

where $\tau^2 = \mathbf{P} \text{id}^2$ is the second moment of \mathbf{P} .

Additionally, $B_{\text{EIS}} = (\text{Cov}_{\mathbf{P}}(T))^{-1} = \frac{\sigma^2}{\tau^2}$ and

$$\begin{aligned} M_{\text{EIS}} &= \text{Cov}_{\mathbf{P}} \left(\left(\log \frac{p(x)}{h(x)} - \lambda_{\text{EIS}} \right) T \right) \\ &= \text{Cov}_{\mathbf{P}} \left((\log p - \log h - \mathbf{P}(\log p - \log h)) T \right) \\ &= \frac{1}{\sigma^2} \int p(x) x^2 \left(\log p(x) + \frac{x^2}{2\sigma^2} - \mathbf{P} \left(\log p(x) + \frac{\tau^2}{2\sigma^2} \right) \right)^2 dx. \end{aligned}$$

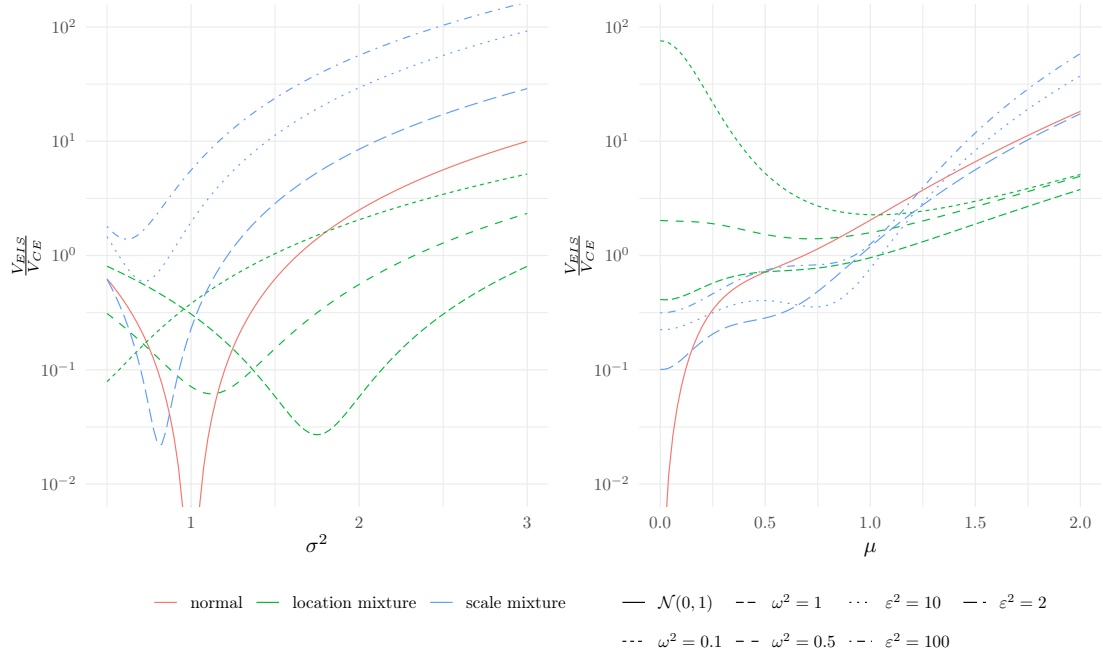


Figure 3.3: Asymptotic relative efficiency $\frac{V_{EIS}}{V_{CE}}$ for the normal distribution from Example 3.2 (left hand side) and Example 3.3 (right hand side). Here \mathbf{P} is either the standard normal distribution, a Gaussian location mixture, or a Gaussian scale mixture. \mathbf{G}_ψ is the normal distribution $\mathcal{N}(\mu, \sigma^2)$, where either σ^2 is fixed (left) and μ determined by the CE-method / EIS, or the other way around (right). Notice the log scale of the y-axis. As μ or σ^2 get close to their true values, EIS outperforms the CE-method in terms of asymptotic variance, see Proposition 3.2. todo: clean up figure legend / linetype, order eps and omega, add global σ^2 chosen by estimating both parameters at the same time?

Thus

$$V_{EIS} = B_{EIS} M_{EIS} B_{EIS} = \sigma^2 \frac{\gamma}{\tau^4},$$

$$\text{where } \gamma = \int p(x) x^2 \left(\log p(x) + \frac{x^2}{2\sigma^2} - \mathbf{P} \left(\log p(x) + \frac{\tau^2}{2\sigma^2} \right) \right)^2 dx.$$

Let us now consider three exemplary choices of \mathbf{P} that illustrate a target that is sufficiently well-behaved (the standard normal), multimodal (a Gaussian location mixture) and has different behavior in the tails than indicated at the mode (a Gaussian scale mixture). For each target, we vary σ^2 from $\frac{1}{2}$ to 3 and obtain relative efficiencies of the CE-method and EIS either analytically or by simulation, the results are shown in the left-hand side of Figure 3.3.

Normal distribution If $\mathbf{P} = \mathcal{N}(0, \tau^2)$ is a normal distribution, this reduces to

$$V_{EIS} = \frac{5}{2} \left(\frac{\tau^2}{\sigma^2} - 1 \right)^2 \frac{\sigma^2}{\tau^2} = \frac{5}{2} \frac{(V_{CE} - 1)^2}{V_{CE}}$$

and so for $\tau^2 = \sigma^2 \hat{\psi}_{EIS}$ converges faster than the standard $\mathcal{O}(N^{-\frac{1}{2}})$ rate. Indeed in this case $\hat{\psi}_{EIS} = \psi_{EIS}$ a.s. for $N > 1$, see Proposition 3.2.

Gaussian location mixture Consider now the case where $\mathbf{P} = \frac{1}{2}\mathcal{N}(-1, \omega^2) + \frac{1}{2}\mathcal{N}(1, \omega^2)$ is a Gaussian location mixture. The second moment is $\tau^2 = 1 + \omega^2 = -\frac{1}{2\psi_{CE}}$. Unfortunately, there is no closed-form expression for many of the terms required for the analysis EIS. Instead, we resort to a simulation study to determine the asymptotic variances and relative efficiencies for three different values of $\omega^2 \in \{0.1, 0.5, 1.0\}$.

To this end we draw $M = 100$ times from the distribution of $\hat{\psi}_{\text{CE}}$ and $\hat{\psi}_{\text{EIS}}$, where we use $N = 1000$ samples from the tractable \mathbf{P} as importance samples. We only iterate a single time for both procedures. From individual estimates, we estimate the asymptotic variances V_{CE} and V_{EIS} by the respective empirical variances, and determine the relative efficiency of EIS over the CE-method as $\frac{V_{\text{EIS}}}{V_{\text{CE}}}$. Again, we vary the fixed variance of the proposals, σ^2 , from $\frac{1}{2}$ to 3.

discuss MC error of this estimate, small enough to ignore?

Gaussian scale mixture Finally we consider $\mathbf{P} = \frac{1}{2} (\mathcal{N}(0, 1) + \mathcal{N}(0, \varepsilon^{-2}))$ for $\varepsilon^2 \in \{2, 10, 100\}$, a scale mixture similar to the one seen in Example 3.1. Contrary to that example, we choose ε big, making the $\mathcal{N}(0, 1)$ component the one with large variance, to make importance sampling with σ^2 in the range considered consistent. Here $\tau^2 = \frac{1}{2} + \frac{1}{2\varepsilon^2}$. Again, we estimate the asymptotic V_{EIS} in the same way as for the Gaussian location mixture, with $M = 100$ estimates using $N = 1000$ samples each.

Note that for fixed σ^2 the asymptotic variance of the CE-method V_{CE} is the same in all of the examples considered, as we sample directly from the tractable \mathbf{P} , so V_{CE} only depends on \mathbf{P} through its second moment τ^2 . The asymptotic variance of EIS however depends on both τ^2 , as well as γ , which depends on global properties of \mathbf{P} .

From the left-hand side of Figure 3.3 we can observe that in the case of $\mathbf{P} = \mathcal{N}(0, 1)$ EIS has smaller asymptotic variance compared to the CE-method, as long as σ^2 is not heavily misspecified. Indeed, if $\sigma^2 = 1$ is correctly specified, by Proposition 3.2, EIS has asymptotic variance 0 and converges already for a single sample.

Consider now the case where \mathbf{P} is a Gaussian location mixture. For $\omega^2 = 1$, the location mixture is unimodal with variance 2 and EIS outperforms the CE-method in terms of asymptotic variance in the range considered. For the smaller values of ω^2 considered here, the location mixture is bimodal. Close to the true variance $1 + \omega^2$, EIS still outperforms the CE-method.

For the Gaussian scale mixture, the case is less clear. Here the true variance is $\frac{1}{2} + \frac{1}{2\varepsilon^2}$. The location of the minimal relative efficiency is still close to this true variance, however, as ε^2 grows, the CE-method starts to dominate EIS. Additionally, recall from Example 3.1 that for large ε^2 EIS becomes inadmissible.

Example 3.3 (univariate Gaussian, μ fixed). Consider the same setup as in Example 3.2, i.e. \mathbf{P} is symmetric around 0 with second moment τ^2 , but let $\mathbf{G}_\psi = \mathcal{N}(\mu, -\frac{1}{2\psi})$ be the single parameter natural exponential family of Gaussians with fixed mean μ and variance $\sigma^2 = -\frac{1}{2\psi}$.

Then

$$\log g_\psi(x) = \psi T(x) + \frac{1}{2} \log(-2\psi) - \frac{1}{2} \log 2\pi$$

for $T(x) = (x - \mu)^2$. Thus $\mathbf{P}T = \tau^2 + \mu^2$ and $\text{Cov}_{\mathbf{P}}T = \nu - \tau^4 + 4\tau^2\mu^2$ where $\nu = \mathbf{P}\text{id}^4$ and $\tau^2 = \mathbf{P}\text{id}^2$.

By matching moments, we obtain $\psi_{\text{CE}} = -\frac{1}{2(\tau^2 + \mu^2)}$ and $I(\psi_{\text{CE}}) = \frac{1}{2\psi_{\text{CE}}^2} = 2(\tau^2 + \mu^2)^2$. In total

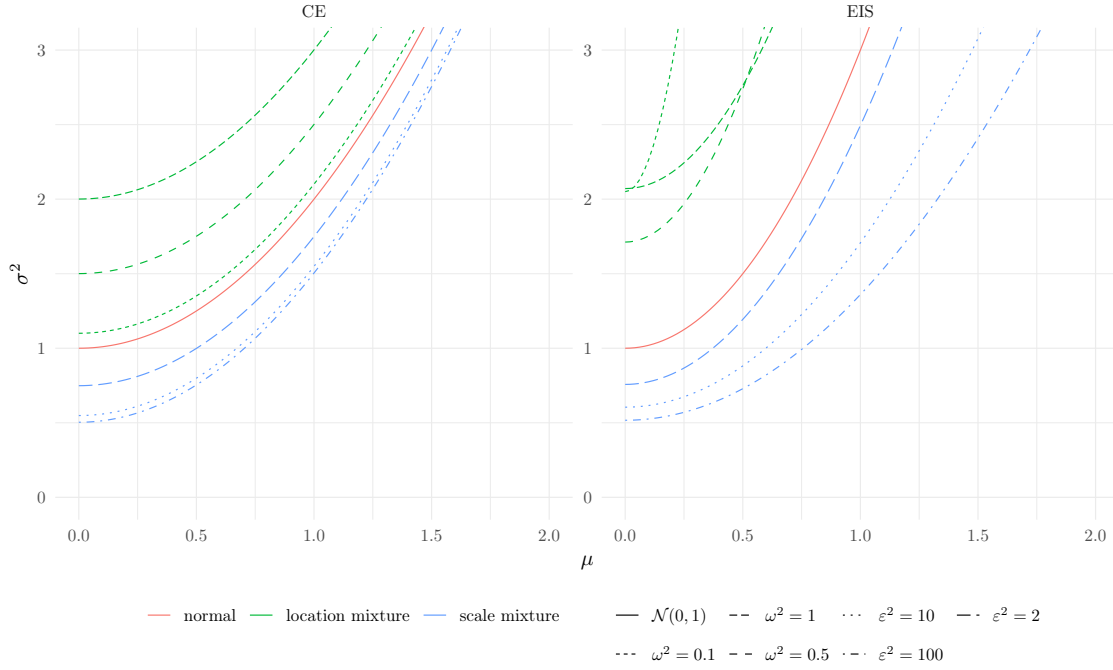
$$V_{\text{CE}} = \frac{1}{4(\tau^2 + \mu^2)^4} (\nu - \tau^4 + 4\tau^2\mu^2) \quad (3.27)$$

For EIS,

$$\begin{aligned} \psi_{\text{EIS}} &= (\text{Cov}_{\mathbf{P}}T)^{-1} \text{Cov}_{\mathbf{P}}(T, \log p) \\ &= (\nu - \tau^4 + 4\tau^2\mu^2)^{-1} \underbrace{\int p(x)((x - \mu)^2 - \tau^2 - \mu^2)(\log p(x) - \mathbf{P}\log p(x)) dx}_{=\gamma} \end{aligned}$$

Then

$$V_{\text{EIS}} = (\nu - \tau^4 + 4\tau^2\mu^2)^{-2} \mathbf{P} \left((\text{id} - \mu)^4 (\log p - \psi_{\text{EIS}}(\text{id} - \mu)^2 - \mathbf{P}\log p + \psi(\tau^2 + \mu^2))^2 \right).$$

Figure 3.4: **TODO**

We now perform the same analysis as in Example 3.2, the resulting ratio of asymptotic variances is displayed in the right-hand side of Figure 3.3. In general, the variances $\sigma_{\text{CE}}^2 = -\frac{1}{2\psi_{\text{CE}}}$ and $\sigma_{\text{EIS}}^2 = -\frac{1}{2\psi_{\text{EIS}}}$ are different, so the ratio is no longer an asymptotic relative efficiency. However, it is still relevant as a measure of the relative speed of stochastic convergence of both methods. Additionally, we display the resulting optimal variances in Figure 3.4.

Normal distribution For the normal distribution $\mathbf{P} = \mathcal{N}(0, \tau^2)$ where $\nu = 3\tau^4$ and $\gamma = -\tau^2$, so

$$\psi_{\text{EIS}} = \frac{-\tau^2}{2\tau^2(\tau^2 + 2\mu^2)} = \frac{-1}{2(\tau^2 + 2\mu^2)}.$$

Thus the EIS proposal uses variance $\sigma_{\text{EIS}}^2 = \tau^2 + 2\mu^2$, which is bigger than the variance of $\sigma_{\text{CE}}^2 = \tau^2 + \mu^2$ optimal for the CE-method.

In this case the asymptotic variances are

$$V_{\text{CE}} = \frac{\tau^2(\tau^2 + 2\mu^2)}{2(\tau^2 + \mu^2)^4}$$

and

$$V_{\text{EIS}} = \frac{\mu^2(2\mu^6 + 45\mu^4\tau^2 + 15\tau^6)}{4\tau^4(2\mu^2 + \tau^2)^4},$$

see the Appendix for details.

reference it

Gaussian location mixture

same setup as before

Gaussian scale mixture

same setup as before

On the left-hand side of Figure 3.3 we see that for μ close to the optimal value, EIS has smaller asymptotic variance than the CE-method, except for the two bimodal location measures. Again, due to the finite sample convergence of EIS, Proposition 3.2, the asymptotic variance V_{EIS} goes to 0 as $\mu \rightarrow 0$. The more μ becomes misspecified, the ratio of asymptotic variances starts to grow.

In Figure 3.4 we see that, except for the extreme scale mixtures, EIS tends to produce proposals that have a larger variance than those produced by the CE-method. As we will see in the discussion of Figure 3.6, this might be advantageous for EIS as proposals with a small variance run the risk of missing a large part of the probability mass of the target.

clean this

In applications, e.g. the model studied in Chapter 4, we are interested in the performance of the importance sampling proposals generated by the LA, CE-method and EIS under more complex circumstances than those discussed in Examples 3.2 and 3.3. In particular, the dimension of ψ is high ($\mathcal{O}(n \cdot m)$ or even $\mathcal{O}(n \cdot m^2)$) and proposals may not come from a natural exponential family, so analysis based on Theorems 3.4 and 3.6 is not possible. Instead, we resort to simulation studies to gain insights into the circumstances when one should prefer one method over the other. As a leading example, we will use the following vector-autoregressive state space model with negative binomial observations. A similar, though more involved, model is studied in Section 4.2 with real data.

Example 3.4 (Negative Binomial VAR(1) SSM). In this example, we consider a SSM where states X_t follow a stationary Gaussian VAR(1) process, initialized in its stationary distribution $\mathcal{N}(0, \Sigma)$ for SPD Σ . For simplicity let the transition matrices be given by a multiple of the identity, i.e. $A_t = \alpha I_m$ for all t where $\alpha \in (-1, 1)$

add I to symbols

. In total, the states are governed by

$$\begin{aligned} X_0 &\sim \mathcal{N}(0, \Sigma) \\ X_t &= \alpha X_{t-1} + \varepsilon_t \\ \varepsilon_t &\stackrel{\text{i.i.d.}}{\sim} \mathcal{N}(0, (1 - \alpha^2)\Sigma), t = 1, \dots, n \end{aligned}$$

where the ε_1, \dots, n and X_0 are jointly independent. The observations follow a conditional negative binomial distribution

$$Y_t^i | X_t \sim \text{NegBinom}(\exp(X_t^i), r), \quad i = 1, \dots, p \quad t = 0, \dots, n$$

and individual observations are conditionally independent given the current state. The parametrization of the negative binomial distribution $\text{NegBinom}(\mu, r)$ is such that the density is

$$p_{\mu, r}(y) = \binom{y+r-1}{r} \left(\frac{\mu}{r+\mu} \right)^y \left(\frac{r}{r+\mu} \right)^r \propto_{\mu} \mu^y (\mu+r)^{-(r+y)},$$

with expectation μ , variance $\mu + \frac{\mu^2}{r}$ and support \mathbf{N}_0 .

Our first simulation study concerns the non-asymptotic behavior of the CE-method and EIS estimators, i.e. finite sample analogs of Theorems 3.4 and 3.6. To this end, we let $m = 1$ in Example 3.4 and fix n to

...

. We then simulate once from the marginal distribution of Y and perform the LA to a prespecified precision ϵ and maximum number of iterations n_{iter} , obtaining a proposal distribution \mathbf{G}_{LA} . Using a large number of samples N_{true} from this proposal we find the optimal \mathbf{G}_{CE} and \mathbf{G}_{EIS} using the same desired precision and number of iterations as for the LA. For the remainder of this section, we ignore sampling variation in these proposals and treat them as exact.

To determine the non-asymptotic sampling behavior we now perform the above procedure again, using only $N \ll N_{\text{true}}$ many samples for both procedures, obtaining proposals $\hat{\mathbf{P}}_{\text{CE}}^N$ and $\hat{\mathbf{P}}_{\text{EIS}}^N$. As the full proposals are Gaussian distributions on $\mathbf{R}^{(n+1) \times m}$, either given as the posterior of a GLSSM (LA, EIS) or by a Gaussian Markov process (CE-method), see Section 3.5. This procedure is repeated M times for every sample size N considered, with different initial random seeds, obtaining $\hat{\mathbf{P}}_{\text{CE}}^{N,i}$ and $\hat{\mathbf{P}}_{\text{EIS}}^{N,i}$ for $i = 1, \dots, M$.

To assess the speed of convergence of the CE-method and EIS we then estimate the mean squared error of means and variances of the $(n+1) \times m$ univariate marginals as N , the number of samples used to obtain $\hat{\psi}_{\text{CE}}$ or $\hat{\psi}_{\text{EIS}}$, grows. For the true value, we take the univariate means and variances of \mathbf{G}_{CE} and \mathbf{G}_{EIS} respectively. Additionally, we perform a bias-variance decomposition to see where the estimation error originates.

More concretely, fix N and denote by $\mu, \sigma^2 \in \mathbf{R}^{(n+1) \cdot m}$ the marginal means and variances of \mathbf{G}_{CE} (\mathbf{G}_{EIS}). Let $\hat{\mu}_i, \hat{\sigma}_i^2 \in \mathbf{R}^{(n+1) \cdot m}$ be the marginal means and variances of $\mathbf{G}_{\text{CE}}^{N,i}$ ($\mathbf{G}_{\text{EIS}}^{N,i}$) for $i = 1, \dots, M$. Now

$$\widehat{\text{aMSE}} = \frac{1}{M} \frac{1}{(n+1)m} \sum_{i=1}^M \|\mu - \hat{\mu}_i\|_2^2 + \|\sigma^2 - \hat{\sigma}_i^2\|_2^2$$

is an estimate of the mean-squared error of (μ, σ^2) , where we divide by $(n+1)m$ to make estimates comparable across models of different dimensions.

In Figure 3.5 we show the $\widehat{\text{aMSE}}$ for both the CE-method and EIS for varying values of N . As is evident from this Figure, the CE-method consistently has a larger $\widehat{\text{aMSE}}$ than EIS, for all values of N . Thus the CE-method requires several orders of magnitude more samples to obtain the same precision as EIS.

For further investigation, we perform a bias-variance decomposition of the $\widehat{\text{aMSE}}$ for both the means μ and variances σ^2 . Consider the average means and variances over the M simulations,

$$\bar{\mu} = \frac{1}{M} \sum_{i=1}^M \hat{\mu}_i \quad \bar{\sigma}^2 = \frac{1}{M} \sum_{i=1}^M \hat{\sigma}_i^2,$$

and the state-average squared bias and variance

$$\begin{aligned} \text{aBias}_{\mu}^2 &= \frac{1}{(n+1)m} \|\mu - \bar{\mu}\|_2^2, \\ \text{aVar}_{\mu} &= \frac{1}{M-1} \frac{1}{(n+1)m} \sum_{i=1}^M \|\bar{\mu} - \hat{\mu}_i\|_2^2, \\ \text{aBias}_{\sigma^2}^2 &= \frac{1}{(n+1)m} \|\sigma^2 - \bar{\sigma}^2\|_2^2, \\ \text{aVar}_{\sigma^2} &= \frac{1}{M-1} \frac{1}{(n+1)m} \sum_{i=1}^M \|\bar{\sigma}^2 - \hat{\sigma}_i^2\|_2^2. \end{aligned}$$

These values are depicted in Figure 3.5.

interpretation of Figure 3.5, equal contribution of bias and var, not much to gain from bias correction

3.8.4 Numerical convergence

3.8.5 Performance of the optimal proposal

change EF to aEF (asymptotic EF) everywhere in this section

For the performance of importance sampling the efficiency factor $\text{EF} = \frac{\text{ESS}}{N}$ plays an important role, see Section 3.4. Additionally, it allows a comparison of the effectiveness of importance sampling across multiple sample sizes N , indeed, as $N \rightarrow \infty$, EF converges to ρ^{-1} , where ρ is the second moment of importance sampling weights, $\int w^2 d\mathbf{G}$.

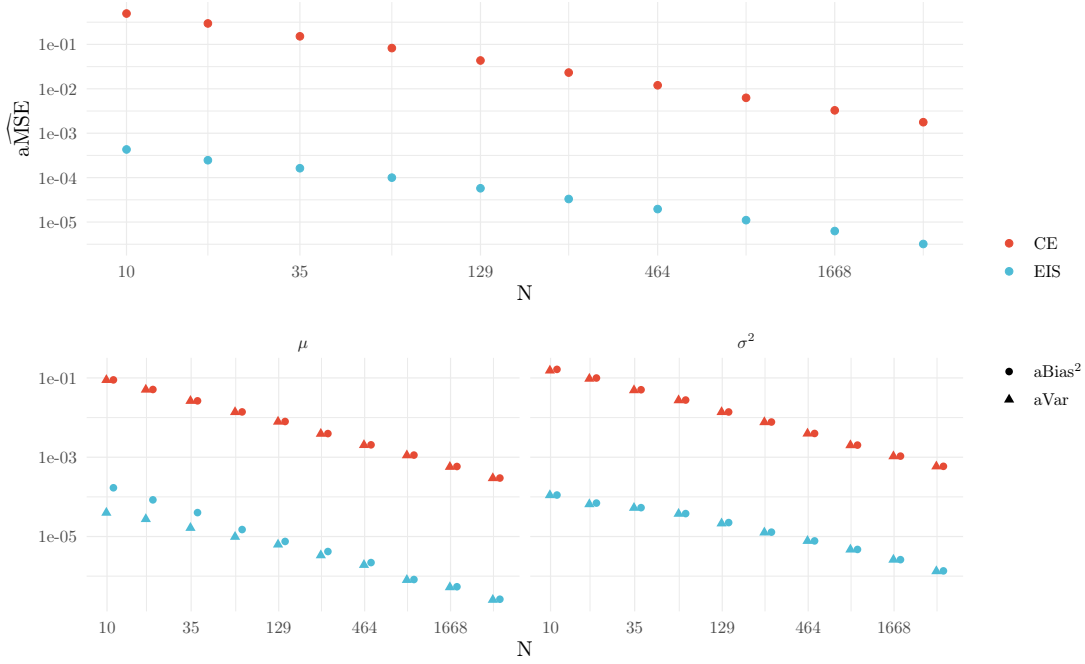


Figure 3.5: TODO

Returning to the distributions studied in Examples 3.2 and 3.3, we now calculate the asymptotic efficiency factor

$$\text{EF} = \frac{1}{\rho} \in (0, 1].$$

As the proposal is always $\mathcal{N}(\mu, \sigma^2)$ with either μ or σ^2 fixed, and \mathbf{P} is a mixture of Gaussians or $\mathcal{N}(0, 1)$, ρ is analytically available.

For Example 3.2, both EIS and the CE-method have, by symmetry, the same optimal $\mu = 0$. Thus the efficiency factor only depends on the fixed σ^2 , see Figure 3.6, and is the same for EIS and the CE-method.

For Example 3.3 the two methods have different optimal proposals, thus also different asymptotic efficiency factors. In Figure 3.7, the first two subfigures show how the efficiency factor depends on the misspecified μ for both methods. The optimal variances are based on the results from Example 3.3, i.e. based on simulation for EIS. The right-hand subfigure shows the relative efficiency factor, i.e. the ratio of the efficiency factor for the CE-method and EIS. Here values smaller than 1 indicate that EIS has a larger efficiency factor than the CE-method.

In this figure, we can observe that, as expected, misspecification in μ almost always results in a smaller efficiency factor, an exception being the scale mixture with $\varepsilon^2 = 100$ for the CE-method. Compared to Figure 3.6, we see that already small misspecification in μ results in a large decline in EF, although we should keep in mind that this is not a fair comparison, as μ and σ^2 live on different scales. If $\mu = 0$ is correctly specified, both methods have comparable performance, except for extreme cases of the mixture models, i.e. when $\omega^2 = 0.1$ or when $\varepsilon^2 = 100$. For small misspecification of μ , this remains true, but for larger misspecification, the CE-method has a larger efficiency factor, especially for the bimodal location mixture with $\omega^2 = 0.1$, where the performance of EIS deteriorates.

stress that cem gives global optimum, eis only approximate

For the model from Example 3.4 we cannot determine ρ analytically, so we fall back to a simulation study. Thus, we also estimate EF for each of the M runs, using the same number of samples $N = N_{\text{true}}$ as was used to determine the true optimal parameter. We display the resulting efficiency

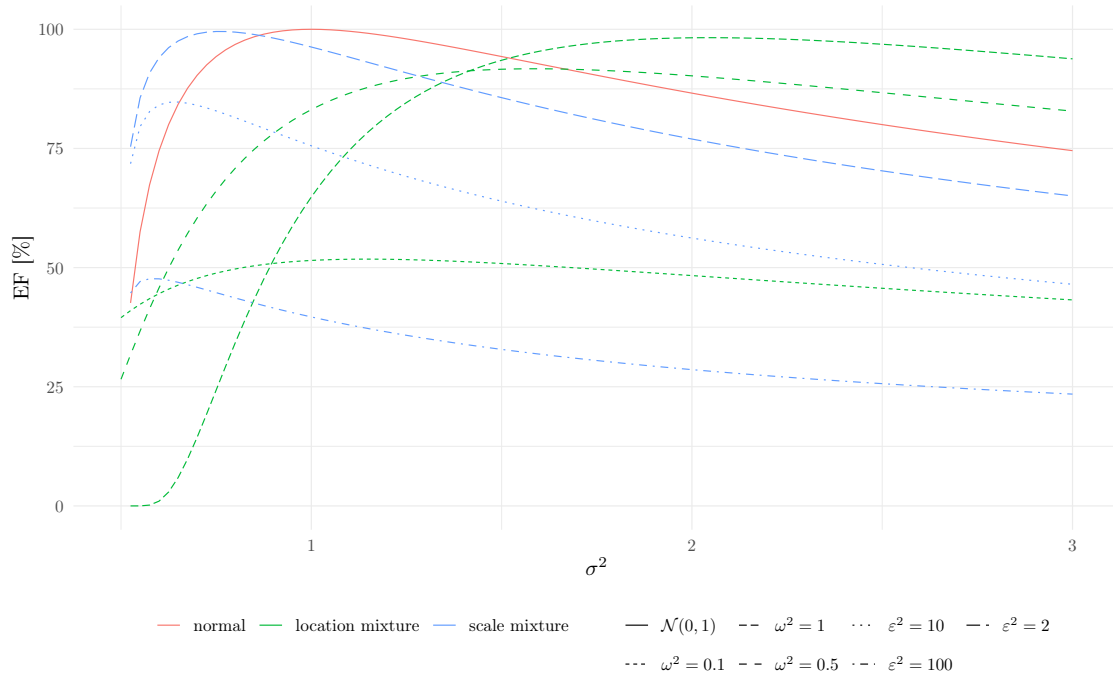


Figure 3.6: TODO

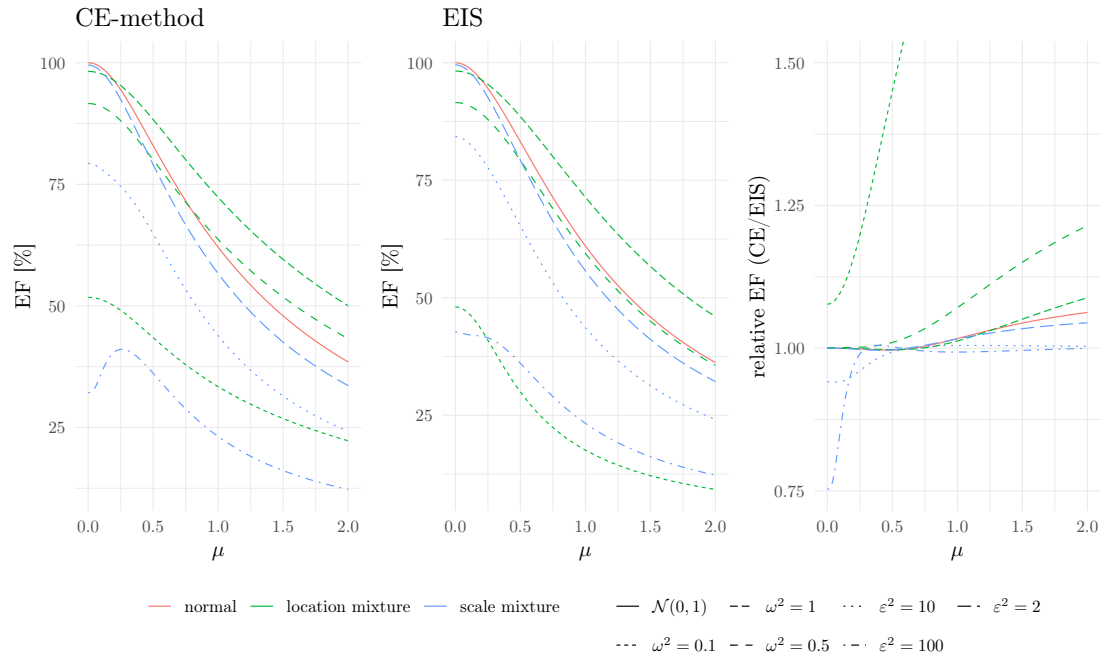


Figure 3.7: TODO

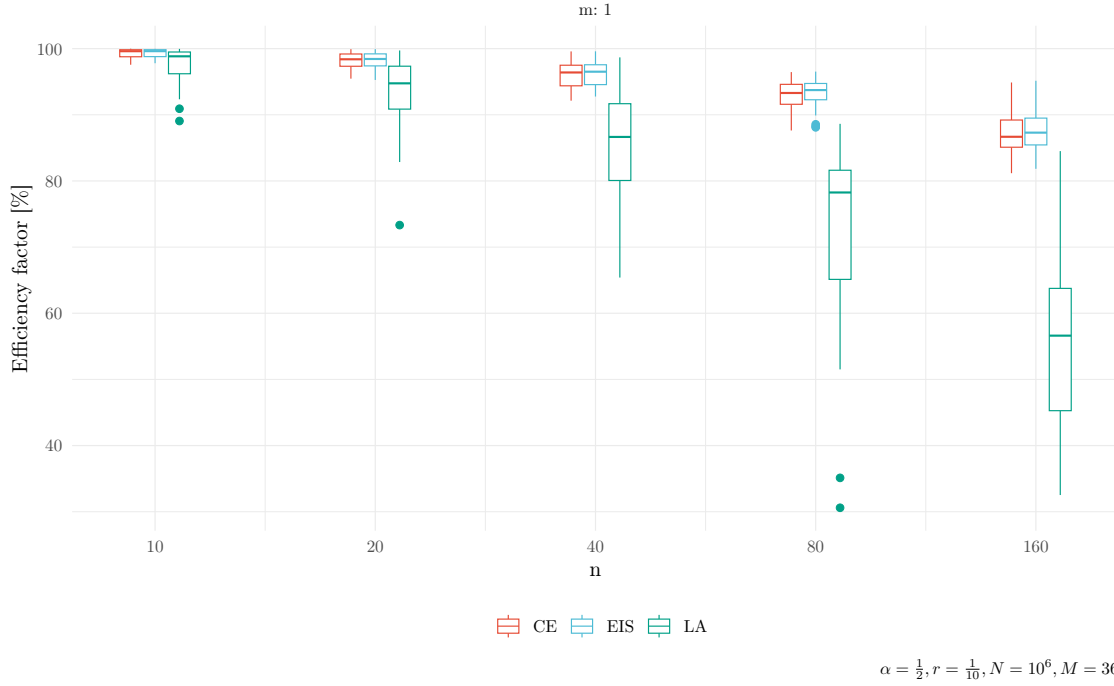


Figure 3.8: The asymptotic efficiency factor degenerates as the number of time steps n increases. We show the estimated efficiency factor over 100 replications of estimating the optimal parameters for Example 3.4 with the CE-method and EIS with $N_{\text{true}} = 10^6$ and the resulting estimated efficiency factors at the optimum. Notice the log scale of the x-axis. The performance of the optimal CE-method and EIS parameters is comparable and superior to that of the LA

factors in Figure 3.8. The parameters α, r, N, M may be found in the bottom right corner of the figure. For a low number of time steps n , all three methods perform comparably. With increasing n , their performance expectedly worsens, however, more so for the local LA, while the CE-method and EIS perform comparably around their optimal value.

Chapter 4

Analysis of selected models

Contributions of this chapter

- ...

4.1 Spatial reproduction number model

1. essentially the Regional model presented in ECMI

4.2 Regional growth factor model

4.3 Nowcasting hospitalizations

4.3.1 Context

Judging the severity of the COVID-19 epidemic has been an ongoing challenge since its inception. As immunization against COVID-19 rose, strict enforcement of social distancing rules eased and testing regimes became less strict, case incidences became a less reliable and harder to interpret indicator of epidemic severity. Instead more direct indicators of morbidity, such as the number of deaths and ICU admissions and occupancy have come to the fore. But these indicators are late due to the substantial delays between infection and occurrence. An alternative indicator that captures the morbidity caused by COVID-19 but is earlier than the others is the number of hospitalisations of positive COVID-19 cases.

While hospitalisations occur earlier, they still come with substantial delay between the infection and subsequent admission to hospital. Additional difficulties arise due to delays in reporting, i.e. the time it takes until the hospital reports the new case to the national health authorities. The problem of accounting for delays in reporting for occurred, but not yet reported events has been termed **nowcasting**, i.e. forecasting of the indicator at time “now”. Predicting the number of hospitalisations is thus a mixture of both forecasting — which reported COVID-19 cases will end up in the hospital — and nowcasting — which cases have yet to be reported — and we will use the term nowcasting in this paper to mean this predictive mixture. In this section we focus on the situation in Germany where data on hospitalisations has been available since April 2021 provided by the German federal health care authority, the Robert Koch-Institut (RKI), via Github [68]. In these data the number of hospitalisations is linked to the date of reporting of the associated case, so the term of nowcasting is accurate: we are interested in the “true” value of the indicator today, that will only be observed after a long delay. While this association requires a careful interpretation of the indicator (see Section 4.3.4) it was, besides case incidences and ICU occupancy, one of the main official indicators in Germany informing countermeasures in 2021 and so there is merit in nowcasting it.

The extent of delays is visible in Figure 4.1: the reported number of hospitalisations will roughly double over the course of twelve weeks. By the aforementioned reporting scheme of hospitalisations there are two reporting dates for a single hospitalised case: the reporting date of the case, i.e. the date when local health authorities were made aware of the positive test, and the reporting date of the hospitalisation, i.e. when the hospitalisation was reported to the RKI. This induces a double weekday effect in the reporting delays which we make visible in Figure 4.2.

Compared to other approaches in the COVID-19 NowcastHub, that tended to exclusively focus on modelling the delay distribution with parametric and non-parametric models, our model sidesteps this complex delay structure by decomposing delayed hospitalisations into weekly chunks (Figure 4.4) and incorporating case data. As cases and hospitalisations are explicitly linked by the case reporting date we forecast the number of hospitalisations in each chunk based on the current incidences and past fractions of hospitalisations in a comparable weekly chunk. We additionally quantify uncertainty by prediction intervals that are informed by the past performance of our model. This makes our model straightforward to understand, easy to implement and fast to run.

reformulate

The origin of nowcasting lie in accounting for incurred, but not reported claims in the actuarial sciences [47], delays in reporting for AIDS [57, 89] and other infectious diseases [33]. Popular statistical approaches include methods from survival analysis [57] and generalized linear regression [89]. In the survival analysis setting one commonly models the reverse time discrete hazard parametrically and assumes multinomial sampling of the final number of cases, potentially accounting for overdispersion.

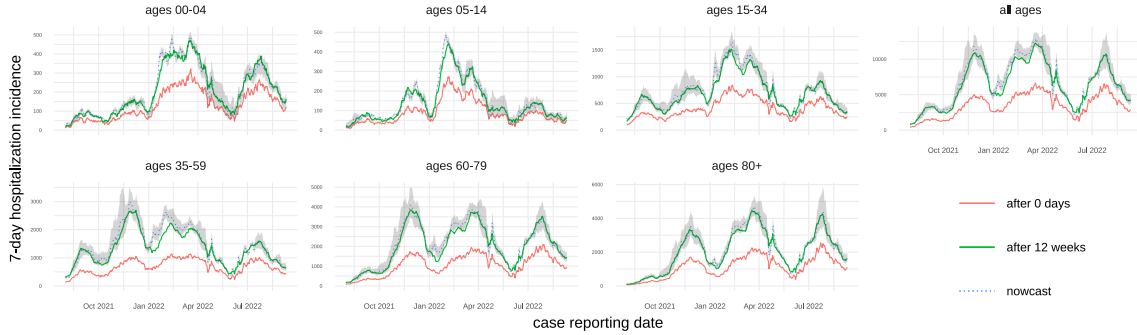


Figure 4.1: Germany's 7-day hospitalisation incidence changes due to various delays such as time to hospitalisation and delays in reporting. This figure shows the extent of these delays: incidences reported at the present date (red lines) severely underestimate the hospitalisation incidence (green solid lines) that is reported after 3 months. Our nowcasting model (blue dotted lines, 95% prediction intervals in shaded gray) deals with this problem by predicting the hospitalisation incidence based on past cases and their delays to hospitalisation.

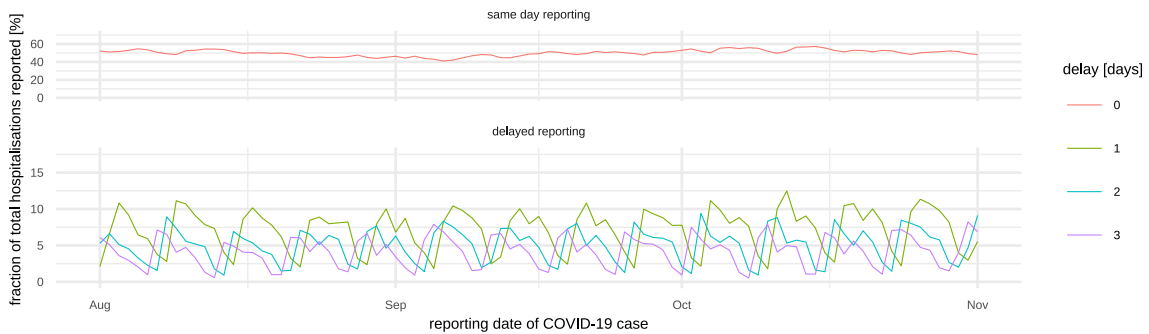


Figure 4.2: The hospitalisation incidence contains a double weekday effect owed to the reporting of both the COVID-19 case and the subsequent hospitalisation. While the weekday effect of the case reporting date is somewhat mitigated by summing over 7 day periods, the weekday effect of reporting date of the hospitalisation is still present in the data. It is most pronounced for hospitalisations that are reported with delays, i.e. where the case reporting date does not match the reporting date of the hospitalisation.

This has been studied with frequentist [60] and Bayesian [5, 40] methods. The generalized linear regression approach has origins in the chain ladder model from actuarial sciences [66] and models the observed counts in the reporting triangle by a Poisson or negative binomial distribution. For both approaches, available covariates can be incorporated in a straightforward way. In the setting of real-time nowcasting, it is often beneficial to incorporate epidemic dynamics into the model, this can be achieved by splines [40, 86] or by a latent process of infections [59].

Nowcasting methods have wide application in accounting for reporting delays [60], early outbreak detection [8, 74], and, in the recent COVID-19 epidemic, improving real-time monitoring of epidemic outbreaks [4, 5, 37, 78]. Evaluating a forecasting model in a real-time public health setting is advantageous as it avoids hindsight bias [24], however nowcasting approach may have difficulties with bias and properly calibrated uncertainty if used in a real-time setting. This includes rapidly changing dynamics [37, 86], both of the delay distribution and the underlying epidemic, retrospective changes in data [60] and long delays with few observed cases [63].

To avoid the aforementioned hindsight bias one can make their predictions publicly available in real-time [12, 65]. For the hospitalisations in Germany, Thomas Hotz and I have participated in the German COVID-19 NowcastHub [64] since November 2021 where nowcasts are available in a public Github repository [42] with the “ILM-prop” model. The ideas, especially the model and the “double-weekday effect”, discussed in this section are based on this model. However, the “ILM-prop” model is based on simple point estimates for the proportion of hospitalisations per reported case, neglecting regularization over time. In this thesis we extend this model to the SSM setting of this thesis and investigate if the increased model complexity results in improved performance.

4.3.2 Data

To predict the number of hospitalisations we consider the reporting process of both reported COVID-19 cases and reported hospitalisations. Recall that the reporting date of a COVID-19 case is shared for both the case and its hospitalisation, i.e. the case and hospitalisation are linked through this date.

As hospitalisations are only available as 7-day rolling sums, we use 7-day rolling sums for daily reported incidences as well. To avoid dealing with the double weekday effect of both reporting date of the case and reporting date of the hospitalisation (see Figure 4.2) we divide the future hospitalisations we wish to predict into chunks of one week, which gets rid of the weekday effect for the hospitalisations. This is depicted in Figure 4.4. Our prediction of each of these weekly chunks then consists of the fraction of hospitalisations of reported cases in the past.

We use publicly available data from the German national health authority (RKI) on daily reported COVID-19 cases [69] and weekly reported hospitalisations [68]. Both datasets are updated on a daily basis.

COVID-19 cases are described by their date of reporting, i.e. the date that the local health authorities were made aware of the case. For a fraction (63 %) of cases the date of symptom onset is also reported. Due to delays in the process from infection to reporting – e.g. the time it takes to get tested, evaluate the test and report the result to local health authorities – the date of reporting is, for most cases, some days after symptom onset (median delay: 3 with interquartile range [2, 6]). As the date of symptom onset is not known for a substantial amount of incident cases, and is not reported for hospitalised cases, we focus our analysis on the date of reporting.

Hospitalisations are associated with the *reporting date of the corresponding case* and no information is available on the actual date of hospitalisation. In addition, hospitalisations are only published as weekly sums over the past seven days. This means that the number of hospitalisations reported for today consists of all hospitalisations that correspond to cases that have a *case reporting date* in the past seven days. In particular if the case reporting date of a hospitalised case is today the case will *not* count towards today's hospitalisation count. The reporting date of hospitalisation is not available in the dataset, but can be inferred by comparing datasets from consecutive days.

Daily incident cases and weekly hospitalisations are reported by federal state and age group (00-04, 05-14, 15-34, 35-59, 60-79, 80+). Incident cases are additionally reported by county and sex.

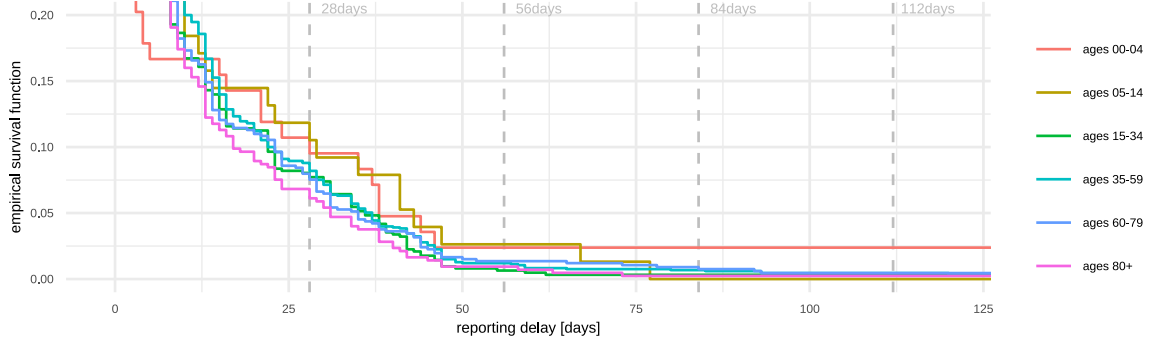


Figure 4.3: Survival function of reporting delays of weekly hospitalisations $H_{t,d}$ with case reporting date 01 September 2021. The delay distribution has long tails with a non-negligible fraction of observed delays longer than eight weeks, in some age groups even twelve weeks.

In line with the structure of the data provided by the RKI we let $H_{t,d}^a$ be the number of weekly hospitalisations in age group a with case reporting date $t-1, \dots, t-7$ that are known on day $t+d$, aggregating over all states. Accordingly we define $I_{t,d}^a$ to be the number of weekly incident cases in age group a with reporting date $t-1, \dots, t-7$ that are known on day $t+d$. Finally we reconstruct the reporting triangles for weekly hospitalisations (Figure 4.4) by differencing the $H_{t,d}^a$ for fixed t : $h_{t,d}^a = H_{t,d}^a - H_{t,d-1}^a$, setting $H_{t,-1}^a$ to 0 by convention. We recover the reporting triangle $i_{t,d}^a$ for incident cases in the same manner.

We show the empirical survival function of hospitalisations for a fixed date in Figure 4.3. We observe that delays have long tails, with most cases reported after 12 weeks (84 days), except for the youngest age group. After such a long delay between infection and hospitalisation we deem it unlikely that hospitalisation is due to COVID and disregard all longer delays accordingly. Given such long delays, it does not suffice to nowcast only today's hospitalisations, but also for dates in the past to monitor hospitalisation, i.e. observe current trends; we thus nowcast for all delays $d = 0, \dots, 28$.

4.3.3 Model

More formally, denote by $h_{t,d}$ the number hospitalisations with reporting date t that are known d days later. Unfortunately we only observe

$$H_{t,d} = \sum_{s=t-6}^t h_{s,d+(t-s)},$$

i.e. a weekly sum of reported hospitalisations. On day T our goal is to predict $H_{t,D}$ for large delays D and days $t \leq T$, of course it suffices to predict $H_{t,D} - H_{t,T-t}$ and add the known $H_{t,T-t}$ to this prediction. We rewrite this into weekly telescoping sum

$$H_{t,D} - H_{t,d} = (H_{t,d+7} - H_{t,d}) + (H_{t,d+14} - H_{t,d+7}) + \dots + (H_{t,D} - H_{t,d+7K}),$$

where $K = \lfloor (D-d)/7 \rfloor$, reducing the task at hand to predict hospitalisations in the k -th week ahead, $H_{t,d+7k} - H_{t,d+7 \cdot (k-1)}$, $k = 1, \dots, K$. To leverage known reported incidences, rewrite this as

$$\underbrace{\frac{H_{t,d+7k} - H_{t,d+7 \cdot (k-1)}}{I_{t,d}}}_{=: p_{t,d,k}} I_{t,d}$$

where $I_{t,d}$ is the 7-day case incidence with reporting date t known at time $t+d$, i.e. the incident case analogue of $H_{t,d}$.

Assuming that the proportions $p_{t,d,k}$ change slowly over time t we estimate them by

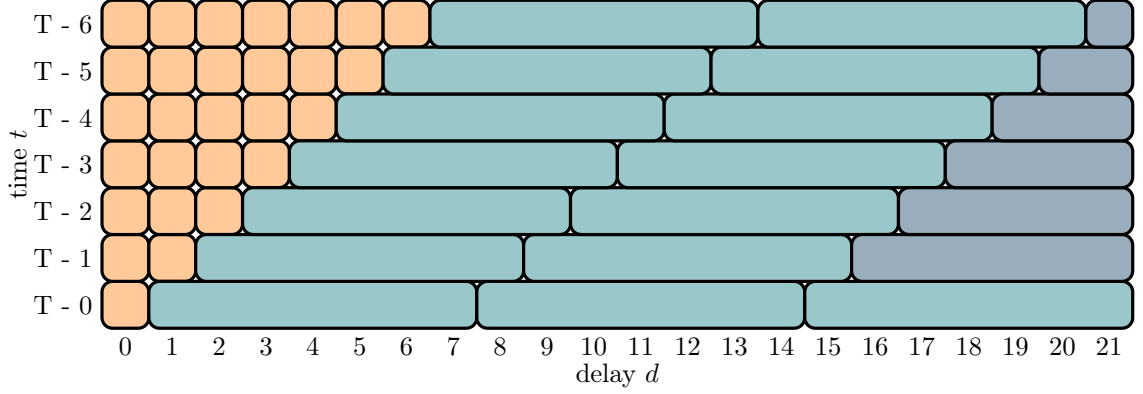


Figure 4.4: Decomposition of the daily reported hospitalisation incidences into the **known incidences**, i.e. the **reporting triangle**, and **the future weekly increments**. The last increment might not be a weekly one, but we expect few cases to occur for such long delays.

$$\widehat{p_{t,d,k}} = \frac{H_{t-7k,d+7k} - H_{t-7k,d+7 \cdot (k-1)}}{I_{t-7k,d}} = p_{t-7k,d,k} \quad (4.1)$$

and finally predict

$$\widehat{H_{t,D}} = H_{t,d} + I_{t,d} (\widehat{p_{t,d,1}} + \dots + \widehat{p_{t,d,K}}). \quad (4.2)$$

As hospitalisation is affected by age, we perform this procedure for all available age groups separately and finally aggregate over all age groups to obtain a nowcast for all age groups combined.

This describes our point nowcast for 7-day hospitalisations. To obtain uncertainty intervals we fit a normal (age groups 00-04 and 05-14) or lognormal (all other age groups) distribution to the past performance of our model. We chose these distributions based on explorative analysis and believe that these should be seen as heuristics rather than as a matter of fact, which is in line with the philosophy of our model to be as simple as possible.

Denote by $\hat{H}_{t,D,s}$ the nowcast made for date t on date $s \geq t$. Starting with date $t + D$ the definite $H_{t,D}$ is known and we can estimate the absolute prediction error $\varepsilon_{t,s} = H_{t,D} - \hat{H}_{t,D,s}$ and the relative prediction error $\eta_{t,s} = \log(H_{t,D} - H_{t,s-t}) - \log(\hat{H}_{t,D,s} - H_{t,s-t})$. For the nowcast for date t made on date s we estimate the standard deviation $\hat{\sigma}$ of $\varepsilon_{t-D-i,s-D-i}$ or $\eta_{t-D-i,s-D-i}$ (age groups 00-04, 05-14 and others respectively), $i = 0, \dots, 27$ by its empirical counterpart. The estimated predictive distribution which informs our prediction intervals is then $\mathcal{N}(\hat{H}_{t,D,s}, \sigma^2)$ (age groups 00-04 and 05-14) or $\mathcal{LN}(\log(\hat{H}_{t,D,s} - H_{t,s-t}), \sigma^2) + H_{t,s-t}$ (all other age groups).

4.3.4 Discussion

Before evaluating the predictive performance of our model we investigate how the fraction of hospitalisations after one up to four weeks changes over time across different age groups. Figure 4.5 shows that these fractions are changing slowly over time, especially in the older age groups. Due to smaller numbers of infections and hospitalisations reported in the younger age groups these fractions vary more strongly, occasionally dropping to 0. Across all age groups we observe a steady decline from October 2021 to December 2021 with a steeper drop in fraction of hospitalisations starting with January 2022. The former period corresponds to a time of mandatory testing at the workplace which may improve ascertainment of asymptomatic and less severe cases. The latter effect is most recognizable in the 35-59 age group and coincides with the time that the Omicron

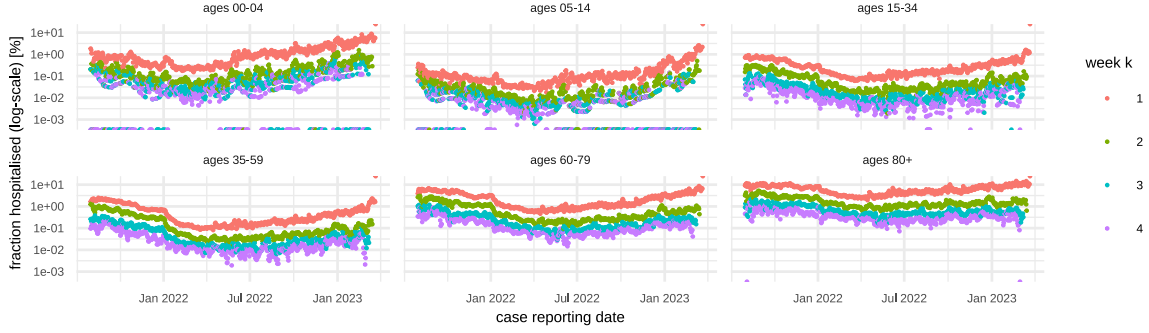


Figure 4.5: We show the fractions of hospitalisations in the k -th week after case reporting date t of initially reported cases in different age groups, i.e. $p_{t,0,k} = (H_{t,7k} - H_{t,7 \cdot (k-1)}) / I_{t,0}$. Note the log-scale of the y -axis. During periods of low incidence, e.g. July – September, we find large fluctuations, but no discernable weekly pattern. With rising case numbers the fractions stabilise and decrease in most age groups. This might be due to changes in testing regime detecting less severe cases. As changes occur on slow time scales, estimating these fractions by Eq. (4.1) is a promising approach.

variant became dominant in Germany [70]. Additionally there is no visually discernible weekday effect present in Figure 4.5.

In Figure 4.1 we depict the nowcasts produced from our model including 95% prediction intervals, whose lengths are based on the past performance of our model. Except for the period from January to April 2022, the model produces reasonable nowcasts with prediction intervals that have sensible widths. In the aforementioned period the nowcasts overpredict the final hospitalisations, except for the oldest age group, and, after a transitional period, have larger uncertainty.

To investigate the quality of point predictions we display the time-evolution of absolute (AEP) and relative errors of predictions (REP, \log_{10} -scale) across all age groups in Figure 4.6. From this figure one can infer that the point nowcasts produced by our model tend to slightly overpredict the final number of hospitalisations. Indeed, the interquartile range of REPs for all age groups and dates combined spans $[-1.56, 8.33]$, demonstrating the same tendency. The highest REPs occurred in October / November 2021 and January/February 2022; the first corresponding to introduction of mandatory testing at the workplace and the second to the arrival of the Omicron variant in Germany. In both circumstances the number of cases rose while hospitalisations did not increase proportionally, a similar effect to the one observed in Figure 4.5.

We further quantified uncertainties in estimation by uncertainty intervals based on an assumption of a (log)-normal distribution for the errors with standard deviation based on past performance of our model. In Figure 4.7 we show the coverages of the 50% and 95% prediction interval across all age groups and delays for the whole time period of our study. For most age groups the 50% prediction interval has close to nominal coverage, while the 95% intervals have less than nominal coverage.

As our goal is to capture all of the uncertainty in this prediction, we chose to assume a sensible distribution for the prediction, a normal distribution for the two young age groups and a log-normal distribution for all other age groups. This has the advantage of producing more honest, wider, prediction intervals than those based on parametric distributions. The estimated standard deviation will also account for periods of low coverage, such as January 2022, albeit only after the maximum delay of 12 weeks.

We base our choice of 12 weeks of delay on the empirical survival function displayed in Figure 4.3. One could, however, argue for shorter maximum delay such as 6 weeks because time from reported infection to hospitalisation is much shorter, on the order of ≈ 10 days [32], so hospitalisations after this (shorter) period are unlikely to be due to the acute infection with SARS-CoV-2. This would have two main benefits: The model would adapt faster to changing circumstances and the indicator nowcasted describes the severity of the epidemic more appropriately.

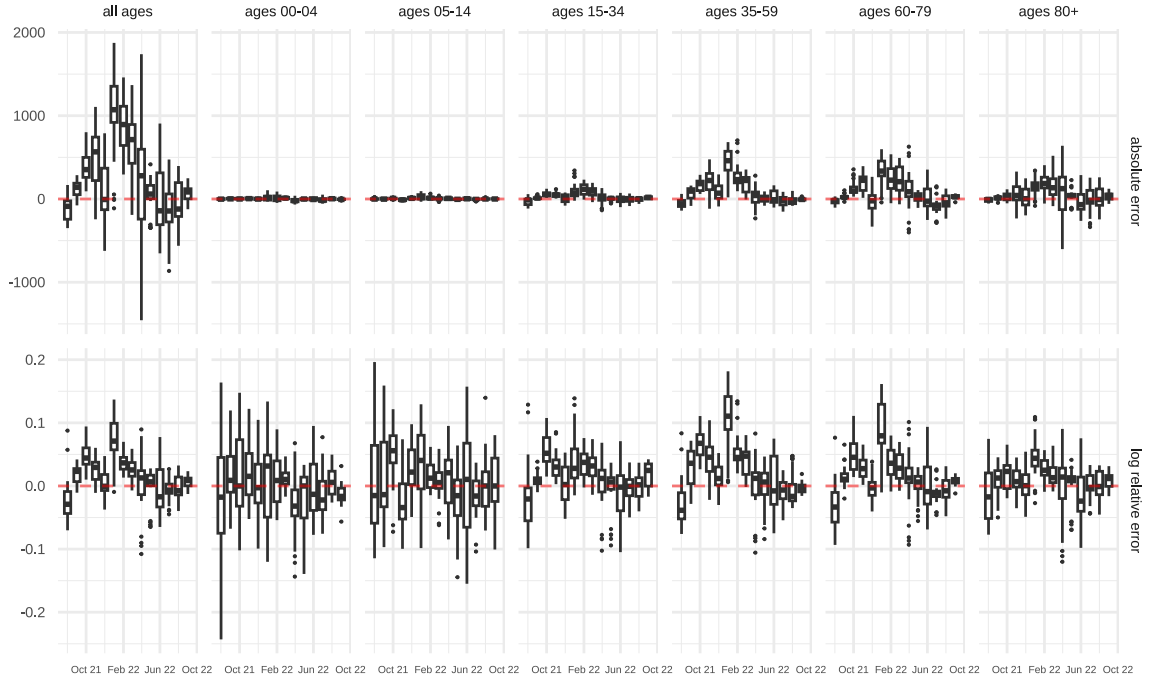


Figure 4.6: We show relative and absolute errors of prediction of our model for same day nowcasts by month of forecast and selected age groups. Relative errors are displayed on the log10 scale, i.e. as $\log_{10}(\text{predicted}) - \log_{10}(\text{actual})$. Up to December 2021 the model performs well, especially in the older age groups where most hospitalisations occur. The sharp increase in cases in January 2022 coupled with a lower probability of hospitalisation, most likely due to the appearance of the Omicron variant in Germany, lead to overpredictions across all age groups.

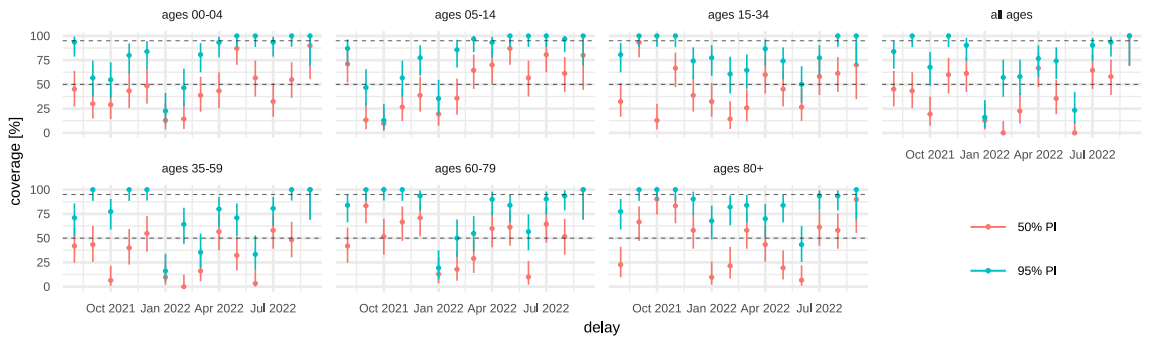


Figure 4.7: Empirical coverage of 50% and 95% prediction intervals (PI) based on same-day nowcasts for dates 2021-08-01 to 2022-09-10 (406 dates) for which the true amount of hospitalisations after 12 weeks is known as of the writing of this paper. We also display pointwise 95% binomial confidence intervals for the coverage. Given the difficulties of real-time forecasting [24] we deem the coverages good, except for the transitional period in the end of 2021 where changing testing schemes and the change from Delta to Omicron cause our model to be overly confident. Coverage is generally better in the older age groups.

The main advantage of our model over established nowcasting approaches is its simplicity, making it easy to understand, straightforward to implement and, once the reporting triangles for incidences and hospitalisation are created, fast to run; taking only $< XX$ minutes on a standard notebook(**TODO: check!**).

The problem of nowcasting hospitalisations is different from previously studied nowcasting settings in several ways. At the time of nowcast a large fraction of hospitalisations are not only unobserved, but are yet to occur - in this sense the nowcast is more accurately termed a forecast. As the date of hospitalisation is not known, the hospitalisations are associated by the date of reporting of the COVID-19 case, creating the double-weekday effect displayed in Figure 4.2. While daily updated data on hospitalisations are available, these consist only of moving weekly aggregates, consecutive observations are strongly auto-correlated.

We sidestep all of these issues by splitting the hospitalisations to nowcast into weekly chunks, incorporating leading indicators of hospitalisation – the weekly reported case incidences – and modelling the number of hospitalisations to come in each chunk by binomial thinning of incidences. Let us stress that this approach is only possible in the special situation where case and hospitalisation are explicitly linked, however we believe that incorporating leading indicators into nowcasting models is a promising approach.

An additional advantage of our model is that the hospitalisation probabilities can further be analysed, e.g. by investigating association between the publicly available vaccination rates and the probability of hospitalisation and delay to hospitalisation. Sudden changes in these fractions, as observed in Figure 4.5, can also hint towards worse model performance, especially if this change can be attributed to changing probability of hospitalisation due to new variants or changing testing regime.

Real time forecasting of epidemiological indicators is a difficult task [24], in particular quantifying uncertainty [12]. To test our model under real-time circumstances we submitted daily nowcasts to the German COVID-19 NowcastHub [64] since November 2021. In the nowcasting context, [57] goes to great lengths to account for overdispersion due to changes in delay distribution, introducing gamma and Dirichlet priors and explicitly modelling trends. Such an approach would also be feasible for our approach, e.g. model incidences by an appropriate Poisson or negative binomial distribution and, conditional on incidences, model hospitalisations by a binomial distribution. As this increases the complexity of our model and relies on the assumed distributions being sensible we opted for another approach.

Regarding the indicator we stress that its value on a given date does not represent the current occupancy of hospitals in Germany with COVID-19 patients but is rather an approximation to the morbidity caused by COVID-19 on that date. The reason for this discrepancy is that hospitalisations are attributed to the reporting date of the associated case, not that of hospitalisation. While the reporting date of the hospitalisation can be recovered from the publicly available data, the date of hospitalisation cannot. Additionally, no information on the duration of stay is available, making it impossible to create an indicator for the occupancy of hospitals based solely on data provided by the RKI.

Implicit in all of these approaches is an assumption of “stationarity”, i.e. that future reported hospitalisations will behave as they did in the past. Thus, all of these approaches might still be insufficient if circumstances change drastically, for example introduction of new testing schemes (school, 3G at workplace), changes in the delay distribution due to new variants, or hospitals close to capacity taking longer to process cases.

In summary, because models usually only capture a small part of the highly dynamic data-generating process, we believe that uncertainty in such circumstances should not come from unrealistic parametric assumptions but rather be based on past model performance. Given the discussed difficulties and the changing epidemiological dynamics in the period studied, the observed errors of prediction (Figure 4.6) and coverages of prediction intervals (Figure 4.7) are satisfying.

In this paper we provide a straight-forward model for nowcasting hospitalisations associated with COVID-19 in Germany. By leveraging known incident cases, we can estimate fractions of hospitalisa-

tions in weekly chunks which in turn avoids a complicated model of the two weekday effects present in the data. As the circumstances of the epidemic are changing constantly, e.g. vaccination coverage, testing regimes and emerging variants, we based uncertainty not on parametric assumptions but on the past performance of our model, assuming a (log)normal predictive distribution. We contributed nowcasts based on this model since November 2021 to the German COVID-19 NowcastHub [64], a collaborative platform collecting and aggregating such nowcasts from multiple research groups. The performance of the nowcasts in this Hub and presented in this paper (Figure 4.6 and Figure 4.7) are, regarding the simplicity of the model and the highly dynamic situation, quite satisfying.

There are multiple extensions to our model worth investigating. Firstly hospitalisations are also available at the federal state level so nowcasting on a spatial scale is naturally of interest due to heterogeneity in immunisation status and testing regimes across states. However, splitting hospitalisations into six age groups and 16 federal states will result in small numbers with larger variability which in turn increases variability in estimates $p_{t,d,k}$ and thus predictions which may require some regularisation thus increasing the models complexity. Secondly, in a similar vein, modeling the temporal evolution of hospitalisation probabilities by smooth functions, e.g. splines [78, 86], may help in early detection of changing circumstances and thus lead to better forecasts. Thirdly our uncertainty intervals account for the variance of past performance, but Figure 4.6 suggests that there is substantial bias in periods of changing circumstances which could be incorporated into our model in a straightforward way. Finally to predict the future course of the epidemic forecasting hospitalisations for dates t that lie in the future is of interest, which could be accomplished if one has a model that produces forecasts for incidences for all age groups.

Chapter 5

Discussion

Appendix A

Implementation in Python

Appendix B

Proofs (?)

Bibliography

- [1] Sam Abbott et al. “Estimating the Time-Varying Reproduction Number of SARS-CoV-2 Using National and Subnational Case Counts.” In: *Wellcome Open Res* 5 (June 1, 2020), p. 112. ISSN: 2398-502X. DOI: [10.12688/wellcomeopenres.16006.1](https://doi.org/10.12688/wellcomeopenres.16006.1).
- [2] Barbara Adamik et al. *Mitigation and Herd Immunity Strategy for COVID-19 Is Likely to Fail*. May 5, 2020. DOI: [10.1101/2020.03.25.20043109](https://doi.org/10.1101/2020.03.25.20043109). preprint.
- [3] S. Agapiou et al. *Importance Sampling: Intrinsic Dimension and Computational Cost*. Jan. 14, 2017. DOI: [10.48550/arXiv.1511.06196](https://doi.org/10.48550/arXiv.1511.06196). arXiv: [1511.06196](https://arxiv.org/abs/1511.06196) [stat]. preprint.
- [4] Andrei R. Akhmetzhanov. “Estimation of Delay-Adjusted All-Cause Excess Mortality in the USA: March-December 2020.” In: *Epidemiology and Infection* (2021). DOI: [10.1017/s0950268821001527](https://doi.org/10.1017/s0950268821001527). pmid: [34210370](https://pubmed.ncbi.nlm.nih.gov/34210370/).
- [5] Matthias An Der Heiden and Osamah Hamouda. “Schätzung Der Aktuellen Entwicklung Der SARS-CoV-2- Epidemie in Deutschland – Nowcasting.” In: *Epidemiologisches Bulletin* (Apr. 22, 2020). DOI: [10.25646/6692.4](https://doi.org/10.25646/6692.4).
- [6] Richard Arratia, Larry Goldstein, and Louis Gordon. “Poisson Approximation and the Chen-Stein Method.” In: *Statistical Science* 5.4 (1990), pp. 403–424. ISSN: 0883-4237. JSTOR: [2245366](https://www.jstor.org/stable/2245366). URL: <https://www.jstor.org/stable/2245366> (visited on 01/11/2024).
- [7] Francisco Arroyo-Marioli et al. “Tracking R of COVID-19: A New Real-Time Estimation Using the Kalman Filter.” In: *PLOS ONE* 16.1 (Jan. 13, 2021). DOI: [10.1371/journal.pone.0244474](https://doi.org/10.1371/journal.pone.0244474). pmid: [33439880](https://pubmed.ncbi.nlm.nih.gov/33439880/).
- [8] Leonardo Soares Bastos et al. “A Modelling Approach for Correcting Reporting Delays in Disease Surveillance Data.” In: *Statistics in Medicine* (2019). DOI: [10.1002/sim.8303](https://doi.org/10.1002/sim.8303).
- [9] Patrick Billingsley. *Probability and Measure*. 3rd ed. Wiley Series in Probability and Mathematical Statistics. New York: Wiley, 1995. 593 pp. ISBN: 978-0-471-00710-4.
- [10] Mohitosh Biswas et al. “Association of Sex, Age, and Comorbidities with Mortality in COVID-19 Patients: A Systematic Review and Meta-Analysis.” In: *Intervirology* 64.1 (Dec. 9, 2020), pp. 36–47. ISSN: 0300-5526. DOI: [10.1159/000512592](https://doi.org/10.1159/000512592).
- [11] Rebecca K. Borchering et al. “Public Health Impact of the U.S. Scenario Modeling Hub.” In: *Epidemics* 44 (Sept. 1, 2023), p. 100705. ISSN: 1755-4365. DOI: [10.1016/j.epidem.2023.100705](https://doi.org/10.1016/j.epidem.2023.100705).
- [12] J. Bracher et al. “A Pre-Registered Short-Term Forecasting Study of COVID-19 in Germany and Poland during the Second Wave.” In: *Nature Communications* 12.1 (1 Aug. 27, 2021), p. 5173. ISSN: 2041-1723. DOI: [10.1038/s41467-021-25207-0](https://doi.org/10.1038/s41467-021-25207-0). URL: <https://www.nature.com/articles/s41467-021-25207-0> (visited on 09/30/2021).
- [13] Johannes Bracher et al. “National and Subnational Short-Term Forecasting of COVID-19 in Germany and Poland during Early 2021.” In: *Communications Medicine* 2.1 (1 Oct. 31, 2022), pp. 1–17. ISSN: 2730-664X. DOI: [10.1038/s43856-022-00191-8](https://doi.org/10.1038/s43856-022-00191-8). URL: <https://www.nature.com/articles/s43856-022-00191-8> (visited on 11/16/2022).
- [14] Mary Ann Branch, Thomas F. Coleman, and Yuying Li. “A Subspace, Interior, and Conjugate Gradient Method for Large-Scale Bound-Constrained Minimization Problems.” In: *SIAM J. Sci. Comput.* 21.1 (Jan. 1999), pp. 1–23. ISSN: 1064-8275, 1095-7197. DOI: [10.1137/S1064827595289108](https://doi.org/10.1137/S1064827595289108).
- [15] Jan M. Brauner et al. “Inferring the Effectiveness of Government Interventions against COVID-19.” In: *Science* 371.6531 (Feb. 19, 2021), eabd9338. ISSN: 0036-8075, 1095-9203. DOI: [10.1126/science.abd9338](https://doi.org/10.1126/science.abd9338).

- [16] Tom Britton et al. *Stochastic Epidemic Models with Inference*. Ed. by Tom Britton and Etienne Pardoux. Springer, 2019.
- [17] Steve Brooks et al., eds. *Handbook for Markov Chain Monte Carlo*. Boca Raton: Taylor & Francis, 2011. 592 pp. ISBN: 978-1-4200-7941-8.
- [18] Lawrence D. Brown. *Fundamentals of Statistical Exponential Families: With Applications in Statistical Decision Theory*. Lecture Notes-Monograph Series v. 9. Hayward, Calif: Institute of Mathematical Statistics, 1986. 283 pp. ISBN: 978-0-940600-10-2.
- [19] Oyungerel Byambasuren et al. “Estimating the Extent of Asymptomatic COVID-19 and Its Potential for Community Transmission: Systematic Review and Meta-Analysis.” In: *Journal of the Association of Medical Microbiology and Infectious Disease Canada* 5.4 (Dec. 31, 2020), pp. 223–234. DOI: [10.3138/jammi-2020-0030](https://doi.org/10.3138/jammi-2020-0030).
- [20] Stephen Chan et al. “Count Regression Models for COVID-19.” In: *Physica A: Statistical Mechanics and its Applications* 563 (Feb. 1, 2021), p. 125460. ISSN: 0378-4371. DOI: [10.1016/j.physa.2020.125460](https://doi.org/10.1016/j.physa.2020.125460).
- [21] Sourav Chatterjee and Persi Diaconis. “The Sample Size Required in Importance Sampling.” In: *Ann. Appl. Probab.* 28.2 (Apr. 1, 2018). ISSN: 1050-5164. DOI: [10.1214/17-AAP1326](https://doi.org/10.1214/17-AAP1326).
- [22] Nicolas Chopin and Omiros Papaspiliopoulos. *An Introduction to Sequential Monte Carlo*. Springer Series in Statistics. Cham, Switzerland: Springer, 2020. 378 pp. ISBN: 978-3-030-47844-5.
- [23] Anne Cori. *EpiEstim: Estimate Time Varying Reproduction Numbers from Epidemic Curves*. manual. 2021. URL: <https://CRAN.R-project.org/package=EpiEstim>.
- [24] Angel N. Desai et al. “Real-Time Epidemic Forecasting: Challenges and Opportunities.” In: *Health Security* 17.4 (Aug. 2019), pp. 268–275. ISSN: 2326-5094. DOI: [10.1089/hs.2019.0022](https://doi.org/10.1089/hs.2019.0022).
- [25] O. Diekmann, Hans Heesterbeek, and Tom Britton. *Mathematical Tools for Understanding Infectious Diseases Dynamics*. Princeton Series in Theoretical and Computational Biology. Princeton: Princeton University Press, 2013. 502 pp. ISBN: 978-0-691-15539-5.
- [26] Zhanwei Du et al. “Reproduction Numbers of Severe Acute Respiratory Syndrome Coronavirus 2 (SARS-CoV-2) Variants: A Systematic Review and Meta-analysis.” In: *Clinical Infectious Diseases* 75.1 (July 1, 2022), e293–e295. ISSN: 1058-4838. DOI: [10.1093/cid/ciac137](https://doi.org/10.1093/cid/ciac137).
- [27] J. Durbin and S. J. Koopman. *Time Series Analysis by State Space Methods*. 2nd ed. Oxford Statistical Science Series 38. Oxford: Oxford University Press, 2012. 346 pp. ISBN: 978-0-19-964117-8.
- [28] James Durbin and Siem Jan Koopman. “Monte Carlo Maximum Likelihood Estimation for Non-Gaussian State Space Models.” In: *Biometrika* 84.3 (Sept. 1, 1997), pp. 669–684. ISSN: 0006-3444. DOI: [10.1093/biomet/84.3.669](https://doi.org/10.1093/biomet/84.3.669).
- [29] James Durbin and Siem Jan Koopman. “A Simple and Efficient Simulation Smoother for State Space Time Series Analysis.” In: *Biometrika* 89.3 (2002), pp. 603–616. DOI: [10.1093/biomet/89.3.603](https://doi.org/10.1093/biomet/89.3.603).
- [30] Max Ehre et al. “Certified Dimension Reduction for Bayesian Updating with the Cross-Entropy Method.” In: *SIAM/ASA J. Uncertainty Quantification* 11.1 (Mar. 31, 2023), pp. 358–388. DOI: [10.1137/22M1484031](https://doi.org/10.1137/22M1484031).
- [31] Michael Engel et al. “Bayesian Updating and Marginal Likelihood Estimation by Cross Entropy Based Importance Sampling.” In: *Journal of Computational Physics* 473 (Jan. 15, 2023), p. 111746. ISSN: 0021-9991. DOI: [10.1016/j.jcp.2022.111746](https://doi.org/10.1016/j.jcp.2022.111746).
- [32] Christel Faes et al. “Time between Symptom Onset, Hospitalisation and Recovery or Death: Statistical Analysis of Belgian COVID-19 Patients.” In: *International Journal of Environmental Research and Public Health* 17.20 (20 Jan. 2020), p. 7560. ISSN: 1660-4601. DOI: [10.3390/ijerph17207560](https://doi.org/10.3390/ijerph17207560).
- [33] C. P. Farrington et al. “A Statistical Algorithm for the Early Detection of Outbreaks of Infectious Disease.” In: *Journal of The Royal Statistical Society Series A-statistics in Society* (1996). DOI: [10.2307/2983331](https://doi.org/10.2307/2983331).
- [34] Seth Flaxman et al. “Estimating the Effects of Non-Pharmaceutical Interventions on COVID-19 in Europe.” In: *Nature* 584.7820 (Aug. 2020), pp. 257–261. ISSN: 1476-4687. DOI: [10.1038/s41586-020-2405-7](https://doi.org/10.1038/s41586-020-2405-7). pmid: [32512579](https://pubmed.ncbi.nlm.nih.gov/32512579/).

- [35] Sylvia Frühwirth-Schnatter. “Data Augmentation and Dynamic Linear Models.” In: *Journal of Time Series Analysis* 15.2 (1994), pp. 183–202. ISSN: 1467-9892. DOI: [10.1111/j.1467-9892.1994.tb00184.x](https://doi.org/10.1111/j.1467-9892.1994.tb00184.x).
- [36] “Discrete Spatial Variation.” In: *Handbook of Spatial Statistics*. Ed. by Alan E. Gelfand et al. CRC Press, 2010. ISBN: 978-0-429-13650-4.
- [37] Felix Günther et al. “Nowcasting the COVID-19 Pandemic in Bavaria.” In: *Biometrical Journal* 63.3 (2021), pp. 490–502. ISSN: 1521-4036. DOI: [10.1002/bimj.202000112](https://doi.org/10.1002/bimj.202000112).
- [38] Sumedha Gupta, Kosali I. Simon, and Coady Wing. *Mandated and Voluntary Social Distancing During The COVID-19 Epidemic: A Review*. Nov. 2020. DOI: [10.3386/w28139](https://doi.org/10.3386/w28139). National Bureau of Economic Research: [28139](https://doi.org/10.3386/w28139). preprint.
- [39] Stefan Heyder and Thomas Hotz. “Measures of COVID-19 Spread.” In: *Covid-19 pandisziplinär und international: Gesundheitswissenschaftliche, gesellschaftspolitische und philosophische Hintergründe*. Ed. by Alexander Kraemer and Michael Medzech. Medizin, Kultur, Gesellschaft. Wiesbaden: Springer Fachmedien, 2023, pp. 51–66. ISBN: 978-3-658-40525-0. DOI: [10.1007/978-3-658-40525-0_3](https://doi.org/10.1007/978-3-658-40525-0_3). URL: https://doi.org/10.1007/978-3-658-40525-0_3 (visited on 10/21/2023).
- [40] Michael Höhle and Matthias An Der Heiden. “Bayesian Nowcasting during the STEC O104:H4 Outbreak in Germany, 2011.” In: *Biometrics* 70.4 (2014), pp. 993–1002. ISSN: 1541-0420. DOI: [10.1111/biom.12194](https://doi.org/10.1111/biom.12194).
- [41] Tito Homem-de-Mello. “A Study on the Cross-Entropy Method for Rare-Event Probability Estimation.” In: *INFORMS Journal on Computing* (July 20, 2007). DOI: [10.1287/ijoc.1060.0176](https://doi.org/10.1287/ijoc.1060.0176).
- [42] *Hospitalization Nowcast Hub*. KITmetricslab, Oct. 31, 2022. URL: <https://github.com/KITmetricslab/hospitalization-nowcast-hub> (visited on 11/09/2022).
- [43] Thomas Hotz et al. “Monitoring the Spread of COVID-19 by Estimating Reproduction Numbers over Time.” Apr. 18, 2020. arXiv: [2004.08557](https://arxiv.org/abs/2004.08557) [q-bio, stat]. URL: <http://arxiv.org/abs/2004.08557> (visited on 07/20/2020).
- [44] Thomas D. Hughes et al. “The Effect of SARS-CoV-2 Variant on Respiratory Features and Mortality.” In: *Sci Rep* 13.1 (Mar. 18, 2023), p. 4503. ISSN: 2045-2322. DOI: [10.1038/s41598-023-31761-y](https://doi.org/10.1038/s41598-023-31761-y).
- [45] Norman Lloyd Johnson, Samuel Kotz, and N. Balakrishnan. *Continuous Univariate Distributions*. 2nd ed. Wiley Series in Probability and Mathematical Statistics. New York: Wiley, 1994. 2 pp. ISBN: 978-0-471-58495-7 978-0-471-58494-0.
- [46] Borus Jungbacker and Siem Jan Koopman. “Monte Carlo Estimation for Nonlinear Non-Gaussian State Space Models.” In: *Biometrika* 94.4 (Dec. 1, 2007), pp. 827–839. ISSN: 0006-3444. DOI: [10.1093/biomet/asm074](https://doi.org/10.1093/biomet/asm074).
- [47] Kenneth S. Kaminsky. “Prediction of IBNR Claim Counts by Modelling the Distribution of Report Lags.” In: *Insurance Mathematics & Economics* 6.2 (Apr. 1, 1987), pp. 151–159. DOI: [10.1016/0167-6687\(87\)90024-2](https://doi.org/10.1016/0167-6687(87)90024-2).
- [48] H. J. Kappen and H. C. Ruiz. “Adaptive Importance Sampling for Control and Inference.” In: *J Stat Phys* 162.5 (Mar. 1, 2016), pp. 1244–1266. ISSN: 1572-9613. DOI: [10.1007/s10955-016-1446-7](https://doi.org/10.1007/s10955-016-1446-7).
- [49] William Ogilvy Kermack and A.G. McKendrick. “A Contribution to the Mathematical Theory of Epidemics.” In: *Proc. R. Soc. Lond. A* 115.772 (Aug. 1927), pp. 700–721. ISSN: 0950-1207, 2053-9150. DOI: [10.1098/rspa.1927.0118](https://doi.org/10.1098/rspa.1927.0118).
- [50] Sahamoddin Khailaie et al. “Development of the Reproduction Number from Coronavirus SARS-CoV-2 Case Data in Germany and Implications for Political Measures.” In: *BMC Medicine* 19.1 (Jan. 28, 2021), p. 32. ISSN: 1741-7015. DOI: [10.1186/s12916-020-01884-4](https://doi.org/10.1186/s12916-020-01884-4).
- [51] Yeganeh Khazaei et al. “Using a Bayesian Hierarchical Approach to Study the Association between Non-Pharmaceutical Interventions and the Spread of Covid-19 in Germany.” In: *Sci Rep* 13.1 (Nov. 2, 2023), p. 18900. ISSN: 2045-2322. DOI: [10.1038/s41598-023-45950-2](https://doi.org/10.1038/s41598-023-45950-2).
- [52] Augustine Kong, Jun S. Liu, and Wing Hung Wong. “Sequential Imputations and Bayesian Missing Data Problems.” In: *Journal of the American Statistical Association* 89.425 (Mar. 1994), pp. 278–288. ISSN: 0162-1459. DOI: [10.1080/01621459.1994.10476469](https://doi.org/10.1080/01621459.1994.10476469).

- [53] Siem Jan Koopman, Rutger Lit, and Thuy Minh Nguyen. “Modified Efficient Importance Sampling for Partially Non-Gaussian State Space Models.” In: *Statistica Neerlandica* 73.1 (2019), pp. 44–62. ISSN: 1467-9574. DOI: [10.1111/stan.12128](https://doi.org/10.1111/stan.12128).
- [54] Moritz U. G. Kraemer et al. “The Effect of Human Mobility and Control Measures on the COVID-19 Epidemic in China.” In: *Science* 368.6490 (May 2020), pp. 493–497. DOI: [10.1126/science.abb4218](https://doi.org/10.1126/science.abb4218).
- [55] Pierre Simon Laplace. “Memoir on the Probability of the Causes of Events.” In: *Statistical Science* 1.3 (Aug. 1986), pp. 364–378. ISSN: 0883-4237, 2168-8745. DOI: [10.1214/ss/1177013621](https://doi.org/10.1214/ss/1177013621).
- [56] Steffen L. Lauritzen. *Graphical Models*. Oxford Statistical Science Series 17. Oxford : New York: Clarendon Press ; Oxford University Press, 1996. 298 pp. ISBN: 978-0-19-852219-5.
- [57] J. F. Lawless. “Adjustments for Reporting Delays and the Prediction of Occurred but Not Reported Events.” In: *Canadian Journal of Statistics* 22.1 (1994), pp. 15–31. ISSN: 1708-945X. DOI: [10.2307/3315826](https://doi.org/10.2307/3315826).n1.
- [58] J. O. Lloyd-Smith et al. “Superspreading and the Effect of Individual Variation on Disease Emergence.” In: *Nature* 438.7066 (Nov. 2005), pp. 355–359. ISSN: 1476-4687. DOI: [10.1038/nature04153](https://doi.org/10.1038/nature04153).
- [59] Sarah F. McGough et al. “Nowcasting by Bayesian Smoothing: A Flexible, Generalizable Model for Real-Time Epidemic Tracking.” In: *PLOS Computational Biology* (2020). DOI: [10.1371/journal.pcbi.1007735](https://doi.org/10.1371/journal.pcbi.1007735). pmid: 32251464.
- [60] Douglas N. Midthune et al. “Modeling Reporting Delays and Reporting Corrections in Cancer Registry Data.” In: *Journal of the American Statistical Association* 100.469 (Mar. 1, 2005), pp. 61–70. ISSN: 0162-1459. DOI: [10.1198/016214504000001899](https://doi.org/10.1198/016214504000001899).
- [61] M. Morf and T. Kailath. “Square-Root Algorithms for Least-Squares Estimation.” In: *IEEE Transactions on Automatic Control* 20.4 (Aug. 1975), pp. 487–497. ISSN: 1558-2523. DOI: [10.1109/TAC.1975.1100994](https://doi.org/10.1109/TAC.1975.1100994).
- [62] Joël Mossong et al. “Social Contacts and Mixing Patterns Relevant to the Spread of Infectious Diseases.” In: *PLOS Medicine* 5.3 (Mar. 25, 2008), e74. ISSN: 1549-1676. DOI: [10.1371/journal.pmed.0050074](https://doi.org/10.1371/journal.pmed.0050074).
- [63] Angela Noufaily et al. “Modelling Reporting Delays for Outbreak Detection in Infectious Disease Data.” In: *Journal of The Royal Statistical Society Series A-statistics in Society* (2015). DOI: [10.1111/rssa.12055](https://doi.org/10.1111/rssa.12055).
- [64] *Nowcasts Der COVID-19 Hospitalisierungsinzidenz*. 2022. URL: <https://covid19nowcasthub.de/> (visited on 11/09/2022).
- [65] Evan L. Ray et al. “Ensemble Forecasts of Coronavirus Disease 2019 (COVID-19) in the U.S.” In: *medRxiv* (Aug. 22, 2020), p. 2020.08.19.20177493. DOI: [10.1101/2020.08.19.20177493](https://doi.org/10.1101/2020.08.19.20177493).
- [66] Arthur E. Renshaw and Richard J. Verrall. “A Stochastic Model Underlying the Chain-Ladder Technique.” In: *British Actuarial Journal* 4.4 (1998), pp. 903–923. DOI: [10.1017/S1357321700000222](https://doi.org/10.1017/S1357321700000222).
- [67] Jean-Francois Richard and Wei Zhang. “Efficient High-Dimensional Importance Sampling.” In: *Journal of Econometrics* 141.2 (Dec. 1, 2007), pp. 1385–1411. ISSN: 0304-4076. DOI: [10.1016/j.jeconom.2007.02.007](https://doi.org/10.1016/j.jeconom.2007.02.007).
- [68] Robert Koch-Institut. *COVID-19-Hospitalisierungen in Deutschland*. Version 2021-10-01. Zenodo, Oct. 1, 2021. DOI: [10.5281/ZENODO.5519056](https://doi.org/10.5281/ZENODO.5519056).
- [69] Robert Koch-Institut. *SARS-CoV-2 Infektionen in Deutschland*. Version 2022-02-07. Zenodo, Feb. 7, 2022. DOI: [10.5281/ZENODO.4681153](https://doi.org/10.5281/ZENODO.4681153).
- [70] Robert Koch-Institut. *Wöchentlicher Lagebericht Des RKI Zur Coronavirus-Krankheit-2019 (COVID-19)*. Jan. 2022.
- [71] Nathan Ross. “Fundamentals of Stein’s Method.” In: *Probab. Surveys* 8 (none Jan. 1, 2011). ISSN: 1549-5787. DOI: [10.1214/11-PS182](https://doi.org/10.1214/11-PS182).
- [72] Reuven Rubinstein. “The Cross-Entropy Method for Combinatorial and Continuous Optimization.” In: *Methodology and Computing in Applied Probability* 1.2 (Sept. 1, 1999), pp. 127–190. ISSN: 1573-7713. DOI: [10.1023/A:1010091220143](https://doi.org/10.1023/A:1010091220143).
- [73] Reuven Y. Rubinstein and Dirk P. Kroese. *The Cross-Entropy Method: A Unified Approach to Combinatorial Optimization, Monte-Carlo Simulation and Machine Learning*. New York, NY: Springer New York, 2004. ISBN: 978-1-4757-4321-0.

- [74] Maëlle Salmon et al. “Bayesian Outbreak Detection in the Presence of Reporting Delays.” In: *Biometrical Journal* (2015). DOI: [10.1002/bimj.201400159](https://doi.org/10.1002/bimj.201400159). pmid: [26250543](https://pubmed.ncbi.nlm.nih.gov/26250543/).
- [75] Bernd Salzberger et al. “Epidemiology of SARS-CoV-2.” In: *Infection* 49.2 (Apr. 1, 2021), pp. 233–239. ISSN: 1439-0973. DOI: [10.1007/s15010-020-01531-3](https://doi.org/10.1007/s15010-020-01531-3).
- [76] Florian Schäfer, Matthias Katzfuss, and Houman Owhadi. “Sparse Cholesky Factorization by Kullback–Leibler Minimization.” In: *SIAM J. Sci. Comput.* 43.3 (Jan. 2021), A2019–A2046. ISSN: 1064-8275. DOI: [10.1137/20M1336254](https://doi.org/10.1137/20M1336254).
- [77] Frank Schlosser et al. “COVID-19 Lockdown Induces Disease-Mitigating Structural Changes in Mobility Networks.” In: *Proceedings of the National Academy of Sciences* 117.52 (Dec. 29, 2020), pp. 32883–32890. DOI: [10.1073/pnas.2012326117](https://doi.org/10.1073/pnas.2012326117).
- [78] Marc Schneble et al. “Nowcasting Fatal COVID-19 Infections on a Regional Level in Germany.” In: *Biometrical Journal* 63.3 (Mar. 2021), pp. 471–489. ISSN: 0323-3847, 1521-4036. DOI: [10.1002/bimj.202000143](https://doi.org/10.1002/bimj.202000143).
- [79] Wolfgang Schneider. *Der Kalmanfilter Als Instrument Zur Diagnose Und Schätzung Variabler Parameter in Ökonometrischen Modellen*. Arbeiten Zur Angewandten Statistik Bd. 27. Heidelberg: Physica-Verlag, 1986. 490 pp. ISBN: 978-3-7908-0359-4.
- [80] Neil Shephard and Michael K. Pitt. “Likelihood Analysis of Non-Gaussian Measurement Time Series.” In: *Biometrika* 84.3 (Sept. 1, 1997), pp. 653–667. ISSN: 0006-3444. DOI: [10.1093/biomet/84.3.653](https://doi.org/10.1093/biomet/84.3.653).
- [81] K. Sherratt et al. *Predictive Performance of Multi-Model Ensemble Forecasts of COVID-19 across European Nations*. June 16, 2022. DOI: [10.1101/2022.06.16.22276024](https://doi.org/10.1101/2022.06.16.22276024). URL: <http://medrxiv.org/lookup/doi/10.1101/2022.06.16.22276024> (visited on 11/28/2022). preprint.
- [82] Philip B. Stark and Robert L. Parker. “Bounded-Variable Least-Squares: An Algorithm and Applications.” In: *Computational Statistics* 10 (1995), pp. 129–129. URL: <https://digitalassets.lib.berkeley.edu/sdtr/ucb/text/394.pdf> (visited on 06/05/2024).
- [83] Luke Tierney and Joseph B. Kadane. “Accurate Approximations for Posterior Moments and Marginal Densities.” In: *Journal of the American Statistical Association* 81.393 (Mar. 1986), pp. 82–86. ISSN: 0162-1459, 1537-274X. DOI: [10.1080/01621459.1986.10478240](https://doi.org/10.1080/01621459.1986.10478240).
- [84] Luke Tierney, Robert E. Kass, and Joseph B. Kadane. “Fully Exponential Laplace Approximations to Expectations and Variances of Nonpositive Functions.” In: *Journal of the American Statistical Association* 84.407 (Sept. 1989), pp. 710–716. ISSN: 0162-1459, 1537-274X. DOI: [10.1080/01621459.1989.10478824](https://doi.org/10.1080/01621459.1989.10478824).
- [85] Damilola Victoria Tomori et al. “Individual Social Contact Data Reflected SARS-CoV-2 Transmission Dynamics during the First Wave in Germany Better than Population Mobility Data – an Analysis Based on the COVIMOD Study.” In: (Mar. 26, 2021), p. 2021.03.24.21254194. DOI: [10.1101/2021.03.24.21254194](https://doi.org/10.1101/2021.03.24.21254194).
- [86] Jan van de Kastele et al. “Nowcasting the Number of New Symptomatic Cases during Infectious Disease Outbreaks Using Constrained P-Spline Smoothing.” In: *Epidemiology* (2019). DOI: [10.1097/ede.0000000000001050](https://doi.org/10.1097/ede.0000000000001050). pmid: [31205290](https://pubmed.ncbi.nlm.nih.gov/31205290/).
- [87] Aad W. Van der Vaart. *Asymptotic Statistics*. Cambridge: Cambridge University Press, 2000.
- [88] Halbert White. “Maximum Likelihood Estimation of Misspecified Models.” In: *Econometrica* 50.1 (1982), pp. 1–25. ISSN: 0012-9682. DOI: [10.2307/1912526](https://doi.org/10.2307/1912526). JSTOR: [1912526](https://www.jstor.org/stable/1912526).
- [89] Scott L. Zeger, Lai-Chu See, and Peter J. Diggle. “Statistical Methods for Monitoring the AIDS Epidemic.” In: *Statistics in Medicine* 8.1 (1989), pp. 3–21. DOI: [10.1002/sim.4780080104](https://doi.org/10.1002/sim.4780080104).
- [90] Wei Zhang et al. “Applications of the Cross-Entropy Method to Importance Sampling and Optimal Control of Diffusions.” In: *SIAM J. Sci. Comput.* 36.6 (Jan. 2014), A2654–A2672. ISSN: 1064-8275. DOI: [10.1137/14096493X](https://doi.org/10.1137/14096493X).

Declaration

Put your declaration here.

Ilmenau, October 2023